Université de Québec
Institut National de la Recherche Scientifique (INRS)
Énergie Matériaux Télécommunications (EMT)

Gold Nanoparticles for Catalytic and Potential Biological Applications

Par

Jianming Zhang

Thèse présentée pour l'obtention du grade de Philosophiæ Doctor (Ph.D.) en Sciences de l'énergie et des matériaux

Jury d'évaluation

Président du jury et examinateurs interne	Royston Paynter INRS-EMT, Université de Québec
Examinateurs externe	Fabio Cicoira École Polytechnique de Montréal
	Zhifeng Ding University of Western Ontario
Directeur de recherche	Dongling Ma INRS-EMT, Université de Québec
Codirecteur de recherche	Mohamed Chaker INRS-EMT, Université de Québec

Abstract

Gold nanoparticles (AuNPs) have attracted much attention in many applications due to their unique physical and chemical properties, which the bulk material does not possess. Generally, two main approaches can be used for synthesis of AuNPs, namely chemical and physical methods. The chemical reduction method is the most widely used synthesis technique. It involves using various chemical precursors, such as Au salt and a reducing agent. Au ions are reduced to Au atoms followed by the growth of NPs. The laser ablation approach is one of the most used physical synthesis methods, such as pulsed laser ablation in liquid (PLAL), where NPs are synthesized via laser ablation of a solid target placed in a liquid medium without addition of chemicals.

AuNPs based nanomaterials used as catalyst have shown highly active catalytic properties in many reactions, such as selective hydrogenation of organic molecules, carbon monoxide (CO) oxidation, and the water-gas shift reaction. The catalytic activity of AuNPs is strongly dependent on their surface chemistry. Various Au-based nanostructures have been successfully synthesized by chemical methods, however, the surface features of AuNPs prepared by these chemical approaches are not optimal for catalysis, due to the existence of surface stabilizing molecules or tightly adsorbed reaction residues, which exerts a “barrier” effect to catalysis or poisons the catalyst. Therefore, AuNPs with relatively “bare and clean” surfaces are highly desired for catalysis. The unique relatively “bare and clean” surface of AuNPs prepared by PLAL makes them a good candidate for catalysis. However, this potential of applications of PLAL-AuNPs in the field of

catalysis is still not explored. It is therefore of great interest to investigate the catalytic properties of PLAL-AuNPs and the influence of their surface chemistry on catalysis.

AuNPs have also been widely used in the field of biological research. In these applications, small and toxic-chemical-free colloidal AuNPs are highly desired. Nonetheless, the colloidal stability and molecule adsorption ability of the AuNPs are two primary properties for their biological application development, which highly depend on the surface chemistry of AuNPs. Unfortunately, the chemical synthesis of very small AuNPs (less than 10 nm) involves the use of toxic chemicals which renders them unsuitable for biological applications. Another laser technique ─ laser irradiation, which combines chemical reduction and laser methods, is suitable for synthesis of "green" Au colloids with very small sizes. Interestingly, laser irradiation introduces novel surface chemistry to chemically synthesized AuNPs, such as surface oxidation. The effect of the surface chemistry variation introduced by laser treatment on NP colloidal stability and amine molecule-AuNP interaction has not been investigated so far.

The work performed in this thesis was therefore driven by two main objectives: 1) PLAL and chemical synthesis of Au and PtAu NPs and characterization of their catalytic properties and 2) investigation of the surface modification of chemically synthesized Au NPs by laser irradiation and its influence on Au colloidal stability and amine-AuNP interaction. The results obtained in this work are summarized in two sections as follows.

In the first section, the synthesis and catalytic property of AuNPs prepared using the PLAL technique are investigated. To do so, I prepared a novel nanostructured catalyst, composed of small (~5 nm in diameter) and uniform AuNPs and ceria nanotubes (CeO_2 NTs). AuNPs with relatively "bare and clean" surfaces fabricated by PLAL on a bulk Au target in pure water are efficiently assembled onto the surfaces of CeO_2 NTs without performing any surface functionalization of either

component to promote their coupling, thanks to the presence of the –OH groups (that do not block catalysis) on the surfaces of PLAL-AuNPs. The model reaction of reducing 4-nitrophenol to 4-aminophenol catalyzed by our PLAL-AuNP/CeO_2-NT catalyst exhibits a remarkably higher reaction rate than the reaction catalyzed by other supported Au catalysts reported recently by other groups.

Meanwhile the study of the effect of surface chemistry on catalysis shows that the catalytic activity of the PLAL-AuNP/CeO_2-NT catalyst is much higher in comparison to that of similar catalysts composed of chemically prepared AuNPs (Chem-AuNPs) and/or commercially available CeO_2 powder as support. Its superior catalytic activity is found to be due to the unique, relatively "bare" surface of the PLAL-AuNPs as well as oxidized Au species induced by the strong interaction between the "barrier-free" surface of PLAL-AuNPs and surface defects (oxygen vacancies) of CeO_2 NTs. The important role of the unique surface chemistry of PLAL-AuNPs in catalysis was further demonstrated in the CO oxidation reaction in the gas phase. Our results suggest that the use of PLAL-AuNPs enables easy and efficient attachment of AuNPs onto the surface of the CeO_2 NTs and their unique combination leads to the development of highly efficient catalysts.

In order to overcome the aggregation issue induced by centrifugation when recycling AuNPs during catalysis, and to expand the application of PLAL-AuNPs for catalysis in liquid phases, I further developed a novel *in situ* recyclable AuNP catalyst for 4-NP reduction using PLAL-AuNPs and CO_2-switchable polymers. The surface of PLAL-AuNPs is relatively "bare and clean" and therefore favours easy surface functionalization. I modified the surfaces of PLAL-AuNPs by coupling a thiol-terminated poly(N,Ndiethylaminoethylmethacrylate) (SH-PDEAEMA) with Au, to form CO_2-switchable AuNPs (PDEAEMA-AuNPs). The structure of PDEAEMA polymer was rationally designed to enable its robust attachment to the NP surface, yet limit the number of polymers that can be anchored onto the NP surface. So the possible, negative "blocking" effect on the catalytic active sites of AuNPs is limited. The dispersion status of PDEAEMA-AuNPs in

aqueous solution can be easily tuned by simply bubbling CO_2 or expelling CO_2 from solution using N_2 bubbling, inducing novel *in situ* recyclable AuNPs in liquid. The PDEAEMA-AuNPs were used as a catalyst in a model catalytic reaction of 4-nitrophenol reduction and compared with the PLAL-AuNPs without polymer functionalization and the Chem-AuNPs. Results show that the limited amount of PDEAEMA on the AuNP surface doesn't noticeably reduce the catalytic activity. More interestingly, this novel catalyst can be easily separated and re-dispersed in solution by CO_2 gas-switching and exhibits better colloidal and catalytic stability during successive reactions than PLAL-AuNPs and similarly sized AuNPs synthesized by the conventional chemical reduction approach (Chem-AuNPs).

In order to further enhance the catalytic activity of PLAL-AuNPs, it is highly interesting to alloy Au with other transition metals, e.g., platinum (Pt) because of the possible synergistic effect of the alloy structure in catalysis. Using a modified PLAL technique, stable PtAu alloy colloids with a wide range of compositions were prepared successfully on novel metal-mixture targets in water, which are made by compression molding a mixture of Pt and Au powders at different ratios. The concentration of Pt in the alloys can be tuned by varying the Pt/Au ratio in the targets, and their composition basically follows that of their corresponding targets. The effect of aqueous solution pH and ablating laser fluence on the formation and structure of alloy NPs was further investigated. It is found that PtAu alloy colloids of identical composition can be achieved over a pH range extending from 4.0 to 11.0 and at fluences varying from 4 to 150 J cm^{-2} as long as targets of the same composition are used. This finding suggests that alloy formation is essentially insensitive to both factors in certain ranges and the method developed herein for the alloy NP formation is quite robust. Moreover, the surface composition, estimated from electrochemical measurements, is identical to the overall composition of the NPs estimated from Vegard's law and X-ray diffraction data, which

is a strong indication of the uniform composition on the surface and in the interior of these alloy NPs.

The as-prepared PtAu alloy NPs were assembled onto CeO_2 nanotubes (NTs) to form hybrid nanocatalysts for 4-NP reduction. As demonstrated in the PLAL-AuNP/CeO_2 study, the unique surface features of alloy NPs resulting from PLAL are mainly responsible for their robust adsorption onto the NTs, without any additional surface functionalization to either component. The as-prepared PtAu alloy NPs exhibit exceptional catalytic activity for the reduction of 4-nitrophenol. All PtAu alloy NPs, and in particular the $Pt_{50}Au_{50}$ sample, outperform the activity of monometallic PLAL-Pt, AuNPs and their mixture, and even outperform most AuNPs reported. Remarkably, the alloying of Au with Pt enhances the catalytic activity by means of a synergistic effect.

In the second section, chemically pre-synthesized AuNPs were treated using a laser irradiation technique, and then the effect of the surface chemistry variation introduced by laser treatment on the colloidal stability of NPs and amine molecule-AuNP interactions was investigated.

First, monodisperse, AuNPs with diameter ~5 nm were prepared at a relatively high concentration by optimized laser irradiation (without the involvement of any hazardous chemicals) on 20-nm AuNPs synthesized chemically via the "green" Frens method. The citate concentration shows an effect on the final particle size and shape during laser treatment. AuNPs after laser irradiation demonstrate a significant improvement in colloidal stability as compared to similarly sized Chem-AuNPs prepared by a purely chemical approach which involves the use of hazardous $NaBH_4$. The stability has been investigated by adjusting the dielectric constant and ionic concentration of the colloidal solutions. The observed enhanced colloidal stability is confirmed by a significant increase in the Zeta potential of the Au colloids and could be explained by the oxidation of gold surface under laser irradiation. The enhanced stability is a key property for the use of AuNPs

in many applications and this study reveals the potential of the laser irradiation treatment (free of hazardous chemicals) for the production of highly-stable ultra-small AuNPs.

Then, I investigated the surface chemistry and surface functionality variation introduced by laser irradiation. The effect of the surface chemistry variation of AuNPs on the AuNP-amine ($-NH_2$) interaction was investigated via conjugating an amine probe ─ 1-methylaminopyrene (MAP) chromophore ─ with three Au colloidal samples of the same particle size yet different surface chemistries. The surfaces of laser-irradiated and ligand-exchanged-irradiated AuNPs are covered with acetonedicarboxylic ligands (due to laser-introduced citrate oxidization) and citrate ligands, respectively, and both surfaces contain oxidized Au species which are essentially lacking for the citrate-capped AuNPs prepared by the pure chemical approach. Both laser irradiated samples show inferior adsorption capacity of MAP as compared with the purely chemically prepared AuNPs. Detailed investigations indicate that MAP molecules mainly complex directly with Au atoms via Au-NH_2R bonds, and the oxidation of the AuNP surface strongly influences the ratio of this direct bonding to the indirect bonding originating from the electrostatic interaction between protonated amine ($-NH_3^+$) and negatively charged surface ligands. The impact of the oxidized AuNP surface associated with the laser treatment is further confirmed by an aging experiment on AuNP-MAP conjugation systems, which straightforwardly verifies that the surface oxidation leads to the decrease in the MAP adsorption on AuNPs.

Acknowledgements

I would like to thank Prof. Dongling Ma and Prof. Mohamed Chaker for giving me the opportunity to study at INRS-EMT, and providing me precious advice and direction throughout my PhD study. They have created a warm and stimulating research environment allowing me explore a complex and fascinating scientific field. Thanks to them for their kindness, patience and support during my PhD path. I learned lots from them. Being able to study under their supervision is one of the most important achievements in my life.

I want to acknowledge the contributions to this work made by Dr. Daria Riabinina. She gave me invaluable help and comments on my research, predoctoral exam and thesis writing. I am grateful to Dr. Guozhu Chen, who collaborated closely with me on many aspects of this research. Thanks to all the group members for their help throughout the work. I am grateful to have been part of such supportive, hardworking, and inspiring groups. Over the course of my research I have been fortunate enough to work with the truly outstanding groups. These people include: Dr. Haiguang Zhao, Ibrahima Ka, Hongyan Liang, Belete Atomsa Gonfa, Maxime Gougis and Dr. Stephano Desigan.

I thank to Prof. Federico Rosei, Prof. Daniel Guay and Ana Tavares at INRS-EMT, Prof. Nianqiang Wu from University of West Virginia and Prof. Yue Zhao from University of Sherbrooke for their important comments during my project research.

I thank Shun Li, Yue Huang, Sébastien Vigne and Maxime Brossard. They always bring me funs and cheer me up.

I thank the departmental and technical staff at INRS-EMT. They are very helpful, particularly Etienne Charette, Georges Lamoureux, Louise Hudon and Christophe Chabanier. I would like to thank Jean-Philippe Masse at Ecole Polytechnique for TEM measurements.

I am eternally grateful to my dearest mother, who has been a constant source of love, encouragement for me. I want to thank to my wife, Meaw-Qian, who loves me deeply and supports me selflessly. I want to say them, I love you. I thank my family and my friends for their continuing love and heartily support.

Finally, I wish to acknowledge the following organizations for their financial support: the Natural Sciences and Engineering Research Council of Canada and Fonds de la recherche sur la nature et les technologies.

Contents

List of Figures

List of Schemes

List of Tables

Chapter 1

Introduction

1.1 Gold Nanoparticles and their Basic Properties

When the size of a material is reduced to the nanometer scale (generally 1–100 nm) in at least one dimension, it can be defined as a "nanomaterial", whether it is dispersed in gaseous, liquid or solid media [1, 2]. At nanoscale, the ratio between the surface and volume significantly increases, which leads to important changes in physical and chemical properties of nanomaterials that are very different from their bulk materials [1-3]. Nanomaterials are likely to impact virtually all fields of physical and chemical sciences, biological and health sciences, and other interdisciplinary region of science and engineering [1-8].

Among various nanomaterials, gold nanoparticles (AuNPs) have attracted considerable attention because of their unique physical and chemical properties and potential technological applications [4-15]. Unlike bulk Au with its familiar yellow color, when the size of Au reaches nanoscale dimensions, its color changes to ruby red or purple (Figure 1.1-a) due to the absorption of the light at certain wavelengths, e.g., 520 nm (green light) [4, 8]. As illustrated in Figure 1.1-b, when light of certain wavelength passes through AuNPs, the NPs are excited, leading to a strong electromagnetic field and an intense absorption attributed to the collective oscillation of excited electrons on the particle surface, known as Surface Plasmon Resonance (SPR) [4, 16]. The presence

of SPR also results in strong light scattering. This resonance can be measured and recorded using a UV-Visible (UV-Vis) spectrometer as a strong absorption peak (SPR peak) as shown in Figure 1.1-c.

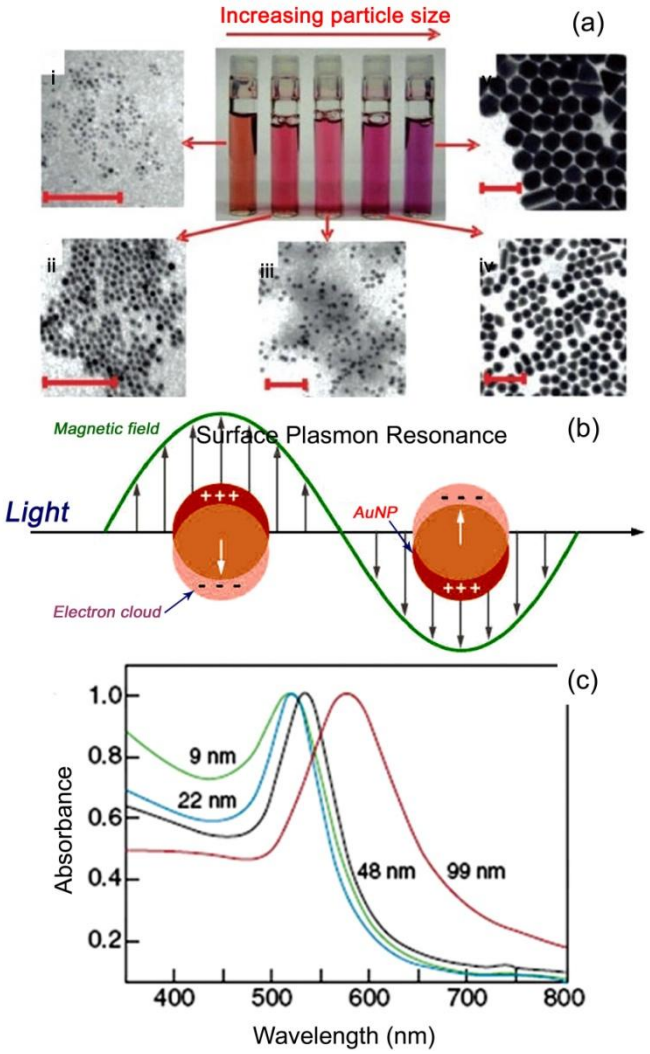

Figure 1.1 (a) Photographs of aqueous solutions of AuNPs as a function of increasing dimensions. Corresponding transmission electron microscopy (TEM) images of the particles (i-v) are shown (all scale bars are 100 nm) [8]. (b) Schematic illustration of a surface plasmon of a metal sphere showing the displacement of the electron charge cloud relative to the NP [4]. (c) UV-Vis spectra of AuNPs of different sizes [17].

Generally, the resonance frequency is highly dependent on particle size, shape, material, and environment [4]. AuNPs in aqueous solution with a particle size of about 10 nm in diameter show a strong absorption at about 520 nm due to their SPR properties. This absorption peak shows a red

shift with an increase in the NP size (Figure 1.1-c) due to the electromagnetic retardation in larger particles, resulting in a color change from ruby-red to purple (Figure 1.1-a) [4, 16]. The NP size can thus be estimated from the position of the SPR peak [18]. This tuneable performance of SPR by varying the size or shape of the NPs leads to particles with tailored optical properties for different applications.

Besides, it is well known that Au has strong affinity with thiol (e.g., R-SH) and amine (e.g., R-NH_2) group-bearing molecules or polymers by forming Au-S and Au-N covalent bonds, respectively [3]. These molecules can thus strongly interact with surface Au atoms to form a stable molecule layer on the AuNP surface. Moreover, appropriately charged ions, molecules or polymers may be able to adsorb on a AuNP surface through electro-static interactions as well [3, 150-158]. The bonding of AuNP with molecules offers a versatile route to modify and functionalize the AuNPs, and brings various possibilities for actual applications.

1.2 Synthesis Techniques for AuNPs

To the best of our knowledge, two main approaches ─ chemical methods and physical methods have been well established for the synthesis of AuNPs [54]. Wet chemical procedures start from the reduction of metal ion precursors to metal atoms, followed by controlled aggregation of atoms into NPs. The physical methods often involve the condensation of vapor-like substances, effective by subdividing bulk materials into NPs.

1.2.1 Chemical Synthesis

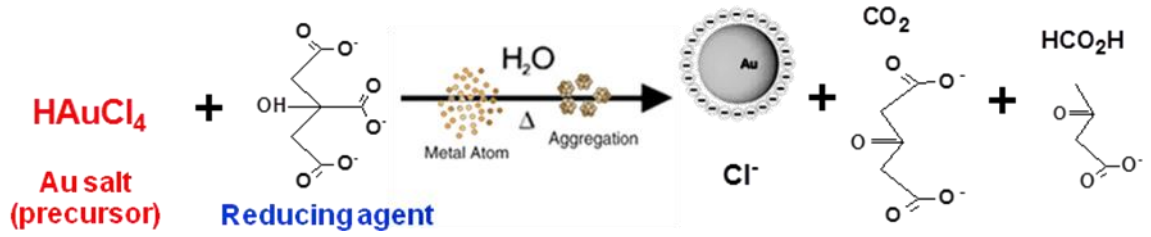

Figure 1.2 A typical AuNP preparation rout ("Frens" method) by chemical reduction [18, 56].

The synthesis of AuNPs with diameters ranging from a few to several hundreds of nanometers has been developed in aqueous solution as well as in organic solvents. As illustrated in Figure 1.2, generally, in a typical chemical synthesis process, the Au precursor (Au salt), e.g., auric acid ($HAuCl_4$), is dissolved in a solution, and then with rapid stirring a reducing agent, such as citrate or $NaBH_4$, is added immediately, which causes Au^{3+} ions to be reduced to neutral Au atoms. The enrichment of Au atoms in solution leads to their nucleation/precipitation to form sub-nanometer particles. The free Au atoms or sub-nanometer particles will attach to the existing NPs, and therefore, they grow into bigger AuNPs [7, 55, 56].

In principle, smaller NPs easily aggregate during synthesis or storage due to their high surface energy, resulting in a large reduction of their quality and application ability. Besides, colloidal NPs are sensitive to their enviroment, for instance, high ionic concentration in dispersing solution or high temperature can induce an irreversible fierce aggregation [7, 57, 58]. In order to prevent the particles from aggregating and control their nucleation/growth to achieve an ideal size, stabilizing agents (such as ligands or surfactants) that bond to the NP surface are usually added during the AuNP synthesis process [34, 35, 57, 59]. For the typical synthesis process of AuNPs in aqueous solution, the stabilizing agent is usually charged, so that the charged NPs repel each other leading to a stable colloidal solution. For particles that need to be dispersed in organic solvent, frequently surfactants, which can bind strongly to the NP surface and are mainly based on hydrophobic alkane chains, are used to provide a good colloidal stability. Another option to stabilize AuNPs is to use support materials, such as ceria (CeO_2), silica (SiO_2) and Zinc oxide (ZnO) [5, 7, 34, 35, 57, 59, 60], to link AuNPs and thus form a hybrid structure to disperse and stabilize the AuNPs. To couple the AuNPs with support, the pre-formed AuNPs are generally surface modified with linker molecules, such as silanes or mercapto alkane acids, during or after the synthesis [5, 7, 60].

Other procedures, such as deposition–precipitation (DP) [15, 59, 61-65], impregnation-incipient wetness [66, 67], and *in-situ* growth methods [39] are widely used to obtain supported AuNPs as well. They are usually composed of two steps [7]: *i)* mixing an Au salt and a solid support in solution for adsorption; *ii)* growth of adsorbed Au salt into AuNPs on the support surface by reduction. The DP method was first reported by Haruta's group to synthesize supported AuNP nanostructures and has since then become one of the most popularly used methods. In a typical DP process, Au salt ($HAuCl_4$) solution is mixed with a support material, such as metal oxide or carbon, and Au anions are hydrolyzed by raising the pH of the solution to form insoluble $Au(OH)_3$ which adsorbs onto the solid support as it precipitates. After the adsorption, the unstable component $Au(OH)_3$ will decompose into neutral Au atoms, followed by their assembly [7, 63]. Finally the AuNPs form on the support surface by nuclearation and growth. For the impregnation-incipient wetness method, an Au complex adsorbing on a support is subject to a thermal treatment under a reductive atmosphere, and is hence reduced to neutral Au atoms that grow into AuNPs on the support surface. Supported AuNP nanostructures can also be synthesized by the *in situ* growth method, where typically Au salt solution is mixed with special support materials, and then a redox reaction occurs between the two components simultaneously leading to the formation of AuNPs on the support surface [7, 39].

1.2.2 Physical Synthesis

The pulsed laser ablation technique is an important physical method for NP preparation [68-86]. As shown in Figure 1.3-a, during laser ablation, high energy pulsed laser beam is focused on the surface of a solid target, creating a directional plasma propagating perpendicularly to the target (plasma plume). Small clusters are formed as a result of the condensation of atoms in the decaying plume. Generally, the size of NPs formed in plasma plume varies from several to hundreds of nanometers, depending on experimental parameters, such as laser density, pulse width, target-

substrate distance, pressure and the composition of the surrounding gas. Unlike the chemical method, chemical reagents are usually not involved in this approach.

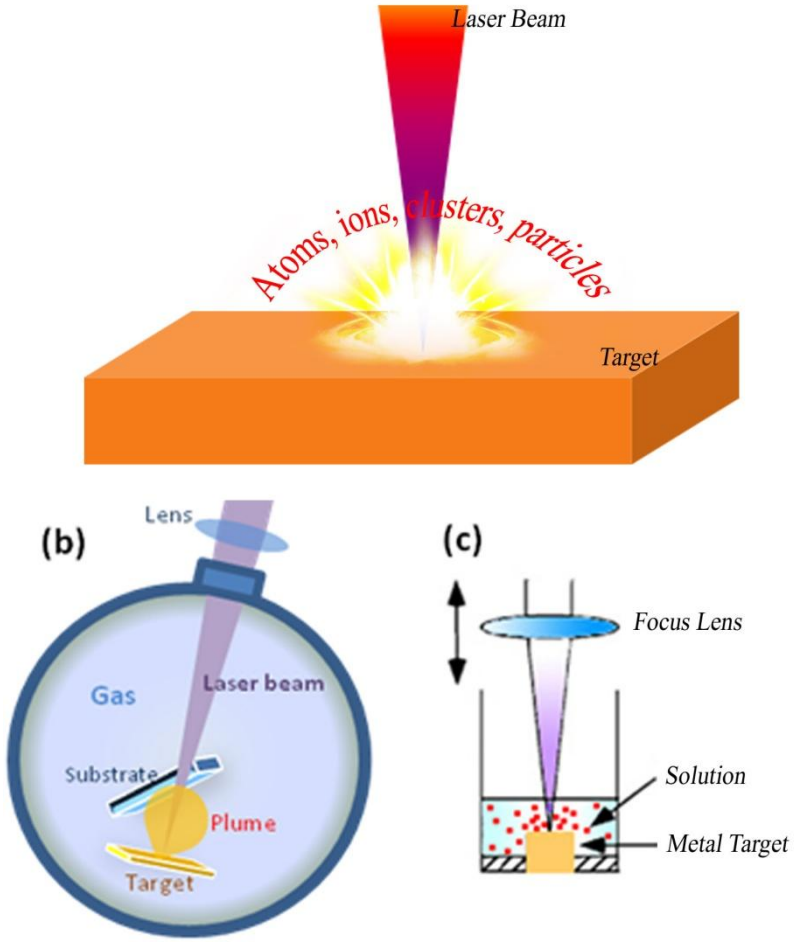

Figure 1.3 Schematic illustration of (a) laser ablation, (b) PLD and (c) PLAL for NPs.

AuNPs prepared by pulsed laser deposition (PLD) in the gas phase are generally collected by a solid substrate (Figure 1.3-b), e.g., a silicon wafer or metal oxide support (such as Fe_2O_3, SiO_2 and MnO_2) [74-76]. Recently, an alternative laser ablation technique, pulsed laser ablation in liquid phase (PLAL), has attracted much interest [68, 69, 71, 73, 78, 79, 81, 82, 85, 87, 88]. The bulk target is immersed in a liquid environment instead of the gas of PLD, and the focused beam passes through the liquid to hit the target (Figure 1.3-c). The influence of various conditions on NP fabrication, such as laser parameters, solvents, pH values, temperatures and electrolytes [68, 69, 79,

81, 88, 90, 91], and the surface chemistry of PLAL-AuNPs has been investigated. If the experimental conditions are appropriately optimized, it is able to yield small, mono-dispersed, stable colloidal NPs in a pure solvent (e.g., water) without intentionally introducing any stabilizing molecules. It has been shown that, in contrast to the plasma plume formed in the classical PLD process involving a gas environment, the plume formed during PLAL has very distinct characteristics [71, 73, 85, 89]: *i).* the plasma plume expansion is limited by the ambient liquid and *ii).* the size and lifetime of the plasma in the liquid are much smaller compared to the PLD in a gaseous environment. Due to the confinement of ambient liquid, the laser-induced plasma is rapidly driven into a thermodynamic state of high temperature, high pressure, and high density, which are highly favorable for chemical reactions, and the short lifetime of the ablated species favors the formation of metastable substances [73]. For example, Luong et al. and Mafune et al. reported that Au atoms on the surface of AuNPs freshly prepared by the laser technique in water are partially oxidized [68, 80, 82], Kondow [69], and Muniz-Miranda et al. [70] also showed that metal PLAL NP prepared in pure water without using any surfactants are stable because small OH^- groups from aqueous environment can adsorb on the NP surface to form a negatively charged surface to stabilize the NPs. This unusual surface feature of AuNPs prepared by laser in aqueous solution may lead to interesting impact to NP properties and potential applications.

1.3 Applications of AuNPs

Various applications using AuNPs have been developed based on their unique physical and chemical properties. For example, AuNPs have been designed to serve as good conductors in printing electronic chips [2]. Since the electronic chips or devices become smaller, NPs are acting as important components for the chip design. AuNPs are being used to connect resistors, conductors, and other elements of an electronic chip [2]. The non-toxicity and unique SPR feature of AuNPs have led to wide applications in biological field [4, 8]. The light absorption of AuNPs can produce

heat at a local region close to NP surface when excited by light at certain wavelengths. Therefore, when light is applied to a tumor containing AuNPs in a treatment, the particles rapidly heat up so as to kill the tumor cells, which is known as AuNP based photo-therapy [8]. Therapeutic agents can also be conjugated onto the NP surface. The large surface area-to-volume ratio of AuNPs enables their surface to be coated with a large number of molecules, such as therapeutics, targeting agents, and anti-fouling polymers [3, 8]. AuNPs can also be used for molecule detection and analysis [5]. For example, surface enhanced Raman signal of small molecules can be significantly enhanced by exploiting AuNP as substrates to enable the measurement of vibrational energies of chemical bonds [4, 5]. Besides, AuNPs also demonstrate outstanding catalytic activity in a number of chemical reactions which will be discussed detailedly in the following content.

1.3.1 Catalytic Applications

Bulk Au is a well-known chemically inert material and has been considered as a poorly active catalyst in many reactions. However AuNPs demonstrate outstanding catalytic properties for many reactions [5, 7, 9, 12, 13, 19-25]. The discovery of the excellent catalytic properties of AuNPs was reported for the first time by Haruta et al. in 1989, who demonstrated that AuNPs can be very active in the promotion of the oxidation of carbon monoxide (CO) at low temperature [26]. Following this discovery, a variety of aerobic oxidation reactions catalyzed by AuNPs have been reported. For instance, the oxidation of alcohols to aldehydes [22], carboxylic acids [5, 27, 28] or esters [29], the oxidation of aldehydes to esters [30] or acids [31], epoxidations of olefins [32], and the oxidation of amines to amides [33] have been investigated.

Recently, the catalytic application of AuNPs in selective hydrogenation has been widely reported as well [9, 12, 34-46]. In particular, it was shown that with the presence of a AuNP catalyst, substituted anilines and related derivatives can be produced efficiently at low temperature from their nitrogenated compounds, which are generally toxic organic by-products produced undesirably

during the industrial manufacturing process of chemicals, such as agrochemicals, dyes and pharmaceuticals [44, 48]. For example, 4-nitrophenol (4-NP), a toxic nitro acromatic chemical, has a delayed interaction with blood and then forms methaemoglobin inducing methemoglobinemia, potentially causing cyanosis, confusion, and unconsciousness to human body. When ingested, it causes abdominal pain and vomiting [49]. On the other hand, 4-aminophenol (4-AP), a hydrogenation product of 4-NP, is a very useful material which can be used as an important intermediate in pharmaceutical synthesis of analgesic and antipyretic drugs [39, 44], as antioxidant in plastics fabrication [44]. More importantly, this reaction is highly constructive for the transferring environmental pollutants into useful chemicals. With AuNPs, unsaturated chemicals can also be selectively hydrogenated. For instance, acetylene and 1, 3-butadiene can be partially hydrogenated into ethylene [48] and butenes [34, 35], respectively. The main advantage of AuNP catalysts is their ability to selectively catalyze the hydrogenation of the C=O group of α,β-unsaturated aldehydes producing allyl-type unsaturated alcohols [19, 48, 50-51].

The reduction of 4-NP to 4-AP on AuNPs with sodium borohydride (BH_4^-) in aqueous solution has also been rigorously used as a model reaction to examine the catalytic performance of noble metal NPs, especially AuNPs prepared from the reduction of auric acid by wet chemical approaches [20, 38-43, 52, 53]. For example, Pal and co-workers report that a decrease in AuNP size leads to the increase of reduction rate [42]. The modification of AuNP surfaces with different functional groups confirmed that the surface structure also largely influences the catalytic properties of AuNPs [38]. The mechanism of the reaction catalyzed by AuNPs has been proposed as follows [44]. Basically, the catalytic reduction can only proceed on the surface of the AuNPs, as illustrated in Figure 1.4. First, BH_4^- or hydrogen (H_2) from the borohydride ions adsorb on the active catalytic sites of a AuNP, and then is dissociated and activated by forming H-Au bonds. Concomitantly, 4-NP molecules adsorbs onto the AuNP surface. Then the hydrogenation reaction takes place between

adsorbed 4-NP molecules and surface-hydrogen to form 4-AP; Afterward, 4-AP desorbs from the AuNP surface.

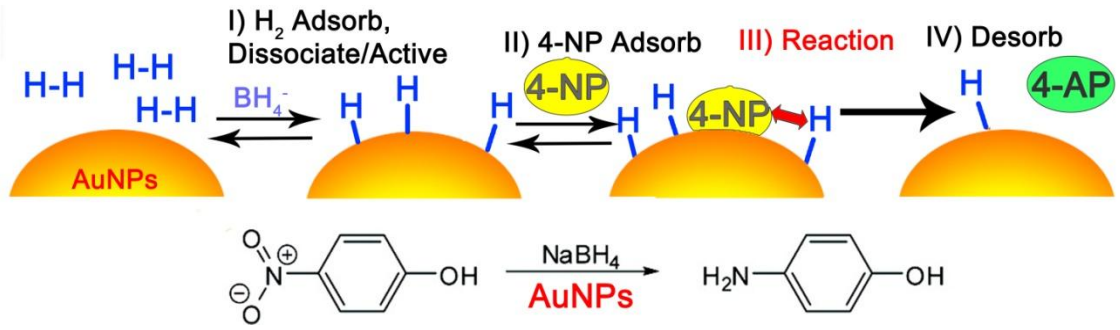

Figure 1.4 Mechanistic model of the reduction of 4-NP by borohydride in the presence of AuNP catalyst.

In the absence of the AuNP catalyst, the reaction does not proceed or only takes place under rigorous conditions. The outstanding catalytic property of AuNP catalysts in 4-NP reduction leads to promising prospects for employing them in industrial applications.

As introduced in 1.2.1, AuNP based nanostuctures has been successfully synthesized by various chemical methods and used as catalysts. Since AuNP catalyzed reactions basically proceed on the surface of the AuNPs, the surface properties of the as-synthesized AuNPs are deemed to influence the catalytic reaction significantly. During the chemical synthesis, using stabilizer or linker molecules leads to successful and reproducible experimental protocols and stable AuNPs in either synthesis or catalysis process; However, it is noted that the presence of these stabilizing molecules on the NP surface can obstruct the access of reactants to the active sites of NPs, namely the “barrier” effect in catalysis, and thus decrease their catalytic activity as illustrated in Figure 1.5-a [58]. The removal of these stabilizing molecules from the surface of AuNPs is still problematic. To date, it has mainly been achieved using thermal and oxidative approaches; however, such methods can lead to extensive changes in the size and shape of the NPs, and thus uncontrolled negative effects on catalytic properties [59, 61]. Also the thermal treatment may affect the support structure [58], so this method is not always highly reproducible.

Supported small AuNPs can be synthesized by the DP method without using stabilizing molecules, which avoids the "barrier" effect, however, impurities, such as chloride ions (Cl^-) from the $HAuCl_4$ precursor and excessive chemical precursors, remaining in the catalyst must be completely removed by an exhaustive washing treatment since these substances contaminate Au catalysts [7]. In particular, residual Cl^- strongly bond to the AuNP surface can poison the Au catalyst [15, 65]. Generally a thermal treatment below 600 ℃ is still not efficient enough to remove most Cl [7]. Thermal treatment at higher temperature will accelerate NP aggregation [64] and hence damage the structure of the nanocatalyst.

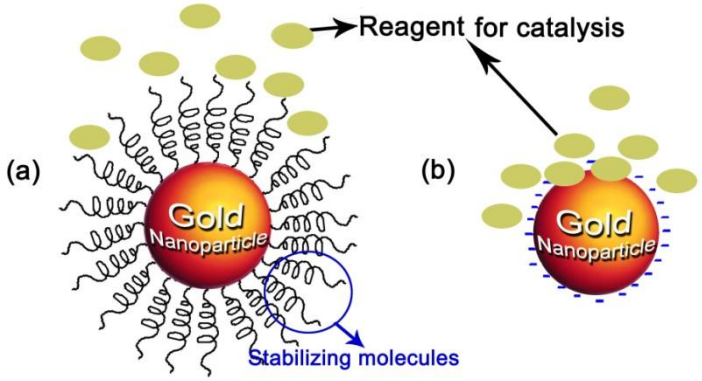

Figure 1.5 Schematic illustration of the access of reagent molecules to the surface of AuNPs prepared by chemical method (a) and physical method (b) during catalysis.

On the other hand, the purely physical approach of laser ablation offers a better way to produce AuNPs for catalysis, since chemical reagents or ions can be avoided in this approach. It is reported that PLD fabricated AuNPs-support structures exhibit high catalytic efficiency in various gas phase catalytic reactions, such as CO oxidation, and low volatility component (e.g., acetone, toluene) oxidation [74-76]. Although the use of stabilizing chemicals is avoided in the PLD approach, which prevents the contamination of metal NPs, the set-up and operation of the PLD system are rather complicated in practice as well as time-consuming. For example, a bigger chamber commonly needs a long time to reach an ideal vacuum, and after refilling with gas, a good

sealability has to been guaranteed. Unlike PLD, the PLAL setup can be an open system without the need for a vacuum or gas refilling. Hence, compared with the PLD technique, PLAL can provide significant improvements in convenience of experimental manipulation. As mentioned previously, the stabilizing molecules on AuNP catalysts prepared by chemical method exert intense "barrier" effects on catalysis, blocking the approach of reagents to AuNP surfaces, reducing the reaction efficiency (Figure 1.5-a). In contrast, as explained in 1.2.2, the surface of a AuNP prepared by PLAL in pure water is only covered by small OH^- groups, therefore this relatively "bare and clean" surface is expected to impose much smaller "barrier" effects on catalysis than most stabilizing molecules, leading to an enhanced reaction efficiency (Figure 1.5-b). Interestingly, the -OH capped surface of a PLAL-AuNP is supposed to easily interact with other materials, e.g., a metal oxide rich in hydroxylgroups in aqueous solution, to form NP/metal-oxide hybrid structures to stabilize the NPs during reactions, which are of high relevance to practical applications. Accordingly, it is highly interesting to apply these stable, colloidal PLAL-AuNPs fabricated in pure water with relatively "bare" surfaces in catalytic reactions in the aqueous phase.

Table 1.1 Comparison of two synthesis methods and surface features of AuNPs.

AuNPs production method	Chemical method	PLAL method
Chemical precursor	Necessary	No need
Additional Stabilizer	Necessary	No need
Purification treatment after synthesis	Necessary	No need
Surface of as-synthesized AuNPs	Stabilizing molecules and/or contaminants	"Bare" and Clean

According to the above discussion of AuNPs prepared by chemical and physical methods, the main differences between them have been summarized in Table 1.1. It is clear that the physical approach, i.e., the PLAL method, demonstrates more advantages for developing AuNPs for catalytic applications.

1.3.2 Stability and Molecule Adsorption for Potential Biological Applications

Au is well known to be a “safe” material, and due to its unique optical/electronic properties, high surface-area-tovolume ratios and diverse possibilities for the surface functionalization of AuNPs using sulfur or amine containing bio-molecules [3, 150-158] for the application in the field of biology, e.g., in drug delivery, cell targeting/imaging, DNA hybridization detection [6, 8, 10, 11, 14, 135, 143-145], etc. For example, biocompatible AuNP carriers have been developed for the application of drug delivery [143, 145]. The AuNPs carry hydrophobic pockets on their surface, which encapsulate drug molecules, and can deliver them into cancer cells [143]. The molecule on the surface is commonly composed of a hydrophobic interior, which can encapsulate drug molecules, and a hydrophilic shell, which has good biocompatibility and binding selectivity with surface functionalities of a targetted cell. After the NP binds with the targetted cell, the entrapped drug payloads can be released into cells by membrane-mediated diffusion to actualize drug delivery [143]. Basically, for certain biological applications, the size of the NP is required to be small enough (less than 10 nm) in order to enable their easy penetration of barriers (for instance, cell membranes), and to enhance their binding capacity with bio-species of interest [10, 11]. Most of these biological applications require the appropriate surface modification of AuNPs with diverse functional molecules in solution. To do so, generally AuNPs are introduced into a buffer solution with various biomolecules or polymers to effect surface functionalization. In this process, a good colloidal stability to avoid the irreversible aggregation of NPs is required, particularly when the salt concentration is high [57]. Therefore, the good colloidal stability of AuNPs is one of the most fundamental requirements [57, 135]. Moreover, the molecule-NP interface directly determines the surface coverage, binding strength and configuration of molecules on the NP surface, all of which could have high relevance to the functionality of these NPs [10, 11]. Au aqueous colloids have been observed to readily bind with amine, thiol and cyanide functional groups [55, 153-155]. Due to the abundance of amine groups in biological and environmental systems and the importance of the

AuNP-amine interaction that is the basis of many biomedical applications, various amine functionalities have been investigated, including amino acid and amine-bearing polymers [150, 156-158]. The study of amine-modified colloidal Au has identified two major bonding modes between amine groups and AuNP surfaces. One is the electrostatic interaction between protonated amine (-NH_3^+) and negatively charged surface ligands, while the other is the direct bonding of Au atoms to the -NH_2 group [150, 156-158]. It is evident that both modes of the AuNP-amine interaction are highly dependent on AuNP surface chemistry [3].

In order to synthesize suitable AuNPs (< 10 nm) for potential biological applications, as discussed in 1.2.1, generally the chemical reaction needs very strong surfactant molecules, e.g., mercaptoalky acid [34, 35, 57, 59], and/or a strong reducing agent [7], such as $NaBH_4$, and in some cases this reaction has to be conducted in organic solution [6]. However, such approaches cannot be considered as "green" because of the introduction of hazardous reducing agents, additives and solvents. Moreover, additional complicated surface modification is necessary for the transfer of AuNPs from an organic solution into aqueous media and for their stabilization in aqueous media with a view to biochemical and biomedical applications [55, 56]. Recently, a method of combining physical and chemical process has been developed to synthesize NPs [68, 82, 91, 146, 147]. In this approach, bigger "parent" AuNPs are first synthesized by a conventional chemical approach, and then they are irradiated by a laser beam. Laser irradiation can break these pre-formed, relatively large metal NPs into smaller ones in a hazardous-chemical-free aqueous medium at high concentration without introducing any additional chemicals [146, 147], which are particularly promising for biological research. Compared with a pure chemical approach, laser irradiation offers unique features when considering the biological application of AuNPs.

More importantly, as described in 2.2, lasers can introduce a unique surface chemistry variation to AuNPs, i.e., oxidized surface Au species, which is not easily achieved by conventional

chemical method due to the inert nature of Au. Considering that such a surface modification may have an interesting impact on the colloidal stability and molecular adsorption of AuNPs, the laser technique appears to be an excellent tool that offers unexplored possibilities for the investigation of the stability of AuNPs with oxidized surfaces and further their interactions with amine molecules.

1.4 Thesis Objectives and Organization

This thesis is divided into two sections with two corresponding objectives:

The first section is mainly devoted to the study of the synthesis and the development of catalytic applications of AuNPs using the PLAL technique.

To the best of our knowledge, although exhaustive research on the synthesis of AuNPs by the PLAL method has been well reported in literature, the study of their catalytic properties is still lacking. Based on the promising surface features of PLAL-AuNPs, I consider that it is of great interest to use this stable, colloidal nanomaterial prepared by PLAL with a relatively "bare" surface for applications in catalysis and compare its catalytic performance with that of NPs synthesized by chemical method. The comparison of the physical and chemical synthesis of AuNPs is also essential for a deep fundamental understanding of the influence of the surface chemistry of AuNPs on their properties.

Additionally, to improve and expand the application of PLAL-AuNPs in catalysis, another two key challenges also need to be considered. 1) the recovery and reuse of the NPs, especially those of very small sizes, i.e., less than 10 nm, are still challenging. The main difficulties consist in the efficient separation of tiny NPs from products without significant mass loss, their re-dispersion after centrifugation or filtration, and their colloidal stability in the new reaction solution. Currently, centrifugation is widely used for separating NPs and the products of reaction; however, it may lead to the irreversible aggregation of NPs, and thus a considerable reduction of their catalytic activity.

Therefore, to achieve optimal catalytic activity, long-term stability and reusability of PLAL-AuNPs, it is desirable to develop a novel, simple yet effective separation technique. 2) the second challenge concerns the increase of the catalytic activity of PLAL-AuNPs. Although it is possible to increase the catalytic activity of AuNPs by reducing the particle size, a meaningful reduction of particle size using the PLAL technique requires the use of strong surfactant additives or ligand molecules. Unfortunately, the use of such additives negates the advantages of surfactant-free synthesis by PLAL. A promising route is to alloy Au with other transition metals, such as platinum (Pt) to form Au based alloy nanostructures which can enhance the catalytic activity of AuNPs by means of synergistic effects. However, such a Au based alloy nanocatalyst has not been developed using PLAL technique.

Therefore, the objective for this section is:

Study the synthesis of the PLAL-AuNP based catalyst and assess its catalytic properties in 4-NP reduction, and understand the effect of surface chemistry on catalysis; Develop a novel, simple yet effective approach offering better recyclability and reuseability to PLAL-AuNPs in catalysis; Secure a new route of alloying Pt into AuNPs based on the PLAL technique to increase the catalytic activity of PLAL-AuNPs.

The second section is mainly focused on the investigatation of the surface modification of chemically synthsized AuNPs by laser irradiation and the study of how this modification influences NP properties. The existing research on the laser irradiation of AuNPs has demonstrated the mechanisms of NP fragmentation and the influence of laser parameters on particle shape and size modification [68, 69, 78, 79, 83, 91, 146]. However, the stability and the interaction with amine molecules of laser irradiated AuNPs have not been well investigated and evaluated. Catalytic properties are not studied in this section. Understanding the influence of surface chemistry on NP

properties not only is of great benefit to fundamental research, but also represents a significant contribution to the development of practical applications. Hence, the objective of this section is:

Investigate the influence of laser irradiation on the surface chemistry of chemically synthesized AuNPs, and explore the effect of surface oxidization on Au colloidal stability and amine molecule-AuNP interactions to gain a deeper fundamental understanding of the influence of the surface chemistry of AuNPs on their properties.

The structure of this thesis is therefore illustrated in Figure 1.6 and organized as follows:

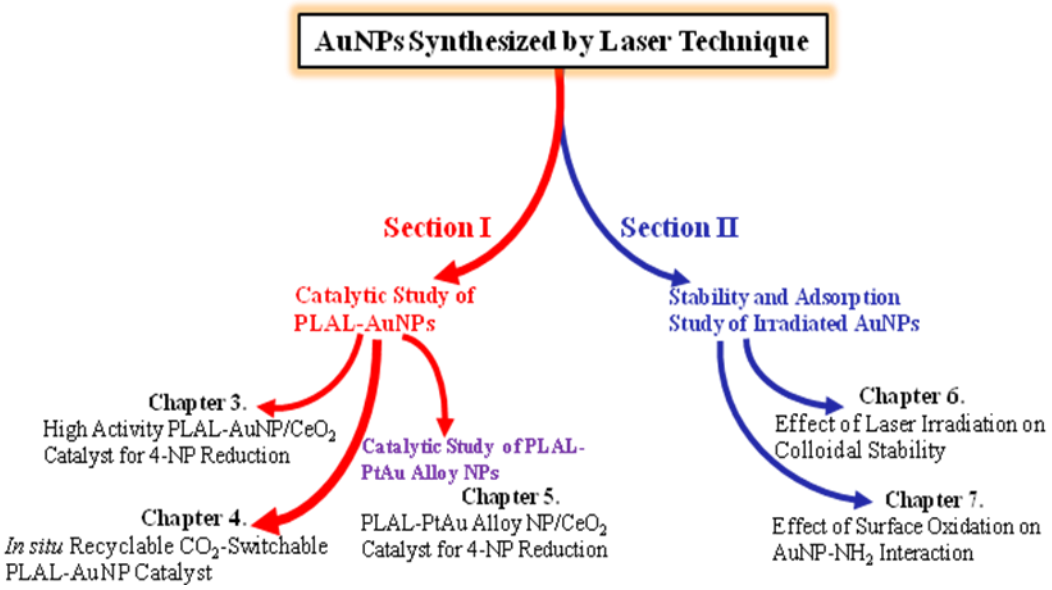

Figure 1.6 A guide illustrating the arrangement of chapters of this thesis.

Chapter 1 introduces the background, motivation and main goals of this thesis;

Chapter 2 describes experimental details of the synthesis process for PLAL-AuNPs, chemically synthesized AuNPs, polymer modified AuNPs, PLAL-PtAu alloy NPs, PLAL-NP hybrid catalysts and catalysis tests. The main characterization techniques of AuNPs and catalysts are also described in this chapter;

SECTION (I): PLAL Synthesized AuNPs and their Catalytic Activity

Chapter 3 details a novel yet simple method to fabricate a PLAL-AuNP/CeO_2 nanohybrid catalyst, which demonstrates higher activity in both 4-NP reduction and CO oxidation than Chem-AuNPs. In order to understand the increased activity of the PLAL-AuNP/CeO_2 catalyst, the effect of the surface chemistry on catalytic activity is studied by designing similar catalysts with different surface characteristics. For the first time, I reported the application of PLAL-AuNPs in catalysis, and the publication related to this chapter is:

[92] Zhang, J., Chen, G., Chaker, M., Rosei, F. and Ma, D. Gold Nanoparticle Decorated Ceria Nanotubes with Significantly High Catalytic Activity for the Reduction of Nitrophenol and Mechanism Study, *Applied Catalysis B: Environmental*, 132-133: 107-115, 2013.

Chapter 4 presents the new concept of combining CO_2-switchable polymers to PLAL-AuNPs to make a CO_2-switchable AuNP catalyst, which demonstrates unique CO_2-controllable, efficient *in situ* recycling behavior upon bubbling or removing CO_2 from a reaction solution. The CO_2-switchable AuNPs show good catalytic activity in 4-NP reduction. The publication related to this chapter is:

[93] J. Zhang, D. Han, H. Zhang, M. Chaker, Y. Zhao and D. Ma, *In situ* recyclable gold nanoparticles using CO_2-switchable polymers for catalytic reduction of 4-nitrophenol, *Chemical Communications*, 48: 11510-11512, 2012 (**Back Cover**).

Chapter 5 introduces the preparation of clean, stable Platinum-Gold (PtAu) alloy colloids with a wide range of compositions using the PLAL technique. The unique solid targets used for PLAL were made by compression moulding a mixture of Pt and Au powders at different ratios. Various characterization techniques confirm the formation of an alloy structure. Meanwhile, I studied the effect of pH and laser fluence in the preparation of PLAL-PtAu NPs. As prepared PLAL PtAu alloy NP catalyst show significantly increased activity in the 4-NP reduction reaction. Also the alloy-NPs

demonstrate good catalytic properties in fuel-cell applications. The publications related to this chapter are:

[71] Zhang, J., Oko, D., Garbarino, S., Imbeault, R., Chaker, M., Tavares, A. C., Guay, D. and Ma, D. Preparation of PtAu Alloy Colloids by Laser Ablation in Solution and their Characterization, *Journal of Physical Chemistry C*, 116: 13413-13420, 2012.

Zhang, J., Chen, G., Chaker, M. and D. Ma, Synergistic Catalysis of PtAu Alloy Nanoparticle in the Reduction of 4-Nitrophenol, *Journal of Physical Chemistry Letters*, to be submitted.

SECTION (II): Surface Modification of AuNPs by Laser Irradiation and its Influence on Colloidal Stability and Amine-AuNP Interactions.

Chapter 6 relates the effect of laser irradiation on preformed chemically synthesized AuNPs. The stability of the AuNPs with and without laser irradiation was investigated. The publication related to this chapter is:

[94] Zhang, J., Riabinina, D., Chaker, M. and Ma, D. Significant Stability Enhancement of Gold Colloids via Nanosecond Laser Irradiation, *Advanced Science Letters*, 4: 59-64, 2011.

Chapter 7 is devoted to the investigation of AuNP-amine molecule interactions of Chem-AuNPs with and without laser treatment. The surface chemistry of Chem-AuNPs before and after laser irradiation was thoroughly studied in this chapter. Amine probe molecules were introduced to the AuNP samples to verify the AuNP-amine molecule interaction. This study demonstrates the high dependences of the AuNP-amine interaction on the AuNP surface chemistry modified by laser irradiation. This chapter related publication is:

[72] Zhang, J., Riabinina, D., Chaker, M. and Ma, D. Effect of Surface Oxidation on the Interaction of 1-Methylaminopyrene with Gold Nanoparticles, *Langmuir* 28: 2858-2865, 2012.

Chapter 8 briefly summarizes most important contributions of this work and discusses the prospects of PLAL-NPs in the catalysis field.

Following the main body of this thesis is an appendix providing a summary of this thesis in French in compliance with INRS policy.

Chapter 2

Experimental

In this chapter, I introduce sample preparation and characterization details. It is divided into two sections. The first section mainly introduces PLAL-NP fabrication, catalyst preparation and catalytic activity measurements. Firstly, I fabricated AuNPs with a PLAL approach in pure water without using any stabilizing molecules, and developed their application as catalyst for 4-NP reduction by anchoring them onto CeO_2 NTs. In another case, I functionalized the PLAL-AuNPs with CO_2-switchable polymers (provided by our collaborators) as a stabilizer material and studied their CO_2-tunable catalytic activity and recyclability. Furthermore, I fabricated PtAu alloy NPs successfully using the PLAL technique, and studied their applications in catalysis.

The second section focuses on the treatment of chemically synthesized AuNPs by laser irradiation. To be more specific, AuNPs were synthesized through a chemical reduction approach, and then laser irradiation was performed on these AuNPs to reduce the particle size and modify the properties of those AuNPs.

In all the above studies, in order to understand the effect of laser-NP interactions on AuNP surface composition and surface-related properties, 5-nm AuNPs were synthesized by a purely chemical approach through the reduction of auric acid by $NaBH_4$ for comparison.

2.1 Materials

Gold (Au) plate target (99.99%), platinum (Pt) micro powder (≥99.9%, 0.5-1.2 μm), Au micro powder (≥99.9%, <10 μm), hydrogen tetrachloroaurate hydrate (auric acid, $HAuCl_4$ $3H_2O$), sodium citrate, $NaBH_4$, ethanol (denatured), 1, 3-acetonedicarboxylic acid, 1-methylaminopyrene (MAP), 4-nitrophenol (4-NP), cerium (III) nitrate hexahydrate ($Ce(NO_3)_3$ $6H_2O$), urea (NH_2CONH_2), deuterium oxide (D_2O) and cerium (IV) oxide powder (CeO_2 powder, mean size ~0.5 μm) were purchased from Sigma-Aldrich Inc. NaOH, hydrochloric acid (HCl, 37.1%), nitric acid (HNO_3, 68.0-70.0%), NaCl, tetrahydrofuran (THF), pressure syringe filter (Millipore Inc.) composed of celluloid membrane filters (0.2 μm) and pressure filter-holder celluloid filter, and Amicon Ultra-4 Ultracel-50K centrifuge filters (Millipore Inc.) for all the centrifugation/separation were obtained from Fisher Scientific Inc. Thiol terminated poly(N,N-diethylaminoethylmethacrylate) polymer (SH-PDEAEMA, Mn≈18,600 g/mol) was obtained from Prof. Zhao's lab at the Université de Sherbrooke. All the chemicals were used without further purification. Water was purified by a Millipore Ultrapure water system and has a resistivity of 18.2 MΩ·cm at 25 °C for aqueous solution preparation.

2.2 Experimental Details Relevant to PLAL Synthesized AuNPs and their Catalytic Study

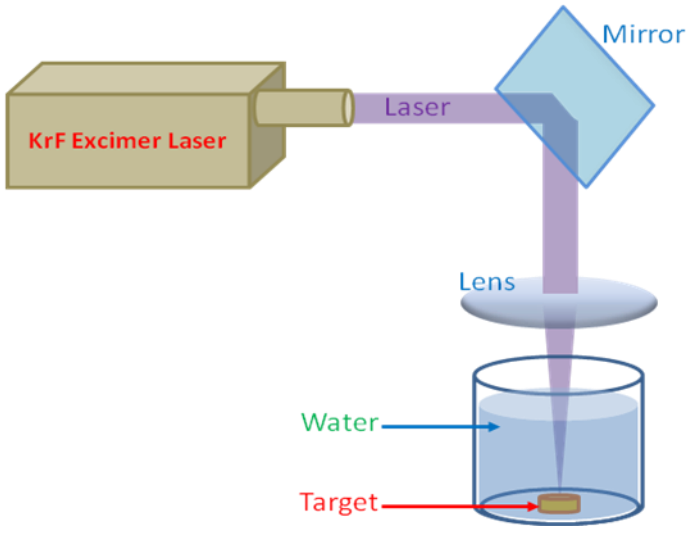

Figure 2.1 Schematic illustration of the PLAL setup for NP colloidal solution preparation.

2.2.1 Laser Ablation Setup

A KrF excimer nanosecond laser (GSI Lumonics PM-846, wavelength: 248 nm; pulse duration: 17 ns; repetition rate: 20Hz) was used for all the laser-related operations. The PLAL setup is simple as shown in Figure 2.1.

2.2.2 Preparation of PLAL-AuNPs

The laser beam was focused by an objective lens, with a focal length of 7.5 cm, onto a gold plate with a diameter of 8 mm and 1.5 mm in thickness. The gold target was placed at the bottom of a 6 mL glass vessel filled with pure water (pH≈6.5). The depth of the water layer above the target was ~10 mm. The lens-to-target distance was fixed to guarantee the consistency of the ablation spot size (~0.4 mm × 0.5 mm) on the target. The laser fluence on the target was set at ~40.0 J/cm^2 during all ablation processes.

2.2.3 Preparation of PLAL-PtAu Alloy NPs

Based on the technique of fabricating PLAL-AuNPs, I used a modified target to fabricate PtAu alloy NPs in solution using PLAL. The preparation process was as follows:

1) Preparation of Targets for Laser Ablation

Pt and Au powders at different ratios (Pt_xAu_{100-x}, x = 0, 30, 50, 70, 100 at.%) were mechanically mixed for 30 minutes for compression molding. Typically, 500 mg of the Pt-Au powder mixture was placed into a steel die with a diameter of 8 mm and pressed with a total pressure of 12 tons for 10 minutes to form a compact plate using a CARVER Press. All the operations were performed at room temperature. The compact plates with a thickness of 1.5 mm and a diameter of 8 mm, were used for laser ablation.

2) Preparation of PLAL-PtAu alloy NPs

The laser beam was focused by an objective lens, with a focal length of 7.5 cm, onto the plate target. The target was placed at the bottom of a 6 mL glass vessel filled with pure water or aqueous

solution at different pH values adjusted using HNO_3 or NaOH. The depth of the solution layer above the target was ~10 mm. The lens-to-target distance was fixed to guarantee the consistency of the ablation spot size (~0.4 mm × 0.5 mm) on the target.

2.2.4 Synthesis of 5-nm AuNPs by Chemical Reduction (Chem-AuNPs) [18]

To evaluate appropriately the properties of the PLAL-AuNPs with respect to that of AuNPs synthesized by a conventional chemical approach, it is necessary to exclude the effect of particle size on their properties and to compare particles of the same size. To do so, citrate capped AuNPs of 5 nm in diameter were synthesized by a solely chemical method by reducing auric acid with $NaBH_4$ as follows:

1) One milliliter (1 mL) of 1 wt % $HAuCl_4$ $3H_2O$ aqueous solution was added to 90 mL of deionized water and mixed well.

2) Two milliliter (2 mL) of 38.8 mM sodium citrate solution was injected into the above solution. The reaction mixture was then stirred for 1 minute.

3) One milliliter (1 mL) of 0.075 wt % freshly prepared $NaBH_4$ solution (in 38.8 mM sodium citrate solution) was added to the above reaction mixture and then the reaction mixture was stirred overnight at room temperature.

After that, the Au colloidal solution was purified to remove any un-attached or un-reacted chemical species, and then 93 mL of 1.25 mM sodium citrate solution was added and sonicated to have AuNPs well re-dispersed for the following operation.

A delicate purification process was performed on the as-prepared Chem-AuNP solution by using ultra-centrifuge filters. In a typical operation, 12 mL of as-prepared Au colloidal solution was centrifuged at ~4500 rpm with an ultra-centrifuge filter into ~4 mL concentrated solution (8 mL of filtrate was discarded). And then ~8 mL of pure water was introduced to re-disperse these highly concentrated AuNPs. After this pre-purification, the additional washing operation was repeated

gently twice in the same way. Finally the AuNPs were re-dispersed in pure water and used immediately for catalyst preparation.

2.2.5 Preparation of Au Based Nanocatalyst

In order to investigate the catalytic activity of the above prepared NPs in catalytic reactions, stabilizing materials, Ceria nanotube (CeO_2 NT) and SH-PDEAEMA were coupled with PLAL-NPs. SH-PDEAEMA was anticipated to endow the NPs with gas-tunable properties.

2.2.5.1 Preparation of NP/CeO_2-NT Catalyst

CeO_2 NTs were synthesized through a solid-liquid interface reaction between $Ce(OH)CO_3$ nanorods and NaOH solution, and mixed with as-prepared NPs. This two-step procedure was performed as follows:

1) Synthesis of CeO_2 NTs [95, 96].

In a typical experiment, 1.736 g of $Ce(NO_3)_3$ $6H_2O$ and 1.44 g of urea were added to 80 mL of water under vigorous magnetic stirring. The clear solution was charged into a 100 mL wide-mouthed jar which was closed and baked at 80 ℃ for 24 h. The solution was then air-cooled to room temperature. The white powder obtained was then centrifuged, washed with distilled water, and dried at 60 ℃. It (0.087 g) was subsequently re-dispersed into 20 mL of distilled water. Upon addition of 2.4 g of NaOH, the mixture was stirred for 30 min and then kept at room temperature. After 4 days of aging, the light yellow precipitate was washed with 1 M HNO_3 solution, distilled water, and absolute ethanol sequentially, and then it was dried in a vacuum at 60 ℃ for 24 h for the following catalyst preparation.

2) Fabrication of NP/CeO_2-NT catalysts.

Typically, for AuNPs, 2 mL of freshly prepared AuNP solution (or purified Chem-AuNPs) was added to 20 mg of CeO_2 NTs (or powder), and mixed by shaking. In the case of PtAu alloy NPs,

5 mL of alloy NP solution was mixed with 50 mg of CeO_2 NTs. The mixture in solution was incubated at room temperature for 30 min. After this, the precipitate was recovered by centrifugation, followed by washing with distilled water twice. Thus, the NP/CeO_2 catalyst was obtained.

2.2.5.2 Synthesis of PDEAEMA-AuNP Catalyst

A typical procedure to couple the SH-PDEAEMA polymer with PLAL-AuNPs is as follows:

1) 1 mL of Au colloidal solution ([Au]=40 ppm, measured by Neutron Activation Analysis) was added drop wise into 10 mL of ~0.625 mM SH-PDEAEMA THF solution under vigorous stirring. The solution was then continuously strongly stirred at room temperature for another ~72 h to complete the surface coupling process.

2) After that, the solution was centrifuged at 2,000 rpm for 15 min to separate and remove aggregates. The light orange supernatant was collected and centrifuged again at 12,000 rpm for 30 min to collect AuNPs and separate them from excess SH-PDEAEMA polymers. The collected AuNPs were washed with THF twice and re-dispersed in THF.

The above synthesized PDEAEMA-AuNP solution was concentrated by partially evaporating the THF solvent for catalysis evaluation.

2.2.6 Catalytic Activity Measurements

The catalytic activity of the Au based catalyst was evaluated in the reduction of 4-nitrophenol (4-NP) to 4-aminophenol (4-AP) in the liquid phase.

2.2.6.1 Catalysis over NP/CeO_2-NT Catalyst for 4-NP Reduction [39]

The aqueous solutions of 4-NP (0.12 mM) and $NaBH_4$ (5mM) were freshly prepared. Typically, 10 mg of AuNP/CeO_2 catalyst (or 50 mg of PtAu-NP/CeO_2 catalyst) was added to 15 mL of 4-NP aqueous solution. Subsequently, 15 mL of $NaBH_4$ solution was mixed with the 4-NP

solution containing the NP/CeO_2 nanocomposite under continuous stirring. All catalytic reactions were carried out at room temperature. In order to monitor the reaction, 1.5 mL of the reaction solution was taken out using a syringe every 60 s, and immediately injected into a quartz cuvette through a pressure syringe filter, which can separate catalyst from the reaction solution and terminate the reaction. The filtrate was then measured with a UV-Vis absorption spectrometer.

2.2.6.2 Catalysis over AuNP/CeO_2-NT Catalyst for CO Oxidation

Catalytic activity was measured using a continuous flow fixed-bed micro-reactor at atmospheric pressure. In a typical experiment, the system was first purged with high purity N_2 gas and then a gas mixture of $CO/O_2/N_2$ (1:10:89) was introduced into the reactor containing 50 mg of AuNPs/CeO_2-NTs (1 wt % Au loading) at a flow rate of 33.6 mL/min (corresponding to a space velocity of 40,000 $mL \cdot h^{-1} \cdot g^{-1}$ of catalyst), which were pre-annealed at 200 ^oC for 2 h. Gas samples were analyzed with an online infrared gas analyzer, which simultaneously detects CO and CO_2 with a resolution of 10 ppm. The results were further confirmed with a Gas Chromatograph.

2.2.6.3 Catalysis over PDEAEMA-AuNP Catalyst for 4-NP Reduction

Above synthesized PDEAEMA-AuNPs were transferred into water and bubbled with CO_2 (~60 mL/min) for ~ 3 hours to blow the THF away and disperse PDEAEMA-AuNPs well in water. Finally a light wine-color, clear solution was obtained. After that, 3 mL of the CO_2 purged PDEAEMA-AuNP clear aqueous solution ([Au]=19 ppm, confirmed by NAA) was mixed with 1 mL of 0.5 mM 4-NP solution. Immediately, 4 mL of 5 mM $NaBH_4$ solution was added and mixed. At certain time intervals, aliquots of the reaction mixture were taken out and injected into a quartz cuvette in order to monitor the reaction process with UV-Vis absorption spectroscopy. After the reaction finished, the solution was bubbled with N_2 to form an opaque suspension. This suspension was allowed to stand for a short time until the AuNPs floated to the solution surface, and then the clear solution containing reaction products was gently extracted to separate the products and the

floating layer containing the Au catalyst. The PDEAEMA-AuNPs were subsequently re-dispersed in water by CO_2 bubbling and re-used for the next round of catalytic reaction.

2.3 Experimental Details Relevant to Laser Irradiated AuNPs and Surface Chemistry Study

2. 3. 1 Preparation of Laser Irradiated AuNPs

2.3.1.1 Synthesis of "Parent" AuNPs [56]

Citrate-capped "parent" AuNPs with average diameter of about 20 nm for laser irradiation were synthesized by the classic "Frens" method. The typical procedure is as follows:

1) Two hundred fifty milliliter (250 mL) of 0.88 mM $HAuCl_4 \cdot 3H_2O$ aqueous solution was brought to a boil under vigorous stirring.

2) Eighteen point thirty five milliliter (18.35 mL) of 1% (w/v) sodium citrate solution was rapidly added. The solution was kept boiling for 15 minutes and then more citrate solution (2~4 mL) was added. The solution was allowed to boil for another 15 minutes.

3) Fifteen milliliter (15 mL) of the as-synthesized Au colloidal solution was filtered, centrifuged and washed to remove any large aggregates and remnant precursors. The clear colorless supernatant was discarded.

4) Fifteen milliliters (15 mL) of sodium citrate solution was added and sonicated to have AuNPs well re-dispersed for the laser irradiation treatment.

2.3.1.2 Laser Irradiation of "Parent" AuNPs

Above purified 20-nm AuNPs were irradiated for 55 minutes (66,000 pulses) by a KrF nanosecond excimer laser (laser fluence: 0.25 J/cm^2) under vigorous magnetic stirring, as illustrated schematically in Figure 2.2. Part of the irradiated AuNP solution was centrifuged and re-dispersed in water. In order to achieve a good size distribution of laser irradiated AuNPs, this laser irradiation process was also carried out while varying citrate concentration in the purified "parent" AuNP solution. This sample is denoted as "**as-irradiated sample**".

Some of the above as-irradiated AuNP solution was repeatedly centrifuged and re-dispersed in pure water several times to remove "free" ligand molecules (i.e., those not attached to the surface of AuNPs). Finally the separated AuNPs were re-dispersed and sonicated in sodium citrate solution for about 2 hours before any further chemical manipulation or characterization. This sample is named as "Ligand-exchanged-irradiated sample".

2. 3. 2 Chemically Synthesized 5-nm AuNPs ($NaBH_4$ reduced sample) [18]

To correctly evaluate the variation in properties of the AuNPs after laser irradiation, it is necessary to exclude the effect of particle size on their properties and to compare the particles of the same size. To do so, citrate capped AuNPs of 5 nm in diameter were synthesized again by a solely chemical method by reducing auric acid with $NaBH_4$. The synthesis procedure is the same as that described in section **2.2.4**. After that, 15 mL of the AuNP solution was centrifuged and purified to remove any un-reacted chemical species, and then sodium citrate solution was loaded and sonicated to have AuNPs well re-dispersed.

2. 3. 3 Stability of Laser Irradiated Au Colloidal Solution

The colloidal stability of the laser irradiated AuNPs was evaluated using the following methods:

2.3.3.1 Ethanol Induced Aggregation

One milliliter (1 mL) of ethanol was introduced into 2 mL of (*i*) as prepared citrate ligand-exchanged irradiated and *(ii)* $NaBH_4$ reduced AuNP solutions. Both solution mixtures were incubated for ~30 min at room temperature for further characterization.

2.3.3.2 Salt Induced Aggregation

As-prepared citrate ligand-exchanged irradiated and $NaBH_4$ reduced AuNPs solutions were mixed with 0.1 M NaCl solution. In a typical process, 2 ml of as-prepared Au colloid solution was added in a 10-mm quartz cuvette; then different volumes (100, 200, 400, 600, and 800 µl) of 0.1 M

NaCl solution were added and incubated for ~10min for characterization. The salt induced aggregation was evaluated by the damping of the SPR peak of the Au colloid.

2.3.4 Adsorption Ability of Amine Molecules on AuNPs

The adsorption ability of amine molecules on AuNPs with and without laser irradiation treatments was measured using 1-methylaminopyrene (MAP), as an amine probe. The experimental details are as follows:

To three kinds of Au colloidal solutions (as-irradiated, ligand-exchanged-irradiated and $NaBH_4$-reduced samples), MAP solution was added for the adsorption testing on AuNPs. In a typical process, 0.75 mL of MAP solution with different concentrations (1000, 1600 and 2000 nM, respectively) was added into 0.75 mL of freshly prepared Au colloidal solution with a particle concentration of ~1.223×10^{-7} M. The conjugation solution was then gently stired at room temperature for 6 hours to complete the surface adsorption process. The pH values of the conjugation solution were set to be 5.5 or 7.0. After that, the conjugation solution was centrifuged with the centrifuge filter at 5600 rpm for 15 minutes to separate AuNPs and aqueous solution. The clear filtrate was collected for the following photoluminescence measurements.

2.4 Characterization

Various characterization techniques were used in order to characterize the material structure, chemical composition and for the measurement of other properties. The technique used are listed and introduced briefly below:

i). Transmission Electron Microscopy (TEM), Selected Area Electron Diffraction (SAED) and Energy Dispersive X-ray Spectroscopy (EDS). TEM is used to directly observe the morphology and size of the nanostructures. The crystal structure and chemical composition of the NPs can be easily identified using SAED and EDS, inside a TEM apparatus. In order to perform these measurement, a small drop of solution containing nanomaterials was deposited onto a Cu grid

coated with a thin (5-50 nm in thickness) carbon film, and excess solution was wicked away by a filter paper. The grid was subsequently dried in air and observed with a JEOL-2100F TEM (École Polytechnique de Montréal, Montréal, Canada). Meanwhile, the SAED pattern and EDS spectra were measured at different locations on the sample. Particle size was determined by measuring more than 100 individually dispersed particles identified in TEM images.

ii). X-ray Photoelectron Spectroscopy (XPS). XPS is a quantitative spectroscopic technique that measures the elemental composition, empirical formula, chemical state and electronic state of the elements that exist within a material. To prepare the samples for this measurement, drops of highly concentrated nanomaterial solution were placed on freshly cleaved non-doped, double-side polished single crystalline (111) silicon substrates, and dried in a vacuum desiccator. All samples were transferred into XPS chamber immediately and were pumped to high vacuum conditions within 1 hour for the XPS measurements. XPS spectra were taken using a VG Escalab 220i XL with a monochromated Al Kα X-ray source (1486.6 eV). XPS acquisition time for Au was ~10 minutes. High-resolution spectra for Au4f and N1s were obtained using a scan step of 0.1 eV and 0.01 eV, respectively, with pass energy of 20 eV. Curve fitting of the XPS data was carried out with Gaussian functions using CasaXPS version 2.2.107 after either Linear or Shirley background substraction. The binding energies were calibrated by referencing them to the designated hydrocarbon C1s binding energy of 284.6 eV.

iii). X-ray diffraction (**XRD).** XRD is a method used for determining the atomic and molecular structure of a crystal, in which the crystalline atoms cause a beam of X-rays to diffract into many specific directions. In order to perform XRD measurements, drops of highly concentrated nanomaterial sample solution were placed on freshly cleaved non-doped, double-side polished single crystalline silicon substrates, and dried in a vacuum desiccator to form a film. The measurements were performed on the film samples using a Panalytical XRD X-pert Pro

diffractometer at a grazing incidence angle of 5^{o} with step size of 0.1^{o} and counting time of 15 seconds per step.

iv). Fourier Transform Infrared Spectroscopy (FTIR). FTIR is a valuable analytical technique to identify materials as it can reveal their molecular structure and chemical bonds. FTIR spectra, in the region of 2200-800 cm^{-1}, were recorded on a Thermo Nicolet 6700 infrared spectrometer with resolution of 0.5 cm^{-1}. Measurements were performed under the protection of N_2 atmosphere on solid samples prepared in the same way as for XPS measurements.

v). Zeta-potential Analysis. The value of the zeta potential can be related to the surface charge of colloidal NPs. The zeta potential indicates the degree of repulsion between adjacent, similarly charged particles in dispersion. Zeta-potential measurements were performed with a Brookhaven ZETAPALS Analyzer for colloidal samples (1.5 mL) at different pH values in standard all-side transparent PMMA cuvettes (length: 10 mm; width: 10 mm).

vi). Nuclear Magnetic Resonance Spectroscopy (NMR). NMR determines the physical and chemical properties of atoms or the molecules where they are contained. It relies on the phenomenon of nuclear magnetic resonance and can provide detailed information about the structure, dynamics, reaction state, and chemical environment of molecules. In my study, Au colloidal samples were centrifuged, and supernatants were discarded to remove most "free" ligands and regular water. The AuNPs were re-dispersed in D_2O. Proton NMR (^{1}H-NMR) spectra were taken at room temperature on the highly concentrated D_2O solutions of AuNPs and recorded by a Varian VNMRS 500 MHz instrument with a pulse sequence of wet1D, a pulse width of 6.9 μs and a pulse power of 61 dB.

vii). Thermogravimetric Analysis (TGA). TGA is a method of thermal analysis in which changes in physical and chemical properties of materials are measured as a function of increasing temperature (with constant heating rate), or as a function of time (with constant temperature and/or

constant mass loss). In my study, TGA was performed on carefully weighted quantities of purified AuNPs (4–8 mg) in air with a TA Instrument TGA Q500 thermogravimetric analyzer. AuNP samples placed in Pt pans were preheated to 50 ℃ and thermally equilibrated for 10 min, followed by a 5 ℃/min temperature increase to 600 ℃.

viii). UV-Visible (UV-Vis) Spectroscopy. A UV-Vis spectrophotometer (Varian 5000) was used to measure the absorption spectra of Au colloids to identify their SPR peak features and monitor the process of catalytic reduction of 4-NP at room temperature in 10 mm PMMA semi-micro cuvettes. The scan speed was set to 600nm/min. For the measurement of Au colloidal samples, all spectra were collected over the range of 350-800 nm. For recording the 4-NP reduction process, the spectra were collected over the range of 250-500 nm. All experimental data were corrected for background absorption by water.

ix). Photoluminescence (PL) Spectroscopy. PL spectroscopy is used to measure the fluorescence properties of dye molecules. PL spectra were taken with a Fluorolog-3 system (Horiba Jobin Yvon) using an excitation wavelength of 278 nm for MAP. All spectra were collected over the range of 350-500 nm from liquid samples (1 mL of solution in quartz micro cuvettes).

x). Elemental Analysis. Neutron Activation Analysis has been used for determining the concentrations of elements numerous materials. In this study, NAA analysis was performed on 1 mL of sample solution using a SLOWPOKE nuclear reactor (École Polytechnique de Montréal, Montréal, Canada) to quantify the Au concentration.

xi). pH Measurement. The pH values of the solutions were measured with an Orion 230A pH meter and adjusted by using NaOH solution (pH=10) or HCl solution (pH=1).

xii). Electrochemical Measurement. Electrochemical characterization was performed on PLAL-PtAu alloy NPs with the assistance of Prof. Daniel Guay and Prof. Ana C. Tavares. Typically, an adequate volume of the PtAu colloidal suspension, corresponding to metal loading of

45 ±3 μg/cm^2, was deposited on glassy carbon (GC) disks (5 mm in diameter, PineChem Inc). After solvent evaporation, 3 μl of 5 wt% Nafion solution was pipetted onto the electrode and allowed to dry overnight. Preceding every electrode preparation, the GC disk was systematically polished with alumina slurries (1.0 μm and 0.05 μm in diameter), and then ultrasonically cleaned in pure water for 5 min.

Prior to each electrode characterization, the glassware and the electrochemical cell were cleaned according to a well-established method. Auxiliary and reference electrodes were a platinum gauze and a Reversible Hydrogen Electrode (RHE), respectively. All electrochemical studies were carried out at room temperature in 0.5 M H_2SO_4 solution. The electrolyte was initially purged with high purity Argon (N5.0, Praxair) for at least 30 min, followed by a continuous light flow of Argon over the solution throughout electrochemical testing. Cyclic voltammograms (CVs) were recorded at 50 mV s^{-1} using a VSP potentiostat (Biologic Science Instruments).

xiii) Surface Area. A Brunauer, Emmett and Teller (BET) device from Quantachrome Autosorb System was used in surface area measurements of CeO_2 nanostructures using nitrogen. The device determines gas quantity needed to cover the sample surface with a molecular layer and calculates surface area using BET theory.

xiv) CO Oxidation. In order to assess the catalytic activity of AuNP based catalysts for CO oxidation, the product gas mixture was analyzed using Gas analyzer (Gasboard-3121, China Wuhan Cubic Co.) and Gas Chromatograph (Shimadzu, GC-14C) to identify and quantify gas composition.

SECTION (I): PLAL Synthesized AuNPs and their Catalytic Activity Study

Chapter 3

High Activity PLAL-AuNP/CeO_2-NT Hybrid Nanocatalyst

In this chapter, I introduce the catalytic application of PLAL-AuNPs. To do so, I synthesized a new nanostructured catalyst composed of PLAL-AuNPs and CeO_2 NTs, and studied its catalytic application in two important reactions (4-NP reduction in the liquid phase and CO oxidation in the gas phase), and further investigated the mechanisms for its high catalytic activity by comparing it with three different yet similar types of catalysts (fabricated from wet-chemically synthesized AuNPs (Chem-AuNPs) and/or commercially available CeO_2 powder as support). This work represents the first demonstration of the application of PLAL-AuNPs in catalysis and a very simple approach for the preparation of the nanostructured catalysts.

3.1 Catalytic Application of AuNPs

As introduced in Chapter 1, due to the relatively "bare and clean" surfaces of NPs prepared by the laser technique, PLAL-AuNPs are expected to serve as a highly promising catalyst in many reactions. However, in most circumstances, during catalytic reactions in liquids, the high ionic strength of the reaction solution causes aggregation of AuNPs [7, 57, 58], which severely reduces their catalytic activity. To avoid this problem, I used CeO_2 to couple with AuNPs to form a composite nanostructure. Among various support materials, CeO_2 is of particular interest due to the wide applications of noble-metal NP/CeO_2 nanocomposites in catalysis including CO oxidation [22, 31] and selective hydrogenation [52]. Moreover, considering the charged surface of some metal

oxide materials in liquids, e.g., CeO_2 [97], immobilizing oppositely charged NPs onto them may be feasible. Additionally, in some catalytic reactions, for example, 4-NP reduction, it has been reported that the catalytic performance of AuNPs is affected by supports [38], but only a few papers have reported the influence of Au─support interactions on metal NP catalytic activity in hydrogenation reactions [34, 98]. On this basis, it is also of great interest to further investigate the influence of support and Au-support interactions on 4-NP reduction in the aqueous phase.

In order to study the catalytic application of the PLAL-AuNPs, I developed a novel strategy for the synthesis of a nanostructured catalyst composed of PLAL-AuNPs and CeO_2 NT supports and studied its application as a highly active catalyst in the model catalytic reaction of 4-NP reduction. The catalyst preparation method developed herein involves the use of PLAL-AuNPs and their uniform immobilization onto the CeO_2 NTs by simply mixing them in solution, as illustrated in Scheme 3.1. I further investigated the mechanisms for its high catalytic activity by comparing it with three different yet similar types of catalysts (fabricated from wet-chemically synthesized AuNPs (Chem-AuNPs) and/or commercially available CeO_2 powder as support). In the following, I present in detail the nanocatalyst preparation using PLAL-AuNPs and the study of their catalytic properties.

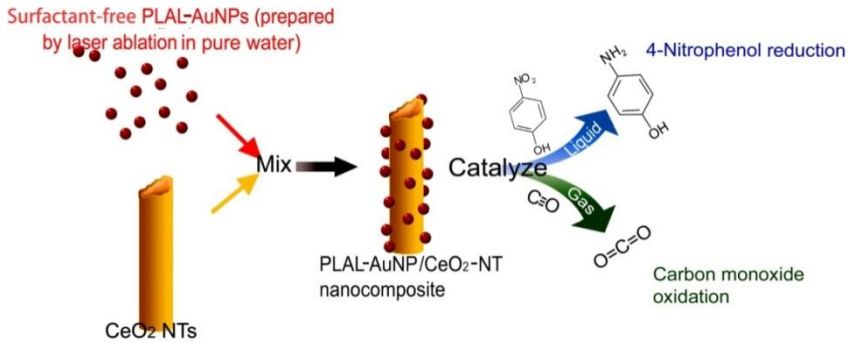

Scheme 3.1 Schematic diagram of the simple route for the preparation of PLAL-AuNP/CeO_2-NT catalyst and its application in 4-NP reduction and CO oxidation.

3.2 Preparation and Structural Characterization of PLAL-AuNP/CeO_2-NT Catalyst

As introduced in Section 2.2.5.1 of Chaper 2, a simple, functionalization-step-free solution process has been established to fabricate the AuNP/CeO_2 nanocatalyst. First, PLAL-AuNPs with a diameter of ~5 nm were fabricated by laser ablation on a bulk Au target in pure water without any additional chemicals, and CeO_2 NTs were synthesized through a solid-liquid interface reaction between $Ce(OH)CO_3$ nanorods, which serve as template, and NaOH solution to first form a CeO_2 shell, followed by acid dissolution of residual $Ce(OH)CO_3$ precursor in the core, as reported in literature [95, 96]. Second, the as-prepared PLAL-AuNP solution was simply mixed with the CeO_2 NTs and incubated for 30 min to assemble AuNPs onto the tube surfaces. Figure 3.1-a shows the UV-Vis absorption spectra of freshly prepared PLAL-AuNP solution before (solid line) and 30 min after the introduction of the CeO_2 NTs (dashed line).. Before the addition of CeO_2 NTs, the UV-Vis spectrum of PLAL-AuNP solution presents a strong SPR peak at ~513 nm. After mixing with the CeO_2-NTs, the PLAL-AuNPs demonstrate a strong affinity for the CeO_2 NTs, reflected in the dramatic decrease of the SPR peak at 513 nm. Nearly all the PLAL-AuNPs are adsorbed onto the NT surface and together they precipitate from the solution. Correspondingly, this considerable difference in the optical absorption of the PLAL-AuNPs in the presence of the CeO_2-NTs is visible in the photographs shown in the insets of Figure 3.1-a. The percentage of "free" (i.e., un-attached) AuNPs in the supernatant (deduced from the absorbance of the SPR peak at 513 nm) as a function of incubation time is summarized and illustrated in Figure 3.1-c (circles). It is found that most (~90%) of the AuNPs are adsorbed onto the surface of the NTs within 10 min. Lengthening the incubation time to 30 min leads to complete attachment. Consistently, it was found that the amount of Au element in the colloidal solution before mixing with CeO_2 NTs is in good agreement with that of the fabricated nanocomposite (confirmed by Neutron Activation Analysis (NAA)), which indicates that with this technique AuNPs entirely attach onto the support without any loss and thus

the Au/CeO_2 ratio can be accurately controlled by simply varying the amount of feeding Au colloidal solution.

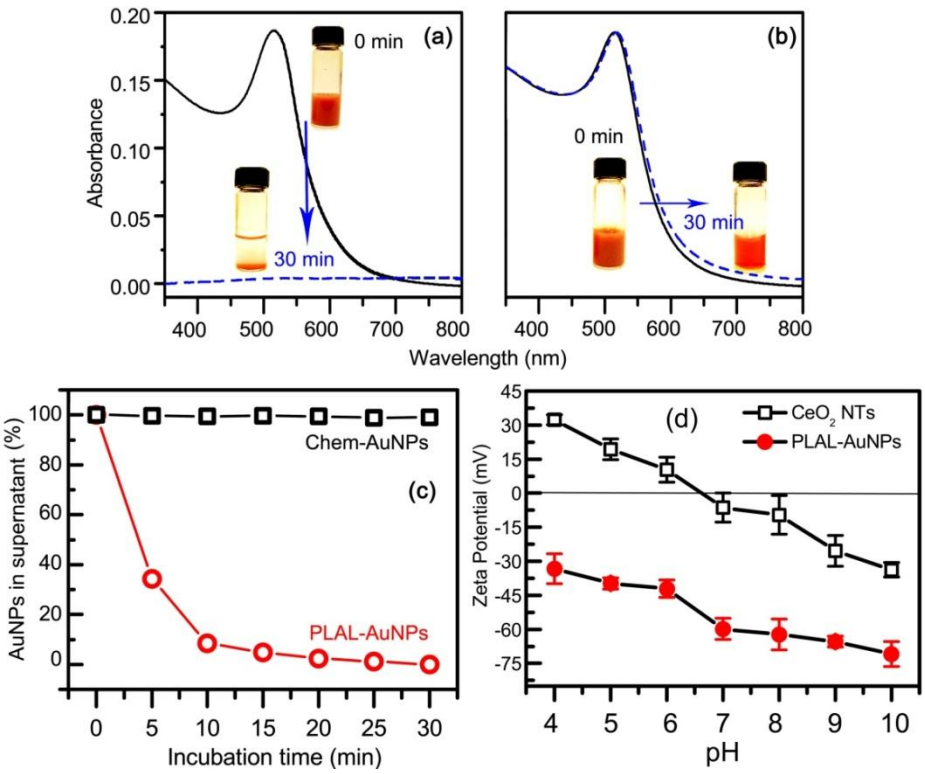

Figure 3.1 UV-Vis spectra of PLAL-AuNPs (a) and Chem-AuNPs (b) solution at 0 min (solid line) and 30 min (dash line) after the addition of CeO_2 NTs. (c) "Free" AuNPs remaining in the solution as a function of incubation time. Insets are corresponding photo-images. (d) Zeta potential of CeO_2 NTs and PLAL-AuNPs.

Of technical importance is that this preparative method for the AuNP/CeO_2 nanocomposite does not require any additional functionalization pre-treatments to either AuNPs or CeO_2 NTs to promote their coupling. The effective immobilization process is associated with the surface chemistry of the PLAL-AuNPs and CeO_2 NTs. Figure 3.1-d shows the Zeta-potential of as-prepared PLAL-AuNPs and CeO_2 NT solution as a function of their pH value. The zeta-potential of the PLAL-AuNP solutions varies between -30 and -75 mV in all pH ranges, indicating negatively charged surface of NPs. For CeO_2 NTs, positive Zeta potential values can be achieved at a pH lower than ~6.5. The pH value of the incubation solution is ~6.0-6.5 which is lower than the Isoelectric

Point (IEP) of CeO_2 (~7.0), therefore the surface of CeO_2 is partially positively charged [97]. The surface features reveal that a static-electric adsorption and hydrogen bonding is dominating the coupling between AuNPs and CeO_2 NTs, leading to the formation of the AuNP/CeO_2 hybrid structure [60]. In terms of nanocomposite fabrication, the unique surface chemistry of PLAL-AuNP does exhibit an attractive specificity.

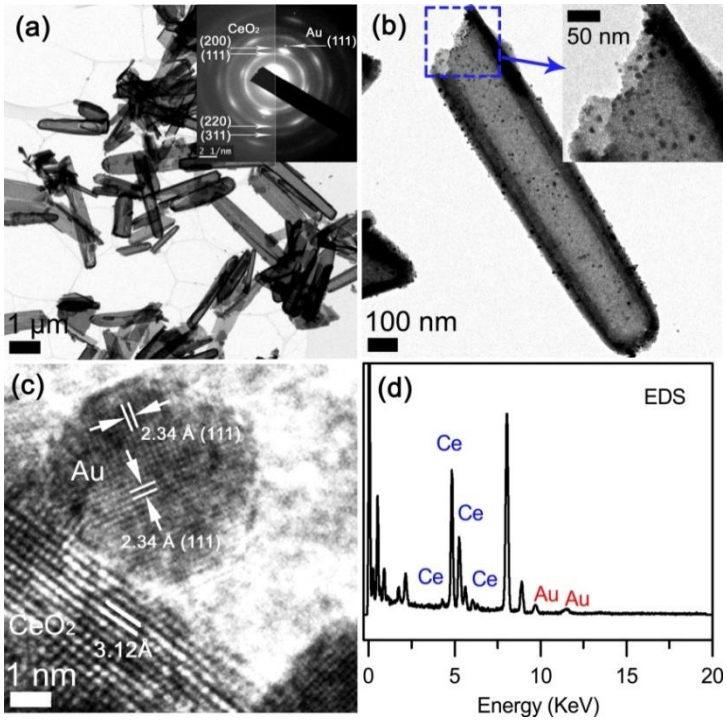

Figure 3.2 TEM (HR-TEM) images (a-c) and EDS spectrum (d) of PLAL-AuNPs/CeO_2-NTs. Insets are the SAED pattern and the magnified TEM image.

Figure 3.2 (a-c) shows TEM images of the PLAL-AuNPs/CeO_2-NTs. The CeO_2 NT structures are quite clear (Figure 3.2-a and b) and at a higher magnification (Figure 3.2-b), the attachment of the PLAL-AuNPs on the tube surface is presented distinctly. The NPs are well distributed on the surface, and no unattached AuNPs are observed, indicating that the PLAL-AuNPs have good affinity with the CeO_2 NTs. The AuNP/CeO_2-NT nanostructures were further characterized by high-resolution TEM (HR-TEM), as shown in Figure 3.2-c. The lattice fringes of an attached AuNP with a diameter of ~5 nm and a CeO_2 NT surface are visible, with the spacing of 2.34 Å corresponding to

that of the {111} planes of face-centered cubic Au [99], and the larger lattice spacing of 3.12 Å matching that of the {111} crystal planes of cubic fluorite-structured CeO_2 [99]. These results regarding crystalline structures are consistent with those obtained from the SAED pattern shown in the inset of Figure 3.2-a. The PLAL-AuNPs/CeO_2-NTs were also characterized by EDS spectroscopy, which reveals the coexistence of both Au and Ce in the nanostructure as presented in Figure 3.2-d.

3.3 Catalytic Activity of PLAL-AuNP/CeO_2-NT Catalyst for 4-NP Reduction

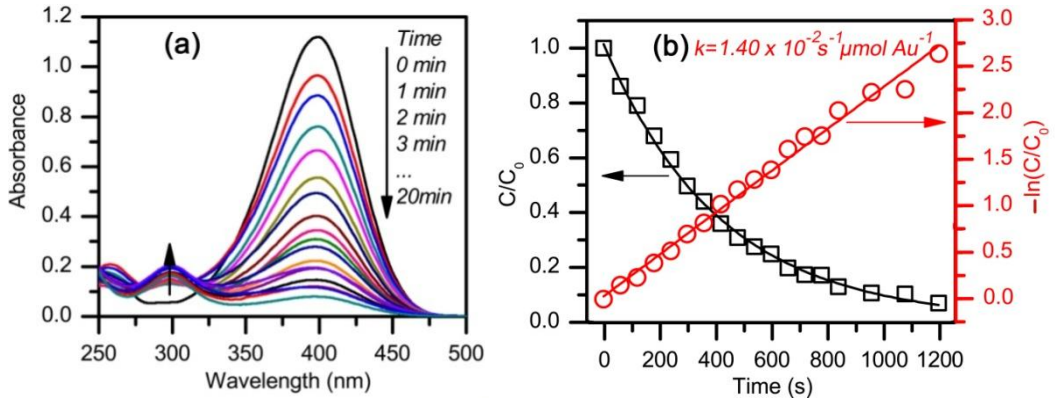

Figure 3.3 (a) UV-Vis absorption spectra during the catalytic reduction of 4-NP over PLAL-AuNPs/CeO_2-NTs; (b) C/C_0 and $-\ln(C/C_0)$ as a function of reaction time for the reduction of 4-NP over PLAL-AuNPs/CeO_2-NTs. Solid lines in (b) are the best-fit polynomials.

The catalytic property of the PLAL-AuNPs/CeO_2-NTs was then evaluated by employing the reduction of 4-NP to 4-AP as a model reaction, in which $NaBH_4$ was used as a reducing agent. In this study, since $NaBH_4$ was added to the reaction in large excess as compared to 4-NP, the reaction kinetics basically follows a first-order rate law [20, 39-41, 43, 92]. The kinetic process of the reaction was monitored by measuring the absorbance of a peak at 400 nm (Abs_{400nm}), directly associated with the concentration of 4-nitrophenolate ions, as a function of reaction time.

Figure 3.3-a shows that after the addition of the catalyst, the Abs_{400nm} value drops gradually as the reaction proceeds, reflecting the steady decrease of the concentration of the 4-nitrophenolate ions in solution. Based on the absorbance data, Figure 3.3-b plots C/C_0 (black square) and $-\ln(C/C_0)$

(red circle) *versus* reaction time, where C_0 and C are the initial concentration of the 4-nitrophenolate ions and the concentration at time t, respectively. The reaction is almost complete within 1200 s in the presence of the PLAL-AuNP/CeO_2-NT catalyst. The linear correlation between $-\ln(C/C_0)$ and reaction time demonstrates that the reaction is of the first-order in 4-NP reduction. Thus, the kinetic equation of this catalytic reaction could be shown as follows

$$dC/dt = -k_{app} C$$

where k_{app} is the apparent reaction rate constant, which can be obtained from the slope of the linear correlation [20, 39-41, 43, 92]. Accordingly, the k_{app} for the PLAL-AuNPs/CeO_2-NTs catalyzed reaction was calculated to be 2.25×10^{-3} s^{-1}. To exclude the effect of Au loading on reaction efficiency, and also for fair comparison with the results reported by other groups on AuNP based catalysts, an intrinsic reaction rate constant, *k*, was introduced by further normalizing k_{app} with Au content [42, 52]:

$$k=k_{app}/M$$

where *M* is the dosage of Au (μmol) in the catalyst. It was found that *k* (1.40×10^{-2} s^{-1} μmol Au^{-1}) of the PLAL-AuNPs/CeO_2-NTs is impressively higher than those reported recently by others on Au-containing nanocatalysts (See Table 3.1 for summary) [37, 39-43].

Table 3.1 Summary of the reaction rate constant *k* according to recent studies on the reduction of 4-NP over AuNP based catalyst.

Entry	Catalyst structure	k_{app} (s^{-1})	*k* (s^{-1} μmol Au^{-1})	Ref. No.
1	AuNPs/Polymer	3.2×10^{-3}	0.225×10^{-2}	37
2	AuNPs/SiO_2-NTs	10.64×10^{-3}	1.064×10^{-2}	39
3	AuNPs/Polymer	6.2×10^{-4}	0.0022×10^{-2}	40
4	AuNPs/Fe_3O_4-NPs	1.7×10^{-4}	0.593×10^{-2}	41
5	AuNPs/Polymer	2.75×10^{-4}	0.01×10^{-2}	42
6	Polygonal AuNPs	11.0×10^{-3}	0.095×10^{-2}	43
7	PLAL-AuNPs/CeO_2-NTs	2.25×10^{-3}	1.40×10^{-2}	This work

3.4 Mechanism for Enhanced Catalytic Activity

In order to understand why the PLAL-AuNPs/CeO_2-NTs show superior catalytic activty, we prepared similar catalysts containing citrate ligand-capped AuNPs synthesized via a common chemical reduction method (Chem-AuNPs) and/or commercial CeO_2 nanopowder support, and then compared their catalytic activity with that of the PLAL-AuNPs/CeO_2-NTs.

3.4.1 Surface Chemistry of NPs: PLAL vs. Chem-AuNPs

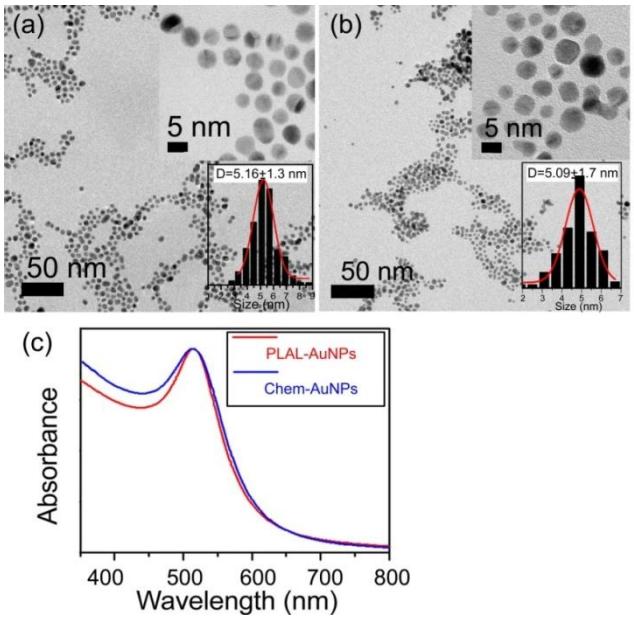

Figure 3.4 TEM images of PLAL-AuNPs (a) and Chem-AuNPs (b). Insets show the high magnification TEM images and histograms of size distribution for each sample; (c) UV-Vis absorption spectra of PLAL- and Chem-AuNPs.

To guarantee a fair comparison, it is necessary to exclude any particle size effect. Therefore, citrate ligand-capped Chem-AuNPs with the same particle size were prepared by reducing $HAuCl_4$ with $NaBH_4$ in citrate solution (see Chapter 2) [18]. TEM observation (Figure 3.4-a and b) shows that as-prepared PLAL-AuNPs and purified Chem-AuNPs have a very similar size (~5 nm in diameter) and size distribution. This was further confirmed by their identical SPR peak position and similar full width at half-maximum (FWHM) (Figure 3.4-c). The Chem-AuNPs and the CeO_2 NTs were then mixed under the same experimental conditions as those used in the preparation of the

PLAL-AuNPs/CeO_2-NTs. Figure 3.1-b shows the UV-Vis spectra and photographs of the as-prepared Chem-AuNP solution before (solid line) and 30 min after (dashed line) the addition of the CeO_2 NTs. It is clear that unlike the PLAL-AuNPs, the Chem-AuNPs do not attach to the CeO_2 NTs (black square, Figure 3.1-c). Abundant "free" citrate molecules in solution have been found necessary to stabilize Chem-AuNPs. Therefore, in general, they are kept in solution for the manipulation of the Chem-AuNPs (such as surface functionalization); otherwise rapid aggregation can easily take place [100]. Based on this consideration, the Chem-AuNPs, which were only purified once to remove un-reacted chemical species and then dispersed in 1.25 mM of sodium citrate solution, were used for coupling with the CeO_2 NTs. Unfortunately, this "standard" stable Au colloidal solution seems inappropriate for the current coupling reaction. Quite likely, free citrate ions in solution are easily adsorbed onto the positively charged CeO_2 NT surface, leading to a negatively charged surface that hinders the adsorption of negatively charged Chem-AuNPs [101].

To promote the coupling yet avoiding rapid NP agglomeration, a delicate purification/washing protocol was developed for as-prepared Chem-AuNPs (see Chapter 2). Our study shows that the Chem-AuNPs with ~0.9 wt% of the citrate ligand content (measured by TGA) can rapidly adsorb on the surface of CeO_2 without evident aggregation. Although successful, the manipulation of the Chem-AuNPs for the catalyst preparation is obviously less convenient and more time-consuming, with respect to the PLAL-AuNPs. The same amount of the Chem-AuNPs as that of the PLAL-AuNPs was coupled with the NTs (examined by NAA) for comparison of catalytic activity. The inset of Figure 3.5-b presents a typical TEM image of the Chem-AuNPs/CeO_2-NTs, whose structure is similar to that of the PLAL-AuNP/CeO_2-NTs. Figure 3.5-a shows the evolution of the UV-Vis spectra of the 4-NP reaction solution when the Chem-AuNPs/CeO_2-NTs are used as a catalyst. It can be seen that the absorbance of 4-nitrophenolate ions only decreases by half after 1800 s in the presence of the Chem-AuNPs/CeO_2-NTs, while it drops to ~0 after the same reaction

time in the case of the PLAL-AuNPs/CeO_2-NTs. Figure 3.5-b displays the variation of C/C_0 and $-\ln(C/C_0)$ with the reaction time as derived from Figure 3.5-a. Both values vary less severely than those shown in Figure 3.3-b, indicating a lower reaction efficiency. The *k* value of the Chem-AuNPs/CeO_2-NTs is 2.86 $\times$ 10^{-3} s^{-1} μmol Au^{-1}, about 5 times smaller than that of the PLAL-AuNPs/CeO_2-NTs. It is noted that the PLAL-AuNP/CeO_2-NT catalyst retains a rather good catalytic activity after four rounds of successive reactions, and its *k* value for each round is much higher than that of the Chem-AuNP/CeO_2-NT catalyst as well (Figure 3.6).

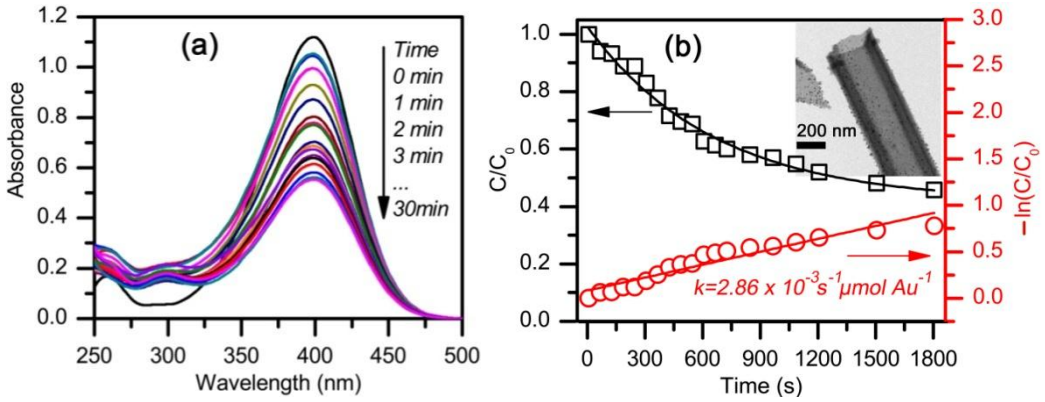

Figure 3.5 (a) UV-Vis absorption spectra during the catalytic reduction of 4-NP over Chem-AuNPs/CeO_2-NTs; (b) C/C_0 and $-\ln(C/C_0)$ as a function of reaction time for the reduction of 4-NP over Chem-AuNPs/CeO_2-NTs. Inset shows the TEM image of the Chem-AuNPs/CeO_2-NTs. Solid lines in (b) are the best-fit polynomials.

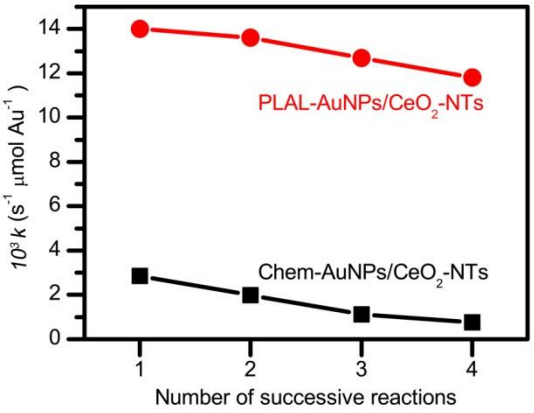

Figure 3.6 One thousand (10^3) times of reaction rate constant (10^3k) against the number of successive reduction reactions catalyzed by PLAL-AuNPs/CeO_2-NTs and Chem-AuNPs/CeO_2-NTs, respectively.

Clearly, chemically synthesized, citrate-capped AuNPs exhibit a considerably inferior catalytic activity than the PLAL-AuNPs which have a relatively "bare" surface. As the PLAL-AuNPs and Chem-AuNPs have similar size distributions and their hybrids with the NTs have similar structures and Au/support ratios, the different catalytic activity for the same reaction must therefore be related to inherent difference between these two types of AuNPs, rather than the morphology of the catalysts.

As described above, after careful purification, most free ligands are removed from the solution. Nonetheless, the Chem-AuNPs are still covered by certain amounts of citrate ligands. They could directly passivate the reactive sites or prohibit the access of reactant molecules to the reactive sites by providing spatial hindrance. As a consequence, probably less reactive sites on the surface of the Chem-AuNPs are exposed, resulting to the lower catalytic activity as compared with the relatively "bare" PLAL-AuNPs. In contrast, the small -OH groups on the latter NP surface leave more reactive sites available for reactants. It is clear that the use of the PLAL-AuNPs is not only beneficial for the easy, time-saving, effective conjugation with the NTs, but also contributes to the increase of catalytic activity. The blocking effect of –OH groups on the PLAL-AuNPs in catalysis is much less than that of citrate, which is commonly used in AuNP preparation. The above observations indicate that the surface chemistry of AuNPs is very important for coupling and catalytic performance.

3.4.2 Au-Support Interaction: CeO_2-NT vs. Commercial Ceria Powder

Among various support materials, NTs are one of the best candidates for NP supporting, because their geometry provides a relatively high surface area to volume ratio for better dispersion of metal NPs. In our case, besides the advantage of the high specific surface area of CeO_2 NTs, it is anticipated that their interaction with Au may also partially contribute to the excellent catalytic activity of the PLAL-AuNPs/CeO_2-NTs [102, 103]. To examine that, commercial ceria nanopowder was introduced as support to disperse and stabilize PLAL- and Chem-AuNPs, and the same

preparation procedures as those applied for the CeO_2 NTs were adopted to fabricate the nanocomposites.

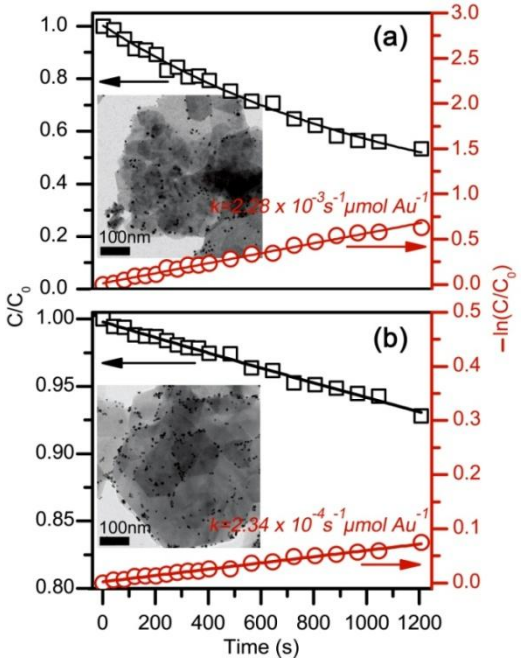

Figure 3.7 C/C_0 and $-\ln(C/C_0)$ as a function of reaction time for the reduction of 4-NP over PLAL-AuNPs/CeO_2-powder (a) and Chem-AuNPs/CeO_2-powder (b), respectively. Insets show the corresponding TEM images of nanocatalyst (a) and (b). Solid lines are the best-fit polynomials.

The insets in Figure 3.7-a and b display the TEM images of the PLAL-AuNPs/CeO_2-powder and Chem-AuNPs/CeO_2-powder, respectively. No obvious aggregation of AuNPs was observed and both types of AuNPs disperse well on the surface of CeO_2 particles. The variation of their C/C_0 and $-\ln(C/C_0)$ with reaction time during the reduction of 4-NP is shown in Figure 3.7-a and b, respectively. The *k* value of the PLAL-AuNPs/CeO_2-powder is nearly 10 times higher than that obtained for the Chem-AuNPs/CeO_2-powder, again indicating that the PLAL-AuNPs are more active than the Chem-AuNPs. However, both *k* values are far below those achieved when the CeO_2 NTs are used as support. Specifically, the *k* value of 1.40×10^{-2} s^{-1} μmol Au^{-1} for the NT supported PLAL-AuNPs is about 6 times higher than that of the CeO_2 powder supported PLAL-AuNPs (2.28×10^{-3} s^{-1} μmol Au^{-1}). These results strongly suggest that the CeO_2 NTs, as supports, have a positive

impact on the catalytic activity; they are at least partially responsible for the significantly higher catalytic activity of the PLAL-AuNPs/CeO_2-NTs in the 4-NP reduction reaction as compared with other Au-containing catalysts [20, 39-42, 53], including those investigated herein.

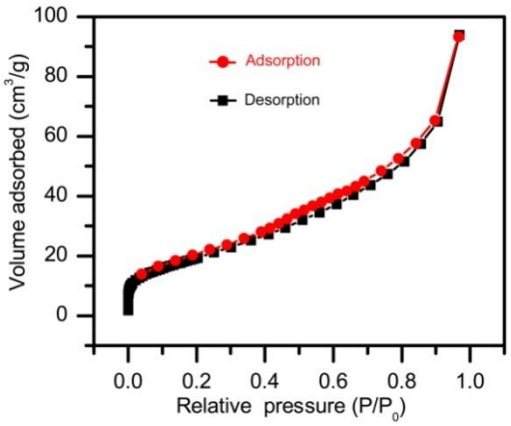

Figure 3.8 Nitrogen adsorption/desorption isotherms at -78 C °of CeO_2 NTs.

The surface area of the CeO_2 NTs is ~74 m^2/g (Figure 3.8), which is much higher than that of commercial powders (~1.58 m^2/g). It seems that the former can allow better dispersion of NPs and thus more effective contact with the reactants, probably leading to an increase of reaction rate. However, in both cases, AuNPs are uniformly distributed without aggregation (insets of Figure 3.5 and 3.7) and are loaded at the same level. Therefore, the surface area difference of CeO_2 supports should not be the dominant factor in the significant difference in catalytic activity. Instead, the Au─NT interaction may play a critical role herein as reported before [7, 13, 15, 34, 59, 61, 63, 66, 102-104].

To test this hypothesis, X-ray photoelectron spectroscopy (XPS) was used as an effective surface analysis tool, to analyze the surface chemistry of both CeO_2 supports and AuNPs. Figure 3.9-a shows the Ce $3d_{5/2}$ XPS spectra of CeO_2 NTs and commercial CeO_2 powder. The proportion of Ce^{3+} indicated by the peak at ~885.8 ev [105] in the NTs is considerably higher than that in the commercial powder, suggesting that there are more defects (i.e., oxygen vacancies) enriched on the

NT surface [62, 102, 103, 106]. It is well-known that the surface defects in CeO_2 can strongly interact with Au atoms to modify their electronic structure and stabilize the oxidation states of Au [62, 102, 103, 106]. These oxidized species have been found to play a positive role in the reduction of 4-NP [98]. From this point of view, it is interesting to examine the chemical status of Au in our nanocomposites.

The XPS spectra of Au 4f were thus taken on the PLAL-AuNPs/CeO_2-NTs, PLAL-AuNPs/CeO_2-powder and Chem-AuNPs/CeO_2-NTs. As shown in Figure 3.9-b, all deconvoluted Au 4f spectra exhibit two main peaks (red doublet) corresponding to metallic Au^0 [105]. For the PLAL-AuNPs/CeO_2-NTs (curve 1), in addition to metallic Au^0, broadened shoulders on the high binding energy side are composed of four distinct additional peaks (blue and green doublets), which can be assigned to the oxidation state of Au (Au^+ and Au^{3+}) [105]. As compared with the Au 4f spectrum of the PLAL-AuNPs/CeO_2-NTs, the intensity of oxidized Au species of the PLAL-AuNPs/CeO_2-powder (curve 2) and Chem-AuNPs/CeO_2-NTs (curve 3) is much lower. Because the Au oxidation states were not observed for unsupported PLAL- and Chem-AuNPs in their XPS spectra (Figure 3.10), the relatively high content of oxidized Au species in the PLAL-AuNPs/CeO_2-NTs must originate from the strong Au/CeO_2-NT interaction [62, 102], which is induced by the defect-enriched CeO_2 NTs [104] and enabled by the highly intimate contact of Au and CeO_2 [104]. In contrast, this interaction is weaker in the hybrids containing either the Chem-AuNPs or CeO_2 powder due to the steric hindrance effect from the citrate ligand on the Chem-AuNPs and fewer oxygen vacancies in the CeO_2 powder, explaining the much lower content of the oxizied Au species in these two samples. The PLAL-AuNPs and CeO_2 NTs together contribute to the strong Au─CeO_2 interaction. The oxidized Au species arising from this interaction may act as electron relay system, which accelerates the electron transfer from BH_4^- to 4-NP in the hydrogenation process [98], leading to the superior catalytic performance of the PLAL-AuNPs/CeO_2-NTs.

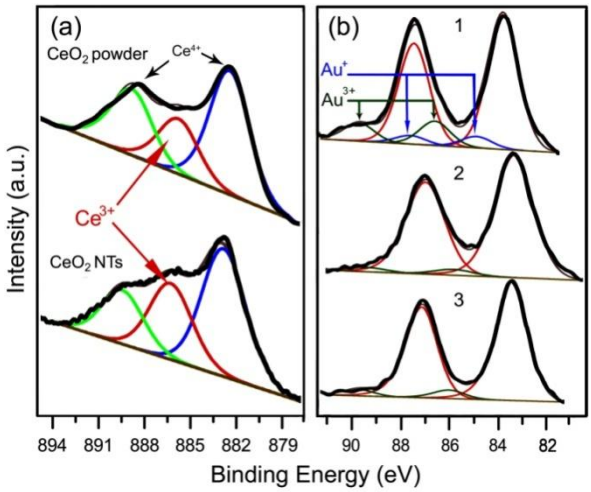

Figure 3.9 XPS spectra of Ce $3d_{5/2}$ (a) for CeO_2 supports and Au 4f (b) of PLAL-AuNPs/CeO_2-NTs (1), PLAL-AuNPs/CeO_2-powder (2) and Chem-AuNPs/CeO_2-NTs (3).

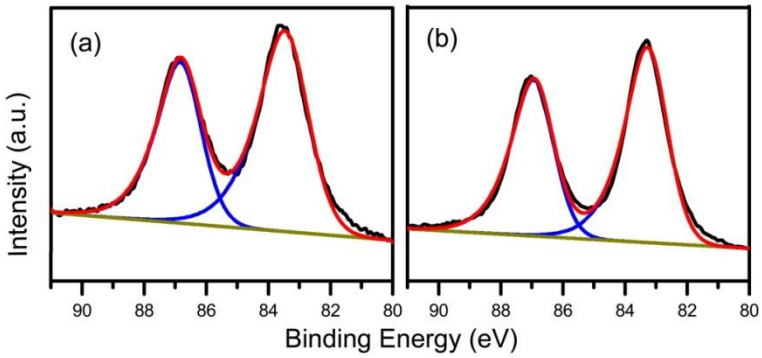

Figure 3.10 XPS spectra of unsupported PLAL-AuNPs (a) and Chem-AuNPs (b).

3.5 PLAL-AuNPs/CeO_2-NTs towards CO Oxidation

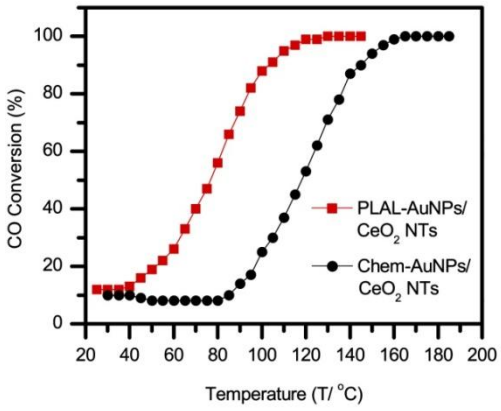

Figure 3.11 Temperature dependence of CO conversion in CO oxidation reaction over PLAL-AuNPs/CeO_2-NTs and Chem-AuNPs/CeO_2-NTs.

To further illustrate the unique, advantageous features of the PLAL-AuNPs/CeO_2-NTs in catalytic reactions, we also studied their catalytic activity towards CO oxidation, which has attracted extensive research due to its fundamental significance in air purification. Figure 3.11 shows the activity curves of the annealed (see Chapter 2) PLAL-AuNPs/CeO_2-NTs along with that of Chem-AuNPs/CeO_2-NTs for comparison. The PLAL-AuNPs/CeO_2-NTs exhibit a higher catalytic efficiency at the same temperature. The reaction rate with the presence of these two catalysts was further calculated at low conversions. For example, at ~45 ^oC the CO conversion reaches ~15% with the use of the PLAL-AuNPs/CeO_2-NTs in contrast to ~8% with the Chem-AuNPs/CeO_2-NTs. Accordingly, the reaction rate for CO oxidation at this temperature proceeding over these two catalysts was calculated to be ~0.42 and ~0.22 mmol $CO_2 \cdot min^{-1} \cdot mg^{-1}$, respectively. The reaction rate on PLAL-AuNPs/CeO_2-NTs is comparable with those calculated from other reports using solely chemically prepared AuNP/CeO_2 catalysts [66, 67, 172, 173]. Since the CeO_2 NT support, and the size and morphology of both types of AuNPs are the same, the higher catalytic activity of the former sample can be attributed to the bare surface of the PLAL-AuNPs and the strong Au-support interaction [62, 102]. The benefit of the bare surface of catalysts in catalysis is expected in most catalytic reactions. As for the contribution of the Au–CeO_2 interaction, it has been well-studied and widely reported for small molecule oxidation reactions [5, 7, 9, 12, 13, 19-25]. For example, by studying Au─CeO_2 and Au─SiO_2 multilayer nanostructures in CO oxidation, Zhou et al. experimentally determined that the active sites for this catalytic reaction are located at the interface of Au and CeO_2 [170]. They further found that the extremely low activity of a pure Au thin film in CO oxidation can be enhanced significantly by decorating it with Ce^{3+}-rich CeO_2 NPs since the strong interaction occurring at the interface between CeO_2 NPs and the Au surface induces a significant increase in number of the active sites on the Au surface [171]. In our study, as shown in the XPS measurements, the CeO_2 NTs containing a higher concentration of Ce^{3+} defects couple

directly with the relatively "bare and clean" PLAL-AuNPs without suffering from any steric hindrance, resulting in a stronger interaction at the CeO_2 –Au interface than that in the samples containing either the Chem-AuNPs or CeO_2 powder. This strong interaction leads to an increase in the number of catalytically active sites, as reflected in the XPS spectra as a higher concentration of oxidized Au. The positive role of oxidized Au species at the interface introduced by the strong interaction in CO oxidation has been widely accepted because they promote CO_2 desorption in the CO oxidation process [61, 62].

3.6. Summary

In summary, a highly catalytically active AuNP/CeO_2-NT nanocomposite was synthesized by simply mixing laser ablated Au colloids with CeO_2 NTs. Due to the OH^- groups on the AuNP surface resulting from the laser ablation process, the PLAL-AuNPs show a good affinity with CeO_2. The PLAL-AuNPs/CeO_2-NTs exhibit a high catalytic activity in the reduction of 4-NP in the liquid phase and CO oxidation in the gas phase. Based on the comparative studies on similar catalysts of the Chem-AuNPs/CeO_2-NTs, PLAL-AuNPs/CeO_2-powder, and Chem-AuNPs/CeO_2-powder, it is found that besides the relatively "bare" surface of the PLAL-AuNPs, the presence of a relatively high content of the oxidized Au species induced by the strong interaction between the bare PLAL-AuNPs and the defects on the surface of the CeO_2 NTs additionally contributes to the superior activity of the PLAL-AuNPs/CeO_2-NTs. This catalyst could be applied to other catalytic reactions, such as the degradation of organic molecules in waste water and exhaust gas, in which AuNPs are involved. This work represents the first demonstration of the use of PLAL-metal NPs in catalysis and the simple approach of preparing the nanostructured catalysts can potentially be extended to other hetero-nanostructured materials, made of PLAL-metal NPs (such as Pt and PtAu alloys) and metal oxide (such as TiO_2 and Al_2O_3). Such hetero-structured materials can find a wide range of applications including, but not limited to, catalysis.

Chapter 4

Novel *In Situ* Recyclable Gas-Sensitive AuNP Catalyst

In Chapter 3, I have demonstrated the promising catalytic properties of PLAL-AuNPs in 4-NP reduction. In this chapter, I continue to introduce my research into the catalytic applications of PLAL-AuNPs.

As mentioned above, the recovery and reuse of NPs in liquids, especially those of very small sizes, are still challenging. Centrifugation has been broadly applied to collect/separate NPs and products; however, it may induce the irreversible agglomeration of NPs, and thus considerable reduction of their catalytic activity. The efficient separation of tiny NPs from products without significant mass loss and with good re-dispersion potential is highly desired. Therefore, to achieve an excellent catalytic activity, long-term stability and reusability, a new, simple, yet effective separation technique needs to be developed. Using "smart", stimuli-responsive stabilizers could represent an interesting strategy.

During the past year, it has been reported that certain organic molecules can not only be used as a good stabilizer for colloidal AuNPs, but can also introduce an interesting environmental sensitivity to the NPs [107, 108]. For example, Li et al. [109, 110] and Zhao et al. [111, 112] reported that AuNPs functionalized by novel thermosensitive polymers exhibit efficient, reversible thermosensitive properties, leading to a new material, which can potentially

be used in temperature-switchable optical devices [109]. Very recently, Zhao et al. have reported a general, simple strategy for making CO_2-swithcable polymers [112]. It was discovered that some polymers containing tertiary-amine side groups, such as poly(N,N-dimethylaminoethylmethacrylate) (PDMAEMA) and poly(N,N-diethylaminoethylmethacrylate) (PDEAEMA), can react with CO_2 in water inducing a change of their solubility. On the basis of this finding, using the amine-containing units as a CO_2-sensitive trigger, we endowed CO_2 switchable solubility to many thermosensitive polymers [112]. With these achievements, it is of high interest to further couple the CO_2-sensitive polymer with AuNPs to control the dispersibility of the NPs in aqueous solution.

On one hand, due to the unique surface features of PLAL-AuNPs, i.e., the relatively "bare" surface, the PLAL-AuNPs are expected to be easily surface-modified by other "smart" molecules, which may import additional, interesting functionalities, e.g., easy recycling ability. On the other hand, it is desired that the functionalization will be performed in such way that the introduction of these "smart" molecules will not significantly hinder the access of reactants to the active sites on the PLAL-NP surface that generally causes a decrease of catalytic activity.

In this work, I use a CO_2-switchable polymer, thiol terminated PDEAEMA (SH-PDEAEMA), to modify the PLAL-AuNPs, so that the PDEAEMA grafted PLAL-AuNPs (PDEAEMA-AuNPs) are CO_2-switchable (for detailed information on the PDEAEMA-AuNP synthesis, please see Chapter 2.2.5.2). The PDEAEMA-AuNPs were characterized and their gas-responsiveness was tested. Finally they were used as catalyst in a model catalytic reaction of 4-NP reduction.

4.1 Characterization of PDEAEMA-AuNPs

Figure 4.1-a and b show TEM images of the PLAL-AuNPs with an average size of ~5 nm

in diameter before and after the functionalization with PDEAEMA. It is clearly seen that both types of AuNPs disperse well without obvious agglomeration, indicating that the surface functionalization process does not cause aggregation. The size distribution, however, becomes slightly broadened following surface functionalization; some larger NPs were observed. These NPs were further characterized by UV-Vis spectroscopy. Figure 4.1-c presents the UV-Vis spectra of PLAL- and PDEAEMA-AuNPs. PLAL-AuNPs exhibit a SPR peak at ~511 nm with FWHM of ~100 nm. For the case of PDEAEMA-AuNPs, slight red shift (~7 nm) of the SPR peak and FWHM broadening (~17 nm) were observed. Correlating with the TEM observations of both samples, the change in the SPR spectrum after functionalization is deemed to mainly originate from the slight size broadening and appearance of some larger NPs, instead of inter-particle electron coupling due to NP aggregation [4, 16].

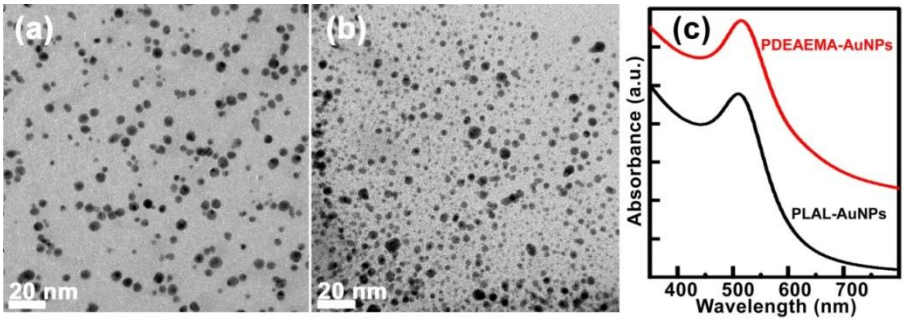

Figure 4.1 TEM image of PLAL-AuNPs before (a) and after (b) functionalization with PDEAEMA, and (c) their corresponding UV-Vis spectra.

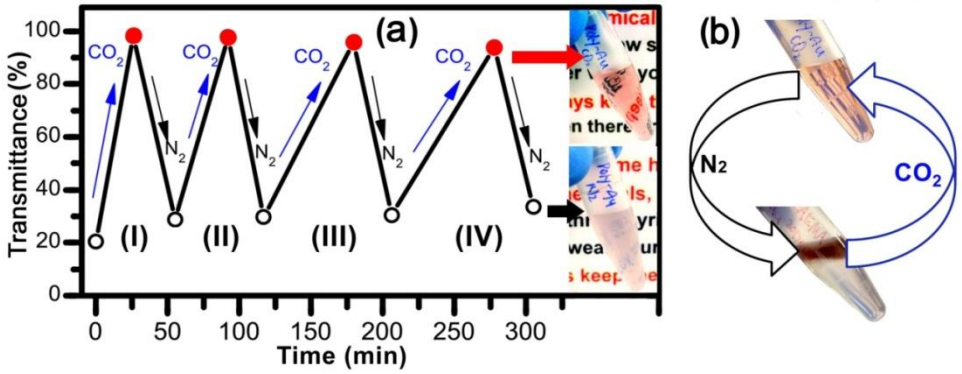

Figure 4.2 (a) Reversible change of transmittance upon four cycles of CO_2/N_2 bubbling; (b) Reversible

in situ phase separation and re-dispersion of PDEAEMA-AuNPs in water upon CO_2/ N_2 purging.

The gas-responsiveness of PDEAEMA-AuNPs was assessed in aqueous solution by purging with CO_2 and N_2 alternately. Figure 4.2-a illustrates the reversible change of transmittance upon four cycles of gas bubbling. The transmittance of the PDEAEMA-AuNP solution bubbled with N_2 for ~30 min is decreased to less than 40%. After CO_2 purging for ~30-60 min, the solution transmittance is restarted. The cloudy-clear transformation of the solution due to the presence of gas-sensitive NPs is also visible in the photo images shown in Figure 4.2-a inset. Interestingly, after N_2 purging was stopped and without any external disturbance, the PDEAEMA-AuNPs in opaque suspension do not precipitate; instead, phase separation was observed after a short time with the PDEAEMA-AuNPs floating on the solution surface, as shown in Figure 4.2-b (bottom). Gently stirring the solution can easily restore its cloudy appearance from this 2-layer phase separated state. After that, a clear, homogeneous, red solution can be obtained by CO_2 purging (Figure 4.2-b, top). This transition between phase separation and re-dispersion of AuNPs in solution is reversible through alternating CO_2/N_2 bubbling. These observations verify that the control of the AuNP dispersion status in aqueous solution using gas-switchable PDEAEMA is highly successful.

In principle, without interaction with CO_2, PDEAEMA polymer is poorly soluble in water as the polymer chains are basically hydrophobic [112]. In this scenario, the polymer chains tend to contract and also to strongly interact and entangle with each other. This explains the "self-aggregation" behaviour of polymer-attached NPs upon CO_2 removal by N_2 bubbling. The buoyancy of the NPs must be due to the formation of a lower-density polymer network. On the other hand, after CO_2 bubbling, water becomes a relatively good solvent for PDEAEMA due to the formation of more water soluble ammonium bicarbonates in the polymer chains originating

from the protonation of the amine groups by carbonic acid as shown in Scheme 4.1-a [112]. The PDEAEMA chains on NP surface are therefore switched from hydrophobic to hydrophilic and become much more extended in solution. Hence, PDEAEMA grafted NPs become well dispersed in water to form a clear colloidal solution.

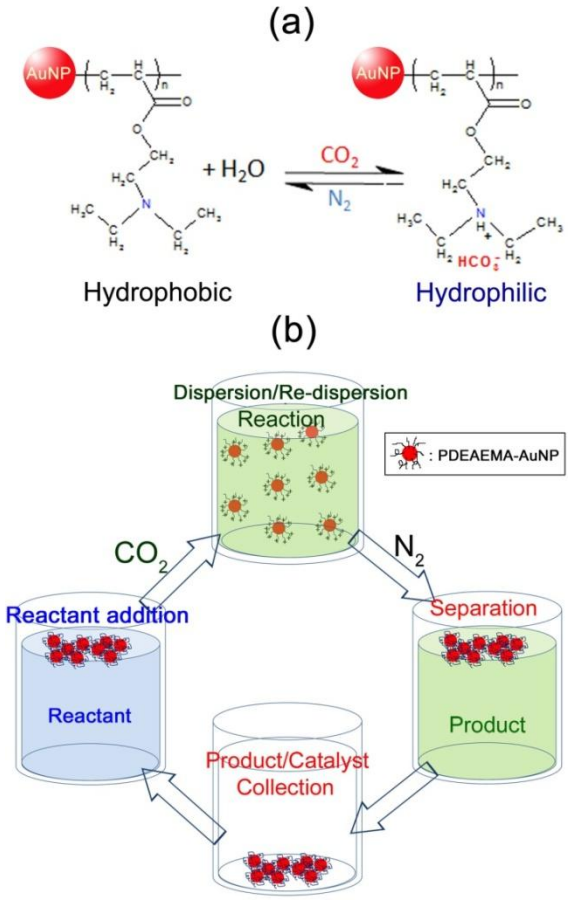

Scheme 4.1 (a) Reactions of the side chains of PDEAEMA on AuNP surface upon CO_2 and N_2 bubbling. (b) Schematic illustration of catalytic cycles using PDEAEMA-AuNPs as catalyst via CO_2/N_2 bubbling.

The structure of PDEAEMA-AuNPs upon cycling gas-bubbling was further confirmed by high resolution TEM (HRTEM) images and selected area electron diffraction (SAED) as shown in Figure 4.3. According to HRTEM and SAED characterization, the spacing (0.234 nm) of the lattice fringes in (c) and (d) matches the interplanar distance of the {111} crystal planes of face-centered cubic Au, consistent with the crystalline structure shown in the SAED patterns [99].

These results suggest that the crystalline structure does not change before and after CO_2 bubbling. Of technical importance is that this *in situ*, reversible phase-separation process in water controlled by gas switching can be employed for recycling NPs in other applications in the liquid phase where conventional methods for NP separation/collection are not efficient or appropriate.

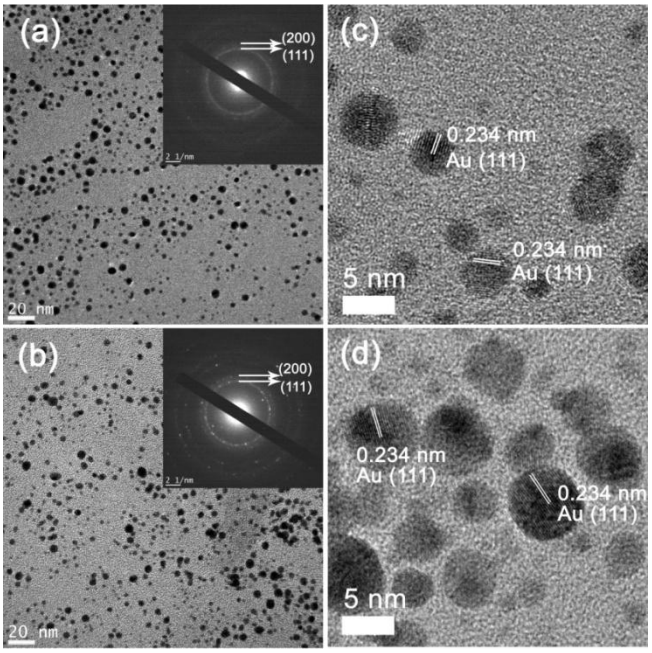

Figure 4.3 TEM images of PDEAEMA-AuNPs before (a) and after CO_2 bubbling (b); Insets show selected area electron diffraction (SAED) patterns; (c) and (d) show corresponding high-resolution TEM (HRTEM) images of (a) and (b), respectively.

4.2 Application of PDEAEMA-AuNPs in Catalysis

The application of these *in situ* recyclable PDEAEMA-AuNPs as catalysts was performed in the reduction of 4-NP to 4-AP in liquid as a model reaction, where $NaBH_4$ was used as a reducing agent. Similarly to the catalytic study in Chapter 3, because a large excess of $NaBH_4$ was added to the reaction as compared to 4-NP, the reaction kinetics basically followed a first-order rate law [20, 39-41, 43, 92]. Through measuring the intensity of UV-Vis absorption peak at 400 nm (Abs_{400nm}), which is directly associated with the concentration of 4-nitrophenolate

ions, as a function of reaction time, the reaction process was monitored.

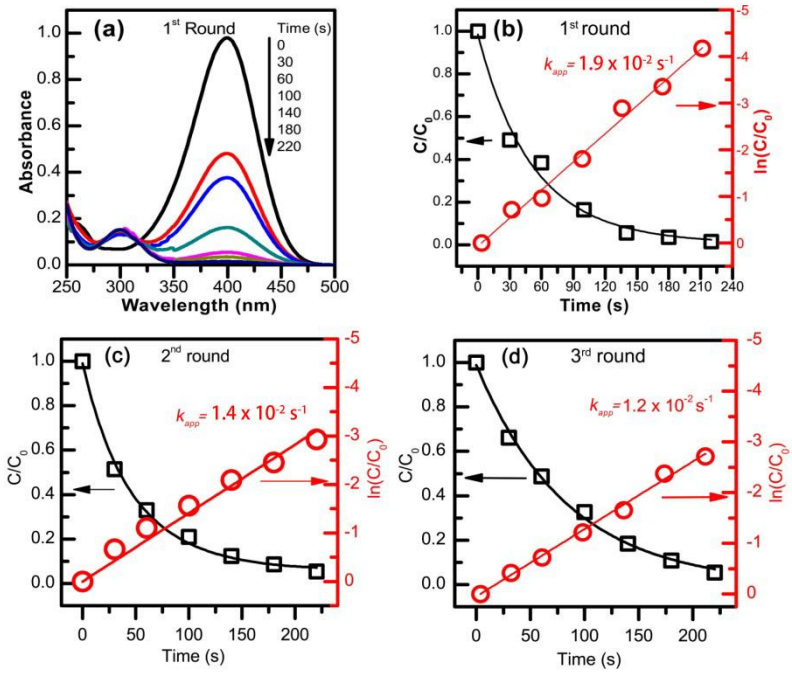

Figure 4.4 (a) UV-Vis absorption spectra during the first round catalytic reduction of 4-NP over PDEAEMA-AuNPs; (b-d) C/C_0 and $-\ln(C/C_0)$ as a function of reaction time for the successive reaction rounds of the 4-NP reduction over PDEAEMA-AuNPs. Solid lines in (b-d) are the best-fit polynomials.

Figure 4.4-a shows that after the introduction of the CO_2-bubbled Au colloidal solution, the Abs_{400nm} value drops rapidly as the reaction proceeds, reflecting the decrease of the 4-nitrophenolate ion concentration. Based on the Abs_{400nm} values, Figure 4.4-b plots C/C_0 (squares) and $-\ln(C/C_0)$ (circle) *versus* reaction time, where C_0 and C are the concentration of the 4-nitrophenolate ions at the beginning and at certain reaction times during the first round reaction, respectively. The reaction finishes within ~220 s with the PDEAEMA-AuNP catalyst. The apparent reaction rate constant k_{app} for the catalytic reaction, estimated from the slope of the linear correlation between $-\ln(C/C_0)$ and reaction time [38, 39, 42, 43, 52] is ~1.9×10^{-2} s^{-1}. After this, the solution was bubbled with N_2 to decrease the dispersibility of PDEAEMA-AuNPs so that they were phase-separated. The reaction product and Au catalyst were easily separated

and collected. Subsequently, the PDEAEMA-AuNPs were re-dispersed homogeneously in water upon CO_2 bubbling for new catalytic reaction rounds (Scheme 4.1-b). The redution kinetic processes of successive reduction reactions are summarized and shown in Figure 4.4-c and d with a slight reaction rate decrease. It was noted that the Abs_{400nm} of 4-NP was almost unchanged within 1 h in the presence of the N_2 purged PDEAEMA-AuNPs floating on the reaction solution (Figure 4.5), indicating that the "self-aggregated" AuNPs do not show any catalytic activity in this reaction. Clearly the removal of CO_2 by N_2 bubbling can easily put the AuNPs in the catalytic "off" state.

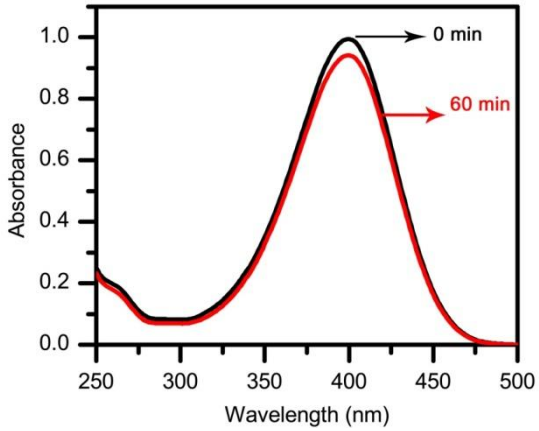

Figure 4.5 UV-Vis absorption spectra of 4-NP in the presence of N_2 bubbled PDEAEMA-AuNPs and $NaBH_4$ for 60 min.

Figure 4.6-a shows the plots of $\ln(k_{app})$ against the reaction cycle where the same amount of PDEAEMA-AuNP (red circles) and PLAL-AuNP (black squares) catalysts were repeatedly used. The latter was separated from the products and collected by centrifugation at the end of each cycle. The PDEAEMA-AuNPs recycled by gas purging demonstrate a much higher catalytic activity in all the following rounds. CO_2/N_2 bubbling reproducibly switches the catalysis state of the AuNPs between "on" and "off". In contrast, although the reaction rate for the first round over these two catalysts is very similar, the decay of the activity for PLAL-AuNPs is considerably faster. This can be mainly attributed to the severe, irreversible

aggregation of the PLAL-AuNPs caused by the centrifugation process. The similar catalytic activity during the first round of reaction for both samples indicates that the polymer on the PDEAEMA-AuNP surface does not largely block the access of reactants to the active sites on AuNPs. This is expected considering the bulky volume of polymers, which limits the number of polymers that can be anchored onto the NP surface. So the "physical" occupation of the active sites is limited. On the other hand, in the catalysis "on" state, the polymers are swollen and in the extended form. This open structure will not prohibit the diffusion of the reactants through the polymer layer to the NP surface. The working mechanism proposed herein is somewhat similar to that of dendrimer-encapsulated AuNP catalyst [43], which however does not have gas-sensitivity.

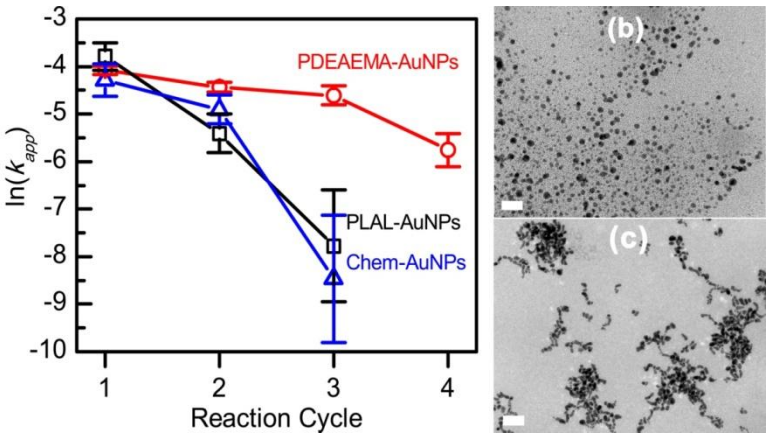

Figure 4.6 (a) Plots of ln(k_{app}) against the reaction cycle in the presence of PDEAEMA-AuNPs, PLAL-AuNPs and Chem-AuNPs respectively; (b) and (c) are TEM images of PDEAEMA-AuNPs and PLAL-AuNPs, respectively, after the third reaction cycle (scale bar is 20 nm).

The colloidal stability difference of both catalysts after three reaction cycles was confirmed by TEM. As shown in Figure 4.6-b, the PDEAEMA-AuNPs basically remain well-dispersed and no fierce aggregation is visible. In clear contrast, Figure 4.6-c shows that PLAL-AuNPs undergo strong agglomeration. Moreover, it is worth pointing out that our CO_2-switchable AuNPs also exhibit better colloidal stability and activity than most commonly

studied citrate ligand-capped AuNPs (Chem-AuNPs) with the same dosage in reactions cycles (Figure 4.6, blue triangle). These observations strongly suggest that the stability and reusability of AuNPs functionalized with PDEAEMA is superior to that of AuNPs without polymer modification, leading to a stable and easily reusable catalyst. Clearly, using CO_2-switchable polymers and processes represents a significant improvement as compared to conventional methods in the recycling and reuse of small NPs (herein: ~ 5nm).

4.3 Summary

In summary, novel gas-switchable AuNPs have been developed with the purpose of producing a highly stable and easily reusable Au nanocatalyst. It is the first time that CO_2-switchable polymer has been introduced into the preparation of 'smart" NPs for catalysis. The PDEAEMA-AuNPs demonstrate a high gas sensitivity to CO_2, leading to a good control of their dispersion status in aqueous solution. As compared to AuNPs manipulated with conventional methods, they show a much more stable catalytic property, and considerably better reusability realized via gas purging. The presence of a limited number of PDEAEMA molecules doesn't seem to noticeably block catalytically active sites on the PLAL-AuNPs. By optimizing the polymer structures, it is expected that even better properties can be achieved. This work successfully demonstrates the novel concept of using CO_2-switchable polymers to make easily recyclable NPs, which can find important applications in homogeneous liquid-phase catalysis.

Chapter 5

Increase of PLAL-AuNP Catalytic Activity by Forming Pt-Au Alloy NPs

In previous Chapters, the PLAL-AuNPs have demonstrated very interesting catalytic properties in 4-NP reduction. In order to enhance the catalytic activity of AuNPs, reduction of particle size could be an appropriate route due to the increase of surface to volume ratio in smaller AuNPs [42]. Another efficient way to improve the catalytic activity of AuNP catalysts is to alloy Au with other transition metals, such as Pt [25, 54, 113-116]. PtAu bimetallic NPs have received increasing attention due to their higher catalytic activity than pure Au and Pt NPs in many applications, such as selective hydrogenation and fuel cells [13, 71, 77, 117-126]. Also, a relatively "bare and clean" surface of the NPs is highly desired to further improve catalysis efficiency [58, 92]. Therefore, the PLAL technique, which can yield "surface-clean" NPs, is considered as a good technique for PtAu alloy NP catalyst preparation. To date, to the best of our knowledge, alloy targets have been largely utilized to produce alloy NPs using PLAL. However, the fabrication of some alloy targets is very challenging due to the miscibility gap of certain metals, i.e., Pt and Au in the current study. It is therefore attractive to develop a general strategy that can potentially lead to the synthesis of a variety of alloy NPs, including those compositions that are not obtainable in the bulk.

In this chapter, surface-clean, stable PtAu alloy colloids with a wide range of compositions were prepared using PLAL on single metal-mixture targets in water. The targets were made by

compression moulding a mixture of Pt and Au powders at different ratios (see Chapter 2 for experimental details). The structure of the NPs was characterized and the effect of experimental parameters on PtAu alloy NP fabrication and structure were studied. The PLAL alloy NPs were then assembled onto CeO_2 NTs to form hybrid nanocatalysts for 4-NP reduction to assess their catalytic activity and compare with CeO_2 NT supported monometallic Pt and Au NPs and their mixtures. It is shown that CeO_2-NT supported $Pt_{30}Au_{70}$ and $Pt_{50}Au_{50}$ NPs demonstrate considerably superior activity as compared with not only supported pure Au and Pt NPs and their mixture in this study, but also Au-based catalysts reported recently by other groups [20, 39-42, 53]. For the first time, volcano-like catalytic activity behavior was observed for the catalysis of 4-NP hydrogenation on PtAu alloy NPs, which clearly suggests a strong synergistic effect between Au and Pt in the alloy structure. The dependence of the activity on the component ratio is most probably due to the unique surface structure induced by laser ablation. This work demonstrates the great technical importance of preparing high activity catalysts using PLAL-NPs.

5.1 Characterization of PLAL PtAu Alloy NPs

PtAu NPs were typically synthesized at a laser fluence of 150.0 J/cm^2 and a solution pH of 11.0. Figure 5.1-a shows the XRD patterns of the NPs prepared at different Pt feeding contents ($[Pt]_{feeding}$), i.e., Pt content in the targets. The pure Au NP sample (A, $[Pt]_{feeding}$ = 0 atom %) clearly exhibits five diffraction peaks, corresponding to the {111}, {200}, {220}, {311} and {222} planes of an fcc structure. After the introduction of Pt, no additional set of peaks are observed and the shape of the diffraction pattern remains similar. According to literature reports, the existence of a large miscibility gap between Pt and Au tends to lead to two sets of diffraction peaks belonging to separate Pt and Au phases [77, 118, 119]. In our case, the observation of a single set of fcc diffraction peaks strongly indicates the formation of an alloy structure. There is a gradual peak shift

toward larger 2-theta values as the $[Pt]_{feeding}$ increases from 0 to 100 atom % (A-E), which can be explained by the replacement of larger Au atoms in the fcc lattice with smaller Pt atoms.

To emphasize the fact that substitutional PtAu alloy NPs are formed, the XRD pattern of a 50:50 mixture of pure Au NPs and pure Pt NPs was measured and compared with that of $Pt_{50}Au_{50}$. As demonstrated in Figure 5.1-b, unlike $Pt_{50}Au_{50}$, the NP mixture exhibits two sets of diffraction peaks. The inset of Figure 5.1-b shows a high resolution scan of the {220} peaks. It is clearly seen that the {220} peak of the $Pt_{50}Au_{50}$ alloy is different from that of the 50:50 mixture of pure Au NPs and pure Pt NPs, emphasizing the fact that an alloy is formed between Pt and Au.

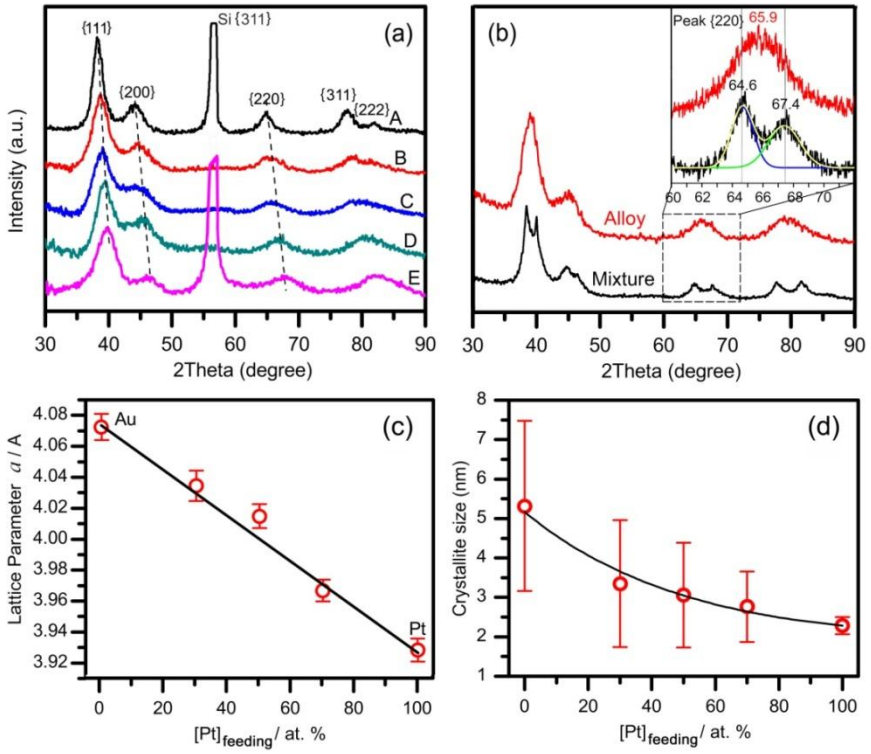

Figure 5.1 (a) XRD patterns of PtAu alloy colloids prepared by PLAL at fluence of 150.0 J/cm^2 and pH of 11.0. The Pt feeding content is (A) 0, (B) 30, (C) 50, (D) 70, and (E) 100 at. %. (b) XRD patterns of $Pt_{50}Au_{50}$ alloy and 50:50 mixture of pure Pt and Au NPs. The inset presents a high resolution scan of {220} peaks. (c) Lattice parameter and (d) crystallite size of NPs, estimated from XRD patterns, as a function of $[Pt]_{feeding}$. Solid lines in (c) and (d) are the best-fit polynomial and a guide for the eye, respectively.

The fcc lattice parameter, *a*, was extracted from an analysis of the {111} diffraction peaks. Figure 5.1-c plots the lattice parameter *a versus* $[Pt]_{feeding}$. It varies nearly linearly with respect to $[Pt]_{feeding}$, i.e., it follows Vegard's law as frequently observed in binary metallic alloys [77, 115, 120]. Not only does this linearity confirm the formation of alloys over a broad composition range, but it also suggests that the Pt content in alloy NPs is indeed close to that in the targets. With $[Pt]_{feeding}$ varying from 30 to 100 atom % (curve B-E of Figure 5.1-a), a peak broadening is observed, indicating a change of crystallite size. The crystallite size of the NP samples was calculated by using the Scherrer equation and the full width at half maximum of the {111} diffraction peak [127]. It is found that the crystallite size decreases from ~5.4 to ~2.5 nm as $[Pt]_{feeding}$ increases from 0 to 100 atom % (Figure 5.1-d). It is clear that the presence of Pt favors the formation of smaller crystallites.

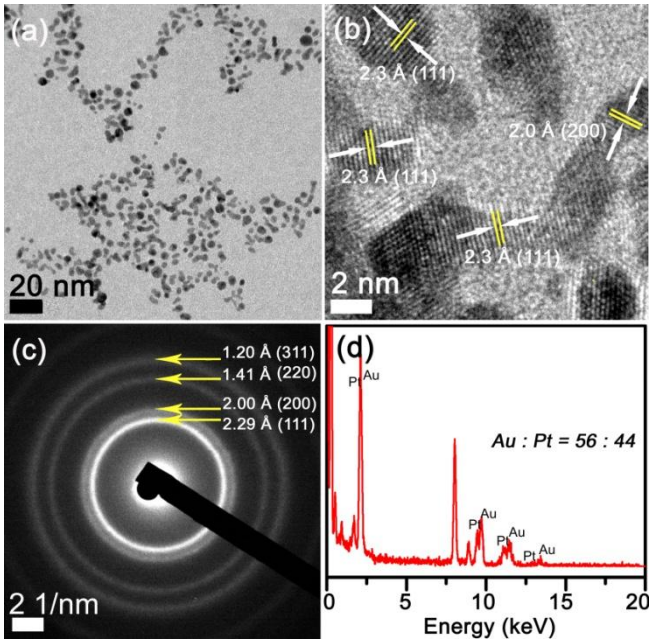

Figure 5.2 TEM (a) and HR-TEM (b) images, SAED pattern (c) and EDS spectrum (d) of $Pt_{50}Au_{50}$ alloy NPs prepared by PLAL at a fluence of 150.0 J/cm^2 and pH of 11.0.

The structure of PtAu alloy NPs was further characterized by TEM, SAED and EDS. Figure 5.2-a shows a typical TEM image of $Pt_{50}Au_{50}$ NPs as a representative example. It can be seen that

the sample is composed of numerous individually dispersed particles, along with partially coalesced particles and some irregularly shaped nanostructures, such as nanorods. The average size, based on the measurement of ~100 non-agglomerated particles, is ~3.3±1.7 nm. This value is close to that obtained from XRD analysis as shown in Figure 5.1-d, implying that these NPs are basically single crystals. A typical high resolution TEM (HR-TEM) image is shown in Figure 5.2-b. Lattice fringes can be clearly observed with spacing of ~2.3 and ~2.0 Å assigned to the {111} and {200} planes of the PtAu alloy, respectively. This sample was further examined with SAED and EDS. The SAED pattern in Figure 5.2-c clearly displays four distinct diffraction rings, the radii of which are 2.29, 2.00, 1.41 and 1.20 Å, indexed as the {111}, {200}, {220} and {311} reflections of the fcc polycrystalline structure, respectively. Taking the {111} plane as a specific example, its lattice separation in $Pt_{50}Au_{50}$ is 2.29 Å, slightly higher than that expected for pure Pt (2.267 Å), but lower than that expected for pure Au (2.355 Å) [99]. Consistent with the XRD results, the lattice spacing of alloy NPs obtained from HR-TEM and SAED is in between that of pure Pt and Au, again supporting the formation of an alloy. Similar results were obtained for other alloy samples prepared at different target compositions. The actual concentration of Pt in this sample was measured by EDS, which yields the value of ~44% (Figure 5.2-d), close to the nominal concentration of 50%.

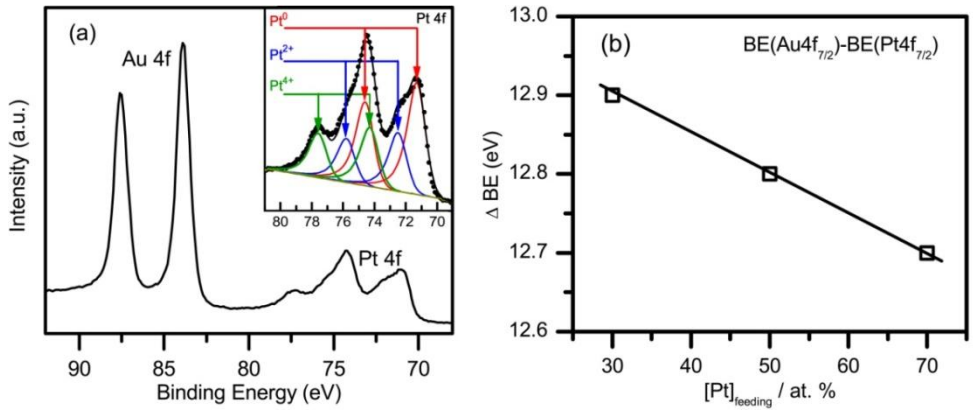

Figure 5.3 (a) XPS spectrum of $Pt_{50}Au_{50}$ (fluence=150.0 J/cm^2, pH=11.0); (b) XPS core electron binding energy difference, ΔBE, defined as Au $4f_{7/2}$-Pt $4f_{7/2}$, of alloy samples as a function of $[Pt]_{feeding}$. Inset shows

the high resolution Pt 4f XPS spectrum of (a) fitted by three pairs of curves. Solid line in (b) shows the linear-fitting.

XPS measurements were conducted to determine the chemical states of the constituent atoms in the alloy samples. Figure 5.3-a shows the XPS spectrum of $Pt_{50}Au_{50}$ NPs. Two distinct, symmetric peaks at a binding energy (BE) of ~84.1 and ~87.8 eV can be assigned to Au^0 [105]. The doublet of the Pt 4f peaks appears in the range ~70 - ~80 eV. It exhibits a considerable asymmetric shape tailing toward higher BE, and an additional peak at ~78 eV. The shape of the Pt 4f peaks is different from that expected for metallic Pt (Pt^0) [105], implying that Pt exists in multiple chemical states in the alloy sample. To identify these states, the Pt 4f peaks were deconvoluted and three components were deemed necessary to yield to a good fit of the experimental data (inset of Figure 5.3-a). The most intense component of the Pt 4f peak occurs at ~71.3 and 74.6 eV, which is attributed to the metallic state of Pt [105]. The higher energy doublet, which is located at ~1.3 eV higher BE than that of Pt^0, can be reasonably attributed to Pt^{2+} species (e.g., PtO and $Pt(OH)_2$) [86, 128]. The highest BE set of peaks, occurring at ~74.3 and 77.6 eV, is assigned to Pt^{4+} species [128, 129]. The observation of oxidized Pt species is not unexpected; they are possibly due to laser induced reactions between ablated metal species and water molecules [86].

Similar XPS spectra were obtained on other samples, $Pt_{30}Au_{70}$ and $Pt_{70}Au_{30}$, but slight peak shifts were noted among all three alloy samples. The $4f_{7/2}$ peaks of Pt^0 and Au^0 in the alloy samples vary from ~70.5 to ~71.3 eV, and ~83.2 to ~84.2 eV, respectively, with the Pt concentrations. This is consistent with previous XPS studies on PtAu having shown that alloying can cause the core-level peaks of Au and Pt to shift to different BE [77, 130]. This again supports the view that formation of PtAu alloy NPs is occurring over a broad composition range under the preparation conditions investigated in the present study (fluence=150.0 J/cm^2, pH=11.0).

In order to avoid a possible size effect on the position of the XPS peak, it was decided to use the BE difference between Au^0 and Pt^0 $4f_{7/2}$ peaks, defined as $\Delta BE = BE(Au\ 4f_{7/2}) - BE(Pt\ 4f_{7/2})$ for comparison [77]. The variation of the ΔBE *versus* $[Pt]_{feeding}$ is summarized in Figure 5.3-b. It can be seen that ΔBE varies linearly from ~12.9 eV to ~12.7 eV, as the $[Pt]_{feeding}$ increases from 30% to 70%. For comparison, ΔBE of the 50:50 physical mixture of Pt and Au NPs is 13.0 eV. These observations are in good agreement with a previous report on bulk PtAu alloy films prepared by crossed-beam PLD in a closed chamber [77]. As reported, when Pt atoms in their fcc structure are replaced by Au atoms, a partial charge transfer from Pt to Au could take place due to the higher electronegativity of Au (2.54) compared to that of Pt (2.20) [124, 130], which induces the BE shift.

5.2 Effect of pH and Laser Fluence on the Fabrication of PtAu NPs

On one hand, it has been reported that in the PLAL process, the liquid environment, including the nature and the concentration of surfactants, has an important impact on the size, morphology and dispersion of Au, Ag and Pt NPs [68, 78-80, 82]. On the other hand, laser parameters (such as pulse energy) were also found to play an important role in the formation of noble metal NPs [78-84]. It is therefore interesting to investigate how these parameters affect the formation of PtAu bimetallic NPs in the approach proposed here. Specifically, the effect of solution pH and laser fluence on the preparation and structure of bimetallic NPs was studied herein.

5.2.1 Effect of pH

Bimetallic PtAu colloids were prepared by PLAL at a laser fluence of 4.0 J/cm^2 with pH values varying from 4.0 to 13.0. All samples prepared from solutions with a pH in the range of 4.0 to 11.0 are stable for weeks at room temperature without any change in their appearance; however, for $Pt_{50}Au_{50}$ and $Pt_{70}Au_{30}$ prepared at pH 12.0, and $Pt_{30}Au_{70}$ at pH 13.0, only turbid, dark suspensions are observed. In those cases, a black deposit forms within 30 minutes. The effect of the

pH on the structure was further studied by XRD and TEM. Figure 5.4-a shows the XRD patterns of $Pt_{50}Au_{50}$ NPs prepared at different pH values (4.0 to 12.0). Two peaks are observed at ~38.9 º and ~45.1 º, which are assigned to the {111} and {200} planes, respectively. However, for the sample prepared at pH 12.0, each diffraction band is composed of two peaks located at the position of pure Pt and pure Au. This is a strong indication of the formation of separated Pt and Au phases. This phase separation is also observed for $Pt_{70}Au_{30}$ at pH 12.0 and $Pt_{30}Au_{70}$ at pH 13.0. Although we cannot clearly explain why a pH higher than 11.0 favors the formation of separate Pt and Au phases, it remains that PtAu alloys can be formed over a broad pH range (from 4.0 to 11.0) by PLAL.

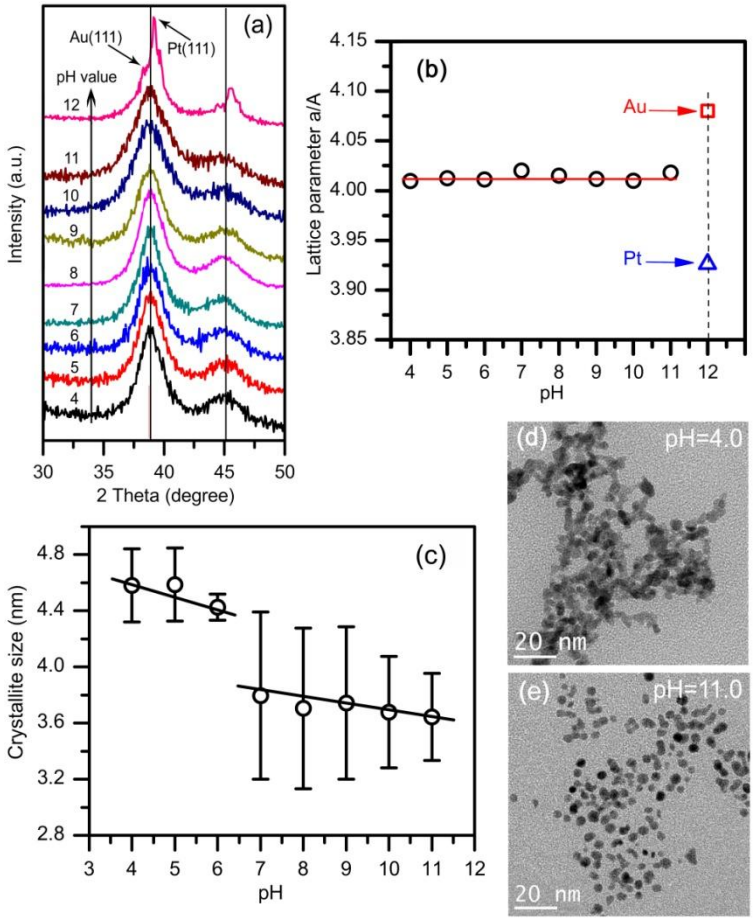

Figure 5.4 (a) XRD patterns of $Pt_{50}Au_{50}$ prepared by PLAL at a fluence of 4.0 J/cm^2 in aqueous solution with different pH values. The pH value increases from 4.0 to 12.0 from bottom to top. (b) Lattice parameter and (c) crystallite size of $Pt_{50}Au_{50}$ as a function of solution pH. (d) and (e) show the TEM images of $Pt_{50}Au_{50}$

prepared by PLAL at pH of 4.0 and 11.0, respectively. Solid lines in (b) and (c) show a linear-fitting and a guide for the eye, respectively.

The variation of the lattice parameter, *a*, with respect to the solution pH is depicted in Figure 5.4-b. In the pH range extending from 4.0 to 11.0, the lattice parameter remains constant at ~4.020 Å, indicating that the composition of the NPs is insensitive to the pH variation in this pH range and is essentially similar to the target composition. This feature makes the control of the alloy composition relatively straightforward in the PLAL process. At pH = 12.0, the values of *a* calculated from different sets of diffraction peaks are ~3.925 and ~4.075 Å, close to the values of pure Pt (*a* = 3.930 Å) and pure Au (*a* = 4.080 Å), respectively, indicating that alloy formation does not take place at this relatively high pH.

Figure 5.4-c shows the variation of the crystallite size of $Pt_{50}Au_{50}$ as a function of the pH. It is found that the average crystallite size remains constant in the pH ranges 4.0 - 6.0 and 7.0 - 11.0. Nonetheless, an abrupt crystallite size reduction is observed at pH 7.0. It is also observed that higher pH favors the formation of individually dispersed NPs. As shown in Figure 4-d, the $Pt_{50}Au_{50}$ sample prepared at pH 4.0 is mainly composed of coalesced and short wire-like structures, making it difficult to identify individual NPs and measure their sizes. In contrast, the TEM image (Figure 5.4-e) of $Pt_{50}Au_{50}$ NPs prepared at pH = 11.0 clearly shows the presence of individually dispersed, non-agglomerated particles with a particle size of ~3.5 ± 1.6 nm. This value is similar to the crystallite size determined from XRD. A similar phenomenon is also observed for all samples prepared under a higher fluence of 150.0 J/cm^2.

The effects of solution pH on the structure of PtAu colloids observed herein are consistent with previous reports for Au and Pt NPs prepared by PLAL [79, 80]. Generally, in a PLAL process, the number of metal atoms ejected from a target depends on laser power, whereas the liquid environment exerts an important influence on the formation of crystallites and nanostructures from

the ablated atoms. It has been reported that in a laser ablated surfactant-free Pt colloidal system, the NPs are slightly charged due to the adsorption of OH^- ions on their surfaces, which provides an electrostatic repulsive force that exceeds the van der Waals attractive force among NPs, thus stabilizing the NPs [79]. The same principle seems to hold true in our alloy colloidal system. At lower pH values (4.0-6.0), there may not be enough surface negative charges to stabilize freshly produced nuclei and small NPs. As a consequence, aggregation and coalescence take place more easily and crystallites also tend to grow bigger, as compared with those prepared at higher pH values [79, 80]. All the above results point to the complicated role of the solution pH in the formation of alloy NPs by PLAL.

5.2.2 Effect of Fluence

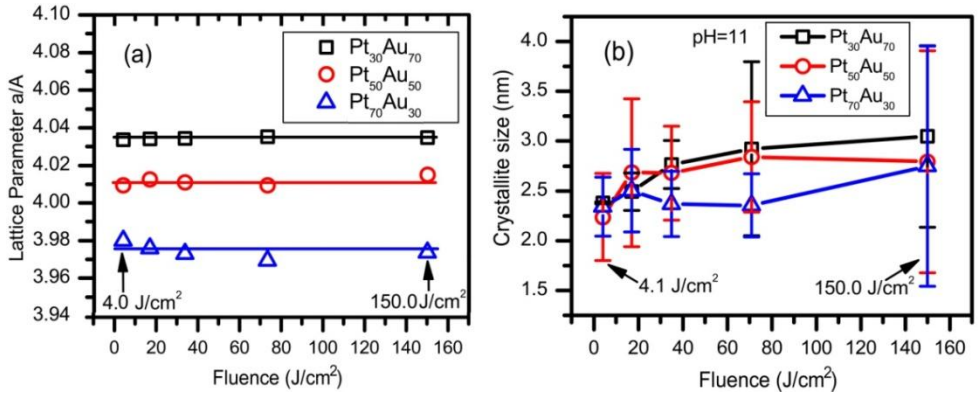

Figure 5.5 (a) Lattice parameter and (b) crystallite size of $Pt_{30}Au_{70}$, $Pt_{50}Au_{50}$ and $Pt_{70}Au_{30}$ prepared at pH 11.0 as a function of laser fluence. Solid lines in (a) show a linear-fitting.

The effect of laser fluence on PtAu alloy NP formation was studied by varying the fluences from 4.0 to 150.0 J/cm^2 at pH 11.0. As-prepared samples were again characterized with XRD, and the variation of the lattice parameter with respect to the fluence is plotted in Figure 5.5-a for three series of samples prepared from three different target compositions. The lattice parameter *a* of each series is constant despite the variation of the fluence over more than one order of magnitude. As expected, the average lattice parameters differ among three series, being 4.030, 4.015 and 3.975 Å

for $Pt_{30}Au_{70}$, $Pt_{50}Au_{50}$ and $Pt_{70}Au_{30}$, respectively. From Vegard's law, the average Pt concentrations were estimated to be 29.3%, 44.8% and 69.8% for $Pt_{30}Au_{70}$, $Pt_{50}Au_{50}$ and $Pt_{70}Au_{30}$, respectively, indicating that alloy NPs with a measured composition close to the target composition can be prepared over a wide fluence range. As illustrated in Figure 5.5-b, the crystallite size does not vary significantly with the fluence. TEM measurements (not shown) further confirm that the variation of the laser fluence hardly influences the NP size. For example, the mean diameter (3.5 ± 1.6 nm) of $Pt_{50}Au_{50}$ NPs prepared at 4.0 J/cm^2 (Figure 5.4-e) is very similar to that of the NPs prepared at 150.0 J/cm^2 (3.3 ± 1.7 nm, Figure 5.2-a). Although the fluence shows a negligible impact on the alloy NP structure, it is noted that a lower fluence, such as 4.0 J/cm^2, is considerably less efficient for NP fabrication, in terms of the quantity of NPs, due to the lower atom ejection efficiency.

5.3 Electrochemical Characterization

Figure 5.6 shows CVs of the alloy NP samples (prepared at: fluence=150.0 J/cm^2; pH=11.0) in 0.5 M Ar-saturated H_2SO_4 solution. On one hand, voltammograms of Pt NPs (Figure 5.6-a) show similar features to the well known electrochemical behavior of bulk Pt with three main potential regions: *i)* from 0.05 to 0.40 V, a pair of anodic (cathodic) peaks attributed to hydrogen desorption (adsorption) ; *ii)* from 0.40 to 0.75V, a featureless potential region attributed to double layer capacitive current, and *iii)* Pt oxide formation/removal potential region at values higher than 0.75V. On the other hand, the CV of AuNPs in Figure 5.6-a displays the characteristic features of bulk Au, i.e. a wide potential region corresponding to the double layer charging current from 0.05 to 1.15 V, followed by Au oxide formation/removal at potentials above 1.30 V. In the case of PtAu alloy NPs, a linear combination of the features of both metals is observed, i.e. well defined hydrogen peaks at 0.12 V and 0.26 V and the Pt oxide reduction peak at 0.75 V in the case of Pt-rich alloys, while an ill-defined hydrogen sorption peak region and a more pronounced Au oxide reduction peak around 1.17 V are observed for Au-rich alloys.

Another interesting aspect correlated with the PtAu alloy NP stoichiometry, is the upper potential region of Figure 5.6-b (E ≥ 1.6V), in which the drastic anodic current increase is attributed to water oxidation, i.e., the Oxygen Evolution Reaction (OER). The onset potential for OER is shifted towards higher values with increasing Au content and eventually vanishes for pure Au NPs, which is attributed to the growth of a continuous monolayer of Au oxide at such potential values. It is therefore obvious that the surface electrochemistry for alloy NPs displayed in Figure 5.6 corresponds to the voltammetric characteristics of both Pt and Au surface atoms.

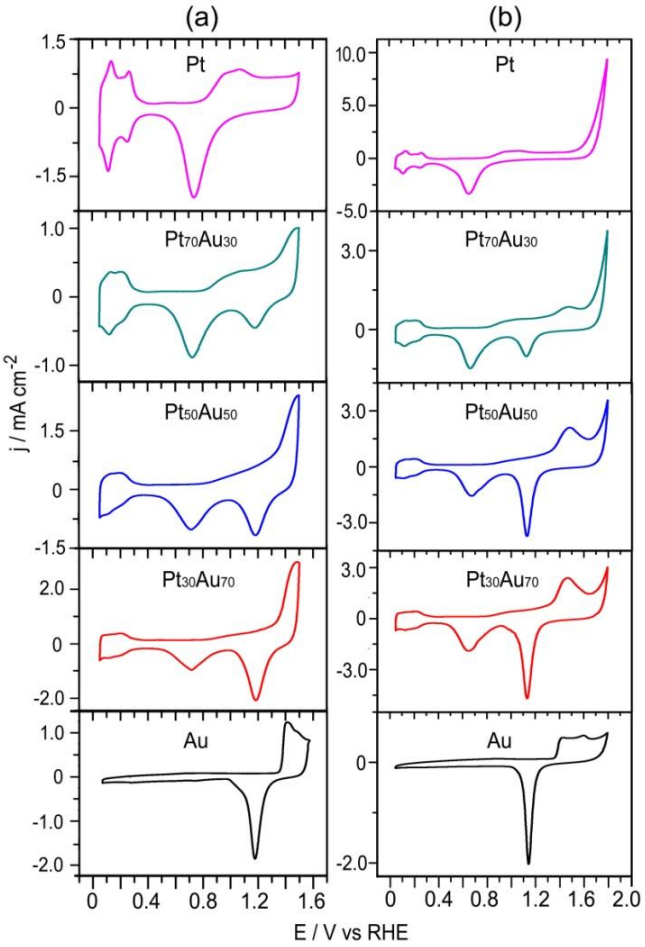

Figure 5.6 Cyclic Voltammetric responses (50 mV s^{-1}) for Pt_xAu_{100-x} NPs (fluence=150.0 J/cm^2, pH=11.0) in 0.5 M Ar-saturated H_2SO_4 solution up to (a) 1.5V and (b) 1.8V vs. RHE.

A detailed investigation of the CVs in Figure 5.6-b reveals that the peak potential value for Au oxide reduction remained constant at ~1.17 V for the whole range of PtAu alloy NPs. On the other hand, in Figure 5.6-a, the peak potential values for Pt oxide reduction was found to shift towards negative values from 0.74 V for pure Pt NPs, to E = 0.73 V for $Pt_{70}Au_{30}$, and further to E = 0.71 V for $Pt_{30}Au_{70}$. This shift reflects a slightly enhanced Pt oxide reduction hindrance as compared to pure Pt, and was already observed on PtAu surface alloys [132, 133]. The negative shift of the Pt oxide reduction peak for the Au-rich alloys reveals stronger Pt-O binding as compared with Pt-rich alloy electrodes. This is related to the increase of the lattice parameter of PtAu alloys with Au content, as previously highlighted in Figure 5.1-c, which has been correlated to the stabilization of oxygen-type adsorbates, such as -O and -OH species, on an expanded lattice [134]. The above mentioned voltammetric features reinforce the earlier conclusions drawn from XPS analyses in Figure 5.3-b, and confirm the formation of alloys on the NP surface for the whole stoichiometry range of PtAu NPs.

As catalytic properties are largely determined by the surface chemistry, it is also necessary to examine whether these PtAu alloy NPs have a uniform composition on the surface and in the interior. To this end, the Pt surface content ($[Pt]_{surface}$) of the PtAu NPs with nominal Pt content of 30%, 50% and 70%, was estimated by analyzing their corresponding CVs displayed in Figure 5.6, viz:

$$[Pt]_{surface} = ECSA_{Pt} / (ECSA_{Pt} + ECSA_{Au})$$ [77, 135]

where $ECSA_{Pt}$ and $ECSA_{Au}$ are the Electro-Chemically Active Surface Areas (cm^2) of Pt and Au, respectively. $ECSA_{Pt}$ was determined from the integration of the electric charge involved in the Pt oxide reduction, centered at ~0.73 V in the reverse scan of Figure 5.6-a, and using the well accepted conversion factor of 440 $\mu C/cm^2$ [122, 136, 137]. From the charge of the Au oxide reduction peak, centered at ~1.17 V in the reverse scan of Figure 5.6-b, $ECSA_{Au}$ was determined using a conversion

factor of 400 μC/cm^2 [138, 139]. On the other hand, as already discussed in section 5.1, the lattice parameters of PtAu alloy NPs follow Vegard's law. From this linear relationship and based on the lattice parameters (Figure 5.1-c) extracted from XRD analysis, the actual, overall concentrations of Pt ([Pt] $_{overall}$) were straightforwardly calculated for these PtAu alloy samples. Figure 5.7 shows a plot of [Pt] $_{surface}$ against [Pt] $_{overall}$. It is clearly seen that [Pt] $_{surface}$ and [Pt] $_{overall}$ values are quite close for all three alloy samples, which indicates that the surface composition of the NPs is nearly identical to the average, overall composition of NPs. This observation supports the viewpoint that there is no surface enrichment of either Au or Pt and that the NPs have a uniform composition. In general, these findings verify that the control of the PtAu alloy NP composition can be successfully achieved by varying the composition of the target.

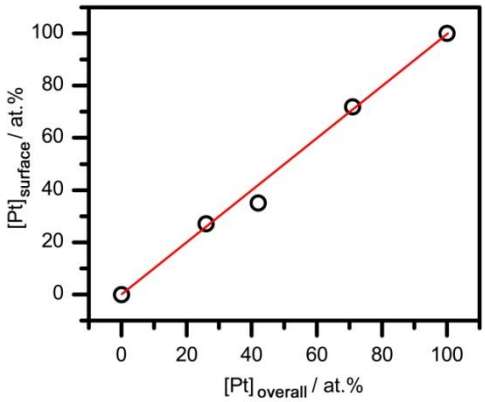

Figure 5.7 [Pt] $_{surface}$ of PtAu alloy NPs, prepared by PLAL at fluence of 150.0 J/cm^2 and pH 11.0, with respect to their [Pt] $_{overall}$. Solid line shows a linear-fitting.

5.4 Catalytic Property of PLAL-PtAu Alloy NPs

5.4.1 Catalyst Preparation

A nanohybrid structure of PLAL-PtAu alloy-NPs/CeO_2 NTs was prepared by mixing PLAL-PtAu alloy NP solution and CeO_2 NTs, which is the same method as that introduced in Chapter 3 (please see Chapter 2 for experimental details). The strong static-electric interaction and hydrogen bonding between NPs and NTs lead to the efficient coupling of them. Again, this

"physical" approach does not require any additional surface-functionalization, such as ligand-exchange with linker molecules, to either NPs or CeO_2 NTs, thereby largely decreasing the risk of contaminating and agglomerating the NPs, which makes the laser approach preferred in catalysis compared to a chemical synthesis.

Figure 5.8-a and b show the TEM images of the $Pt_{50}Au_{50}$ alloy-NPs/CeO_2-NTs as a representative example. The CeO_2 NTs are quite obvious and at a higher magnification (Figure 5.8-b and inset), the presence of the PLAL-$Pt_{50}Au_{50}$ NPs on the tube surface is clearly visible. The NPs are well dispersed on the surface with no unattached metal NPs being observed, indicating a good affinity between PLAL-metal NPs and CeO_2 NTs. The $Pt_{50}Au_{50}$-NP/CeO_2-NT sample was further characterized by HR-TEM; as shown in Figure 5.8-c, the lattice fringes of the attached PLAL-$Pt_{50}Au_{50}$ NPs with diameter of ~3-4 nm and the CeO_2 NT surface are clearly presented and marked [99].

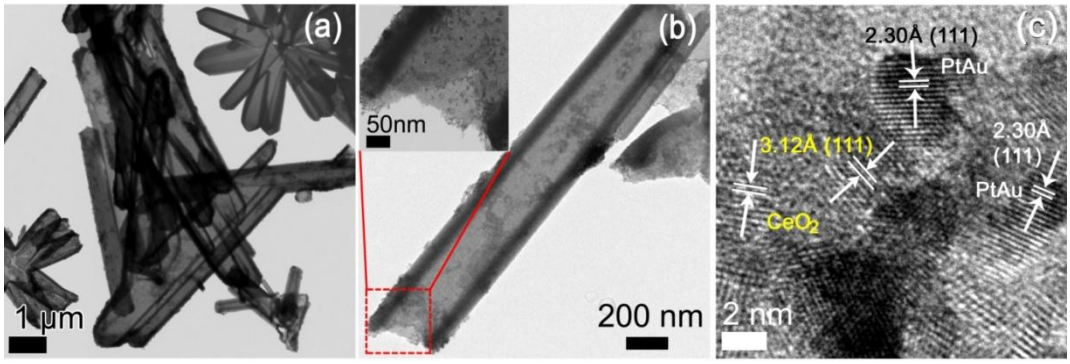

Figure 5.8 TEM (a, b) and HR-TEM images (c) of $Pt_{50}Au_{50}$-NPs/CeO_2-NTs.

5.4.2 Catalytic Measurement

As described in Chapters 3 and 4, the catalytic performance of the Pt_xAu_{100-x}-NPs/CeO_2-NTs was then assessed in the catalytic reduction of 4-NP, where $NaBH_4$ was used as the reducing agent. Figure 5.9-a shows the $Pt_{50}Au_{50}$-NPs/CeO_2-NT catalyzed reaction whose kinetic process was recorded by absorption spectra. Based on the evolution of the absorbance data,

Figure 5.9 (b-f) plots C/C_0 (black squares) and $-\ln(C/C_0)$ (red circles) versus the reaction time upon supported Pt_xAu_{100-x} catalysts, where C_0 and C are the concentration of the 4-nitrophenolate ions at t = 0 s and a time *t*, respectively. In all cases except for the pure AuNP/CeO_2-NT sample, the reduction reaction of 4-NP is almost completed after 180 s, as evidenced by the fact that Abs_{400nm} drops rapidly to zero. The linear correlation between $-\ln(C/C_0)$ and reaction time verifies that the reaction is of the first-order. Thus, the kinetic equation of the reduction can be described by the equation of $dC/dt = -k_{app} C$ again.

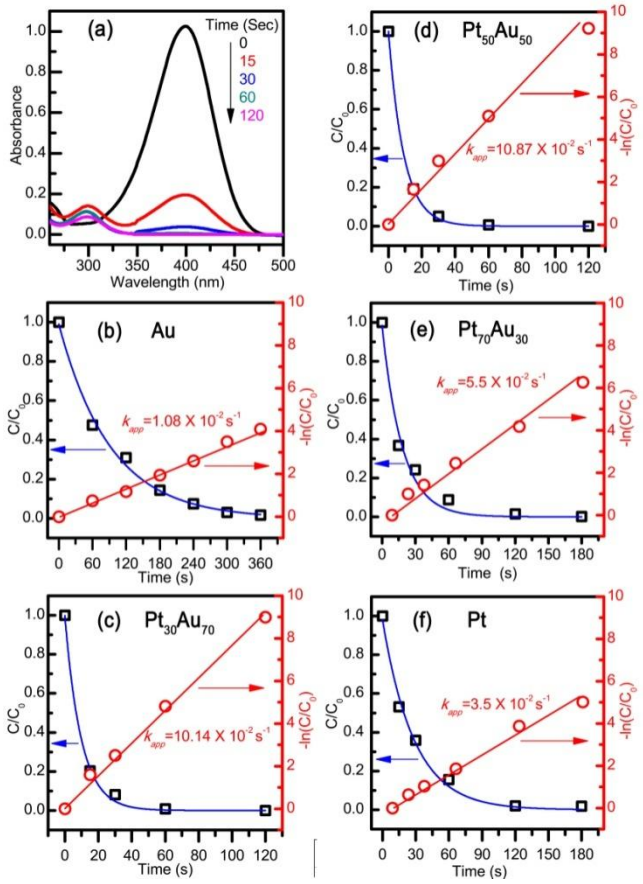

Figure 5.9 (a) UV-Vis absorption spectra of the 4-NP reduction reaction over PLAL-$Pt_{50}Au_{50}$-NPs/CeO_2-NTs; (b-f) C/C_0 and $-\ln(C/C_0)$ as a function of reaction time over hybrid catalysts. Solid lines in (b-f) are the best-fit polynomials.

The catalytic reaction takes place on the surface of NPs, therefore in order to exclude the effect of metal NP loading on the reaction efficiency and also to compare the catalytic activity of the

alloy NPs with different Pt/Au ratios, the catalytic reaction rate k is further defined by normalizing k_{app} to the total surface area of metal NPs (S, m^2), i.e., $k=k_{app}/S$ [42]. The k values for the PtAu alloy-NPs/CeO_2-NTs with respect to the Pt content are summarized in Figure 5.10 (red circles). The reaction over the $Pt_{50}Au_{50}$-NP/CeO_2-NT sample demonstrates the highest reaction rate (k= ~5.11 × 10^{-2} s^{-1} m^{-2}), which is not only impressively higher than that of the pure Au and Pt NPs investigated herein but also those based on AuNPs reported recently by others [20, 39-42, 53]. These observations indicate that the reaction efficiency of 4-NP reduction can be enhanced by alloying Au with Pt at appropriate component ratios. To further verify the influence of alloying on the catalytic activity, the 4-NP catalytic reduction reaction was also performed in the presence of the mixture of Pt and Au NPs loaded onto the NTs at different Pt/Au ratios, and their k values were compared with those of the alloys. As demonstrated in Figure 5.10 (blue triangles), supported NP mixture samples show steadily enhanced activity with increasing Pt content towards that of the pure Pt NPs. However, these k values are much lower than those of alloy NPs of $Pt_{30}Au_{70}$ and $Pt_{50}Au_{50}$, suggesting that Pt and Au in these alloys have a distinctly different and strong synergistic effect in the catalysis.

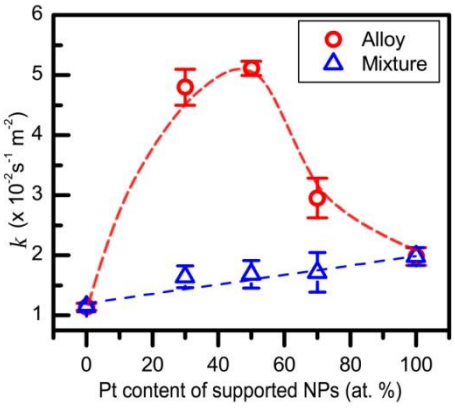

Figure 5.10 Reaction rate constant k on PtAu alloy-NPs/CeO_2-NTs as a function of Pt content. Dashed lines are the guides for eyes.

This synergistic effect was also recently reported by Preussner et al. in that Pt-Au bimetallic nanorods with a Pt content of 17 wt% showed higher catalytic activity for 4-NP reduction than pure Au and Pt nanostructures [117]. Nonetheless, our study clearly illustrates for the first time a "volcano-like" dependence of catalytic activity upon the bimetallic component ratio in the 4-NP reduction reaction. Generally the formation of an alloy structure can change the electronic structure of involved metal atoms, which is highly relevant to their catalytic activity [113]. The variations in the surface electronic structure have been theoretically studied using Density Functional Theory (DFT) computation by assuming some specific structural models [113, 123]. As for the PtAu system, it has been predicted that there is a significant shift of the d-band center from -2.25 eV for Pt atoms in pure Pt metal to -1.80 eV for Pt atoms in PtAu alloys under certain geometries [113, 123]. Importantly the latter value is close to the d-band center of pure Palladium (-1.83 eV), which has been shown to exhibit the highest catalytic activity among noble metal NPs in the 4-NP reduction reaction [131]. Although the actual atomic arrangement of Pt and Au atoms in the PtAu alloy investigated herein can be quite complicated, it is highly likely that the d-band centre of certain Pt atoms shift towards that of Pd, demonstrating much higher, "Pd-like" catalytic activity.

On the other hand, the co-operative effect between nearby Pt and Au sites may also play a role in the largely enhanced catalytic activity. A simple thermodynamic model based on co-operative actions has recently been proposed by Fernondez *et al* [142] as guidelines for the design of improved bimetallic catalysts for the oxygen reduction reaction and experimentally tested. In that study, it was suggested that O can migrate from one metal that can accelerate the dissociative adsorption of oxygen to another metal that is more efficient for adsorbed oxygen atom reduction and together they lead to the enhanced activity [142]. As for the PtAu system, it has been theoretically predicted as well as experimentally proved that strong dissociative adsorption of hydrogen can take

place more efficiently on Pt clusters than on Au clusters (or mixed PtAu sites) [44, 114, 141]. It is possible that, in our case, very small Pt clusters are present on the PtAu alloy NP surface. They adsorb BH_4^-/H_2 dissociatively with a much lower activation barrier as compared with Au (or mixed PtAu) sites [44, 140]. Thus-activated H atoms could then migrate to Au (or mixed PtAu) sites at a very close proximity [142] to react with 4-NP efficiently, followed by much easier desorption of reaction products on these sites than that on the clustered Pt sites [141]. Therefore, the catalysis is promoted by the co-operation between Pt and Au. It should be noted, however, that although the Pt clusters may contribute greatly to catalysis, their number must be insignificant, as evidenced by the absence of current peak associated with the presence of Pt clusters during the cyclic voltammetry measurements of formic acid oxidation (not shown here). We also would like to emphasize that although the local structure at the atomic level may not be uniform, the chemical composition of the PtAu NPs is same on the surface and in the interior as confirmed in our previous work [71].

5.5 Summary

In this chapter, it was shown that PtAu alloy colloids with variable composition can be formed by PLAL using a series of targets. These targets were made by simple compression molding of a physical mixture of Au and Pt powders. Characterizations confirm that the composition of the alloy colloid is the same throughout its volume and that the outermost surface layer has the same composition as that of the interior, even if bulk Pt and Au have a large miscibility gap. Over a wide range of pH and at all laser fluences investigated herein, the formation of alloy NPs and their compositions are insensitive to both parameters, suggesting the robustness of this newly developed approach. I further coupled the alloy NPs onto CeO_2 NTs to form nanohybrid structures for catalysis measurement in 4-NP reduction. The unique surface features of PLAL-NPs are mainly responsible for their robust adsorption onto the NTs, without any additional surface functionalization to either

component. The effect of the Pt content on catalysis shows that supported alloys with lower Pt content significantly increase the reaction rate. This finding can be explained by the improved hydrogen dissociation efficiency on NP surface induced by alloying an appropriate amount of Pt into AuNPs. Last but not least, this colloidal alloy NP fabrication technique, i.e., the liquid phase laser ablation on a single metal-mixture target (not a homogeneous alloy target), can in principle be readily extended to prepare other colloidal alloy NPs, including those with bulk-immiscible metals, at various compositions in a controlled fashion. Thusly prepared alloy NPs may find important applications in a wide variety of catalytic reactions.

SECTION (II): Surface Modification of AuNPs by Laser Irradiation and its Influence on Stability and Amine-AuNP Interactions

Chapter 6

Modification of Chemically Synthesized AuNPs using Laser Irradiation:

(I) Influence on Colloidal Stability

Starting with this chapter, I focus on the second objective of using laser irradiated AuNPs to study the influence of surface chemistry variation introduced by laser treatment on AuNP properties.

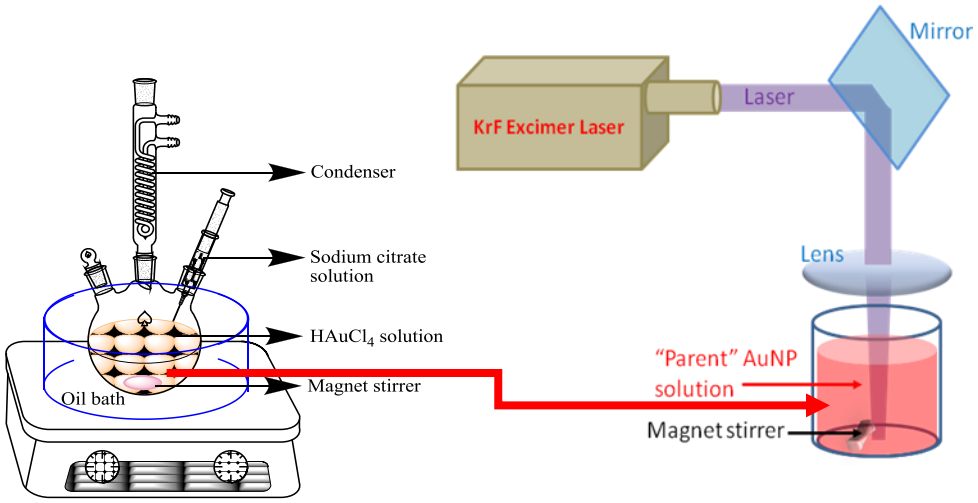

Scheme 6.1 Schematic illustration of the laser irradiation of a pre-synthesized AuNP colloidal solution.

The laser irradiation method is basically a two-step approach combining chemical and physical techniques for the synthesis of small AuNPs. In the first step, "parent" AuNPs with a particle size of around 20 nm in diameter were synthesized by the "Frens" method — reducing auric acid with sodium citrate as a reducing agent [18], and in the following step, a laser irradiation process was performed on the "parent" AuNP solution to reduce particle size and modify the NP

surface chemistry as shown in Scheme 6.1 (please see Section 2.3 in Chapter 2 for experimental details).

It is obvious that the major differences between laser irradiation and PLAL in my study are as follows:

1) A "parent" AuNP solution has to be synthesized by a chemical approach before laser irradiation;

2) During laser irradiation, there is no target submerged in the solution; instead, the "Parent" Au colloidal solution will be irradiated by laser;

3) The beam is not focused in solution.

In the following chapter, I present the treatment of the AuNPs by laser irradiation and the study of their colloidal stability after laser irradiation.

6.1 Preparation of AuNPs by Laser Irradiation

As stability study requires AuNPs to be well dispersed in aqueous systems for assessment, it is necessary to find the optimal experimental conditions for high quality AuNP preparation. In the irradiation process, although the influences of laser parameters on the NP morphology have been previously investigated, the role of the surrounding solution in the fragmentation of AuNPs has not been reported. It is well known that the agglomeration of NPs strongly depends on surface stabilizing molecules or ligands [34, 35, 57, 59]. As laser irradiation leads to a size reduction and a therefore significantly increased surface area of AuNPs in solution, more ligands may be needed in the original solution to support the surface area increase so as to guarantee a similar ligand coverage on surface of the AuNPs and a similar dispersion capability during laser irradiation. On the other hand, it has to be realized that excess, "free" ligands may degrade the stability of gold colloids and lead to the agglomeration of AuNPs by acting as electrolytes. Therefore, it is of great importance to

study the effect of the sodium citrate concentration on the photo fragmentation of AuNPs undergoing laser irradiation.

In this work, 5-nm AuNPs with a narrow size distribution were prepared successfully and efficiently using a combination of citrate reduction of auric acid and laser irradiation in a hazardous-chemical-free environment. The irradiated AuNPs are used for the assessment of the colloidal stability.

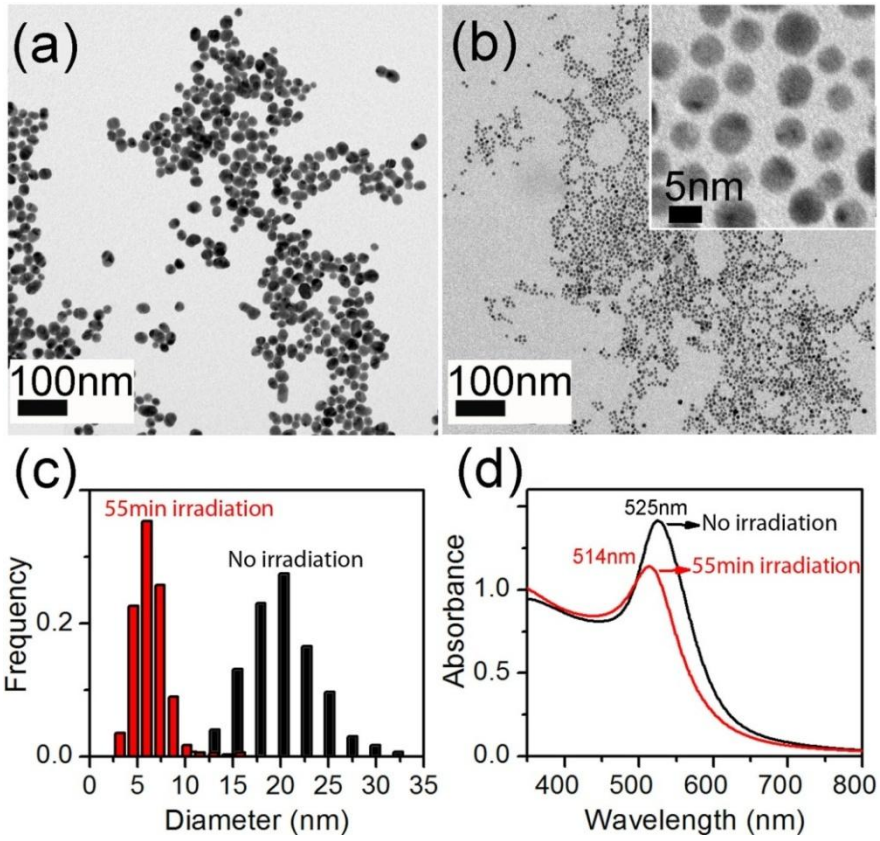

Figure 6.1 TEM images of AuNPs before (a), and after (b) laser irradiation. The inset shows the high magnification TEM image of irradiated AuNPs (b); (c) Histograms of NP size distribution for the original 20-nm (a) and irradiated (b) samples. (d) UV-Vis absorption spectra of gold colloids, before and after laser irradiation.

Figure 6.1 shows the TEM images of the parent 20-nm AuNPs before (a) and after (b) 55 minutes of laser irradiation prepared under the optimized conditions. TEM analysis reveals that laser irradiation leads to a size decrease from (20.2 ±3.4) nm for the original (non-irradiated) sample, to

(5.7±1.5) nm for irradiated AuNPs (Figure 6.1-c). It is important to note that the fragmentation of NPs leads to a significant increase in their number concentration. As supported by NAA, the particle concentration (number of particles per unit volume) from this preparation is about 1.45×10^{15}/mL, which is 10^3 times higher than that achieved by the traditional laser ablation method [92]. The size reduction is consistent with the UV-Vis spectrum change shown in Figure 6.1-d. The SPR peak position of irradiated AuNPs exhibits an 11-nm blue shift, while the FWHM remains similar for both samples.

6.1.1 Effect of Citrate Concentration

Table 6.1 The concentrations of sodium citrate introduced after the particle synthesis and purification, before laser irradiation.

Au colloids for irradiation	Concentration of the loaded sodium citrate solution (mM)
1	0 (pure water)
2	6.2
3	11.2
4	16.2

The effect of citrate ligands on the shape and dispersion of laser irradiated AuNPs was investigated by varying the sodium citrate concentration of the purified "parent" 20-nm Au colloidal solution, as described in section 2.3.1 of Chapter 2. As listed in Table 6.1, the prepared Au colloidal samples are denoted as samples 1−4, with the increasing sample number corresponding to an increasing sodium citrate concentration. It should be noted that although pure water was loaded in the case of sample 1, the NPs in this sample were also covered by citrate groups, which were introduced during the particle synthesis by the Frens method.

Figure 6.2 shows the UV-Vis spectra of samples 1-4 after being irradiated by the UV laser for 55 minutes. For clarity, only one typical spectrum of the sample before laser irradiation is included.

The exact position and the FWHM of the SPR peak of all the samples before and after laser irradiation can be found in Table 6.2.

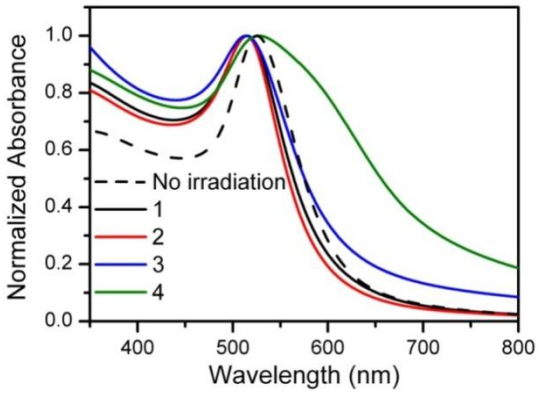

Figure 6.2 UV-Vis spectra of Au colloid samples 1-4 with increasing citrate concentration after the 55-min irradiation. For comparison a typical UV-Vis spectrum (dashed curve) of the original gold colloid without laser treatment is also included.

Table 6.2 SPR peak characteristics of samples before and after laser irradiation

Sample	SPR peak position (nm)		FWHM (nm)	
	Before irradiation	After irradiation	Before irradiation	After irradiation
1	525	515	100	98
2	525	514	100	90
3	525	513	103	120
4	527	528	112	256

Basically, with the addition of sodium citrate, the UV-Vis curves do not alter much among the samples investigated herein, although the sample 4 does show a slight red shift (2 nm) and peak broadening (12 nm). It is clear that except for the sample 4, all the other samples exhibit a blue shift of approximately 10 nm after laser irradiation. As our focus is on the effect of citrate concentration on the morphology of laser irradiated particles, in the following we will mainly compare the spectra of laser irradiated samples 1-4. The spectra of laser irradiated samples 1 and 2 appear quite similar as clearly shown in Figure 6.2. Although centered at the nearly same wavelength as those of samples 1 and 2, the SPR spectrum of sample 3 shows a slightly enhanced absorption at longer wavelengths. A remarkably different spectrum was observed for sample 4, which exhibits a

significantly broadened peak at 528 nm and considerably increased absorption at longer wavelengths. Furthermore, instead of a blue shifts of ~ 10 nm as displayed in all the other samples, the SPR peak of sample 4 red-shifts by 1 nm with respect to that of its initial sample before laser irradiation.

The UV-Vis absorption spectrum of spherical AuNPs has often been correlated with the size and agglomeration status of the particles. Generally, a SPR peak located at a shorter wavelength indicates that the particles are of smaller size, and a narrower peak width reflects a narrower size distribution of particles. On the other hand, the red-shift of the SPR peak, the increased absorption at longer wavelengths and peak broadening have normally been attributed to particle agglomeration [4, 16]. Therefore, according to the data in Table 6.2, we can deduce that laser irradiation causes a significant size reduction in the samples 1, 2 and 3. In addition, from laser irradiated samples 1 to 3, the average size decreases gradually, and among them samples 1 and 2 show similarly narrower size distributions, while sample 3 presents a wider size distribution. Sample 3 may contain either larger particles or some agglomerates, which contribute to the increased FWHM and absorption at longer wavelengths. In order to confirm this interpretation of the UV-Vis spectra, TEM was applied to observe the size and agglomeration status of laser irradiated particles directly.

Figure 6.3 presents the TEM images of the laser irradiated samples. After laser treatment, sample 1 shows individually dispersed particles without any obvious sign of particle coalescence and the particle size is around 6.4 nm in diameter, much smaller than that (20.2 nm) of the initial particles. The sample 2 exhibits a quite similar morphology and most of the particles are still individually dispersed. Consistent with the UV-Vis absorption results, the average size of the NPs (5.7 nm) in sample 2 is slightly smaller than that (6.4 nm) of sample 1. It is worth recalling that this sample shows a narrow SPR peak than sample 1 due to the narrower size distribution (based on TEM images) of individually dispersed particles in this sample even though at the same time it

contains a very small fraction of particle dimers. Obviously, the effect of the former dominates the UV-Vis spectrum in this case.

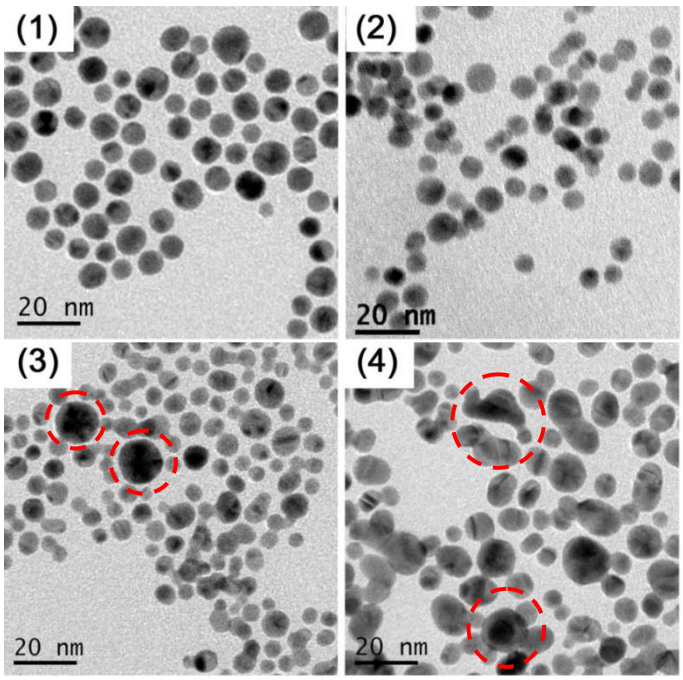

Figure 6.3 TEM images of samples 1-4 with increasing citrate concentration after 55-min laser irradiation; Circles mark the representative fused particles and single bigger particles.

Many more particle dimers, trimers and multimers as well as single bigger particles (>10 nm) were observed in sample 3, which undoubtable account for the increased absorption at longer wavelengths. The average size of non-agglomerated particles was found to be 5.1 nm, which is smaller than those of samples 1 and 2 and explains its more blue-shifted SPR peak. The particle agglomeration is most obvious in sample 4 according to these TEM images. Numerous irregularly shaped large agglomerates were observed in addition to single particles, with the largest ones close to 20 nm in size and the tiniest ones smaller than 5 nm. It is these agglomerates and large particles, which represent a considerably large proportion, that dominate the UV-Vis spectrum of this sample.

In laser irradiation, size reduction arises from the laser-induced fragmentation effect and has been previously reported to be dominated by laser parameters [146, 147]. In our experiment, the

laser parameters have been fixed for all the samples, so the influence of laser parameters on the variations in size and shape of the NPs can be neglected. According to the data obtained, the average size of individually dispersed particles gradually decreases from 6.4 nm to 5.1 nm with increasing citrate concentration. It is known that an increased ligand concentration can make an important contribution to the preparation of smaller NPs during the chemical synthesis process. The same trend observed in our experiment strongly indicates that the concentration of ligands also affects the size of particles prepared from laser processing. On the other hand, it is noted that increasing the citrate concentration induces a more significant coalescence of particles. It is most likely that the excess citrate molecules (i.e., those not attached to the gold particle surface) act as electrolytes and destabilize the colloidal solution, especially in sample 4, and laser irradiation quite possibly aids the formation of permanent agglomerates by melting and fusing initially loosely agglomerated particles. Therefore, the dispersion status seems to depend on the complicated interplay of the laser fragmental and subsequent fusion effect, the ligand stabilization effect and an electrolyte-induced aggregation effect and such interactions between the laser, the particles, ligands and electrolytes must be dynamic and ever changing during laser irradiation. With all these complexities, it is certain that the presence of ligands can significantly modify the laser-matter interaction and alter the morphology of particles during laser irradiation. Our experimental results show that when non-agglomerated NPs are desired, the as-purified colloidal solution (sample 1) without any post-synthesis added citrate should be used for laser irradiation, whereas when a narrower SPR band is most important, a citrate concentration of 6.2 mM (added after synthesis, sample 2) is the optimum concentration under these laser parameters.

6.2 Stability of Laser Irradiated AuNPs

To evaluate correctly the stability of gold colloids after laser irradiation, it is necessary to exclude the effect of NP size on the colloidal stability and to compare NPs of the same size. Besides,

it has been reported that highly intense UV light irradiation on sodium citrate and citrate-capped silver colloids photo-oxidizes citrate groups [151, 152], which changes the surface ligand on NPs. Therefore, a ligand exchange step was performed on the irradiated sample (prepared in 6.2 mM sodium citrate solution) using citrate solution to recover the citrate ligand layer. These ligand-exchanged irradiated AuNPs a with good particle size distribution were chosen for stability assessment. Moreover, the citrate capped Chem-AuNPs of ~5 nm in diameter used in the catalysis study of Chapter 3, were synthesized again for stability comparison. Figure 6.4-a shows the TEM images of the 5-nm AuNPs prepared by the $NaBH_4$ reduction reaction. Figure 6.4-b shows the UV-Vis spectra of the laser irradiated AuNPs and 5-nm AuNPs prepared by $NaBH_4$ reduction. The spectra exhibit SPR peaks located at 514 nm and 513 nm, respectively, and both show a similar FWHM of about 100 nm.

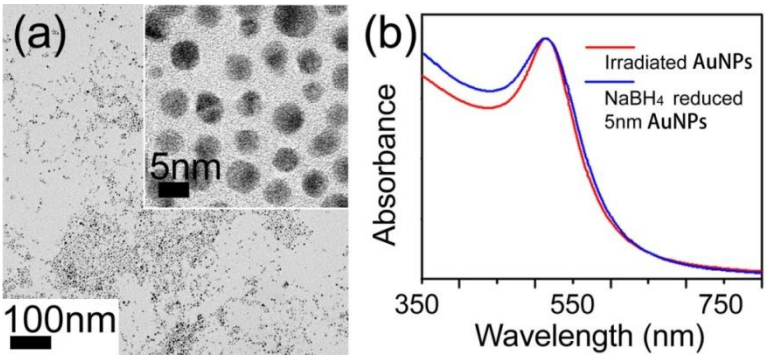

Figure 6.4 TEM image of $NaBH_4$ reduced 5-nm AuNPs (a). Inset shows the high magnification TEM image. (b) UV-Vis spectra of laser irradiated AuNPs and chemically prepared 5-nm AuNPs.

In order to investigate the stability of the AuNPs prepared by laser treatment and compare it to that of chemically prepared AuNPs, the methods of ethanol and salt-induced aggregation were used, in which the dielectric constant and ionic concentration of the dispersion environment respectively, were adjusted. All samples were purified and re-dispersed in 1.25 mM sodium citrate solution to achieve the same particle and electrolyte concentration for a fair comparison.

6.2.1 Ethanol Induced Aggregation

It is well known that the UV-Vis absorption spectra of gold colloids are very sensitive to the change of the particle dispersion status [41, 79]. Generally, the agglomeration of AuNPs yields a significant red shift and broadening in the absorption spectrum due to the perturbation in the SPR related to the inter-particle electron coupling [41, 79]. Also, the NP agglomeration is associated with a considerable decrease in the absorption intensity of AuNPs at the initial SPR peak position and an increase in the absorption intensity at longer wavelengths [79]. Figure 6.5-a shows the UV-Vis absorption spectra of AuNP solutions at pH values of 5.6 and 6.6 before (solid line) and after (dashed line) adding ethanol to the solution and incubating for 4 hours (volume ratio of colloidal solution: ethanol = 2:1). These two pH values are higher than the second (4.8) and third (6.4) dissociation constants (pK_a) of citric acid, respectively. Generally a higher pH (6.4 herein) value indicates more carboxy groups of citric ligand dissociate and thus leads to more negative charges on the NP surface.

The most significant difference in the stability of laser-irradiated and purely chemically prepared AuNPs has been observed for pH 6.6. The absorption spectra of the irradiated AuNPs (red) and $NaBH_4$ reduced 5-nm (blue) NPs before the addition of ethanol exhibit narrow peaks with a similar SPR position and FWHM as shown in Figure 6.5-a. Four hours after ethanol addition, very small changes in peak position (5 nm red shift) and FWHM (118 nm vs. 100 nm) can be observed for the irradiated NPs, while the $NaBH_4$ reduced 5-nm AuNP sample undergoes a remarkable red shift of about 19 nm, and the peak FWHM increases to 176 nm. The noticeable variation in the optical absorption of the colloidal solutions due to the ethanol-induced aggregation of AuNPs is clearly visible in the photographs shown in the right part of Figure 6.5-a. It is worth mentioning that although higher pH values (> 6.6) lead to increased stability for both samples, the laser irradiated sample always appears to be less affected by the addition of ethanol.

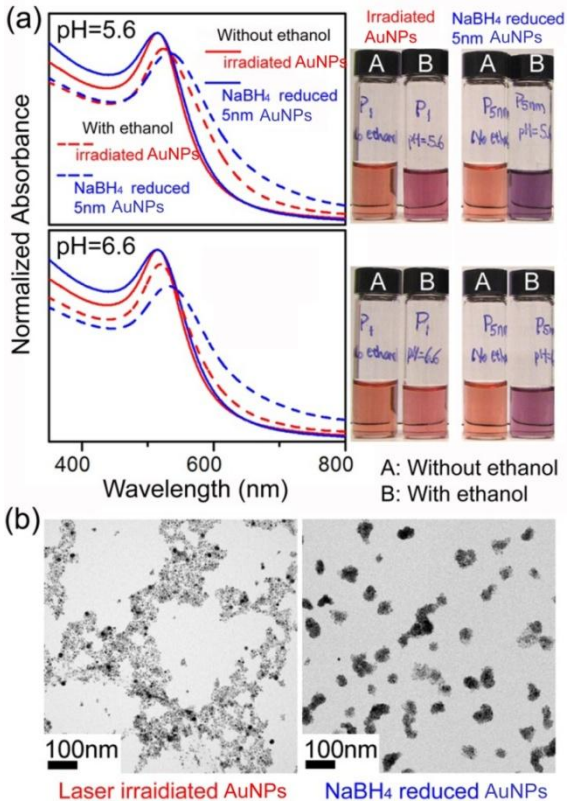

Figure 6.5 (a) UV-Vis spectra of irradiated (red) and $NaBH_4$ reduced (blue) AuNPs at pH 5.6 and pH 6.6. Solid and dashed lines represent the colloids before and after being mixed with ethanol for 4 hrs, respectively; photographs show the color change of the colloidal solutions due to the ethanol-induced aggregation of AuNPs. (b) TEM images of AuNPs prepared after ethanol-induced aggregation experiments of irradiated (left), and $NaBH_4$ reduced 5-nm (right) samples.

The ethanol-induced agglomeration of AuNP samples was also observed by TEM. Figure 6.5-b shows TEM images of AuNPs prepared by laser irradiation (left) and $NaBH_4$ reduction (right) after being mixed with ethanol for 4 hours at pH 5.6. According to these TEM images, the $NaBH_4$ reduced sample undergoes a fierce agglomeration and clusters of about 100 nm in diameter can be easily observed. In clear contrast, the laser irradiated AuNPs basically remain well dispersed. These observations are in excellent agreement with the absorption spectra shown in Figure 6.5-a and thus strongly suggest that the stability of laser-irradiated AuNPs is superior to that of the $NaBH_4$ reduced NPs.

6.2.2 Salt Induced Aggregation

The influence of a monovalent salt on the stability of the AuNPs was investigated by the addition of 0.1 M NaCl aqueous solution into colloidal gold solutions [57]. The electrolyte-induced aggregation can be generally explained as a result of the compression of the electrical double layer and consequently the weakening of electrostatic repulsion forces [148]. UV-Vis absorption spectra were again used to estimate the salt-induced aggregation of AuNPs.

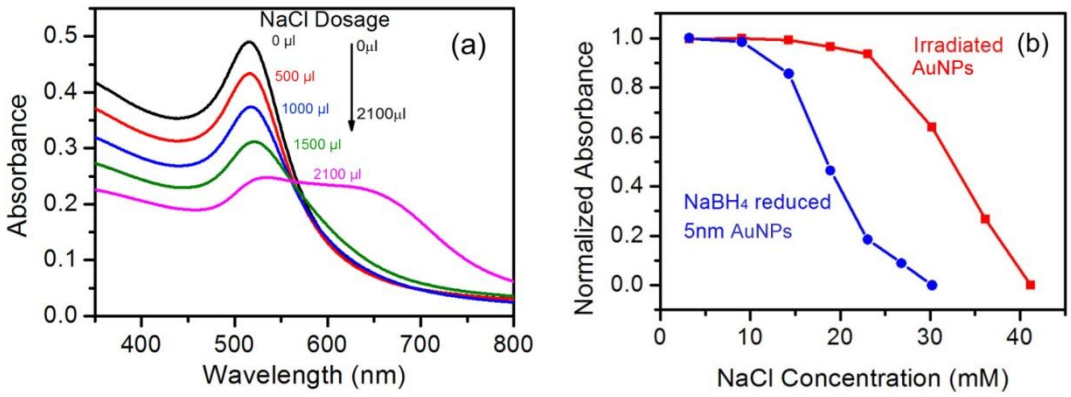

Figure 6.6 (a) The absorption spectra of the laser irradiated AuNPs at pH 5.6 for various quantities of 0.1M NaCl solution; (b) the normalized absorption intensity at a wavelength of 514 nm of the irradiated AuNPs (red square) and $NaBH_4$ reduced 5-nm (blue circle) AuNPs at pH 5.6 as a function of final NaCl concentration in solution mixture.

Figure 6.6-a shows the evolution of the UV-Vis spectra of the laser-irradiated AuNP solution at pH 5.6 upon the addition of different amounts of 0.1 M NaCl solution. For relatively small amounts of NaCl (less than 27 mM), the changes in the absorption spectrum due to the addition of salt solution are insignificant and the decrease in the absorption intensity at the SPR peak position of 514 nm merely results from the dilution of the colloidal solution. However, for the $NaBH_4$ reduced sample the slight intensity decrease proportional to the decreasing AuNP concentration was only observed for NaCl concentrations less than 10 mM (Figure 6.6-b). With the further increase of the NaCl concentration (more than 10 mM), the absorption peak intensity at 514 nm decreases rapidly and this is accompanied by the significant red shift and broadening

of the peak which clearly indicate the formation of AuNP agglomerates in dispersion. The "critical point" associated with a significant decrease in the peak intensity due to NP agglomeration occurs at a much higher NaCl concentration for irradiated AuNPs (27 mM NaCl) than for the $NaBH_4$ reduced NPs (10 mM NaCl). A similar behaviour of the absorption intensity as a function of NaCl concentration was observed for both colloidal gold samples at pH 6.6. These results demonstrate that the stability of the AuNPs created by the laser irradiation method is superior to that of AuNPs prepared by the purely chemical approach, which involves the use of hazardous $NaBH_4$.

6.3 Zeta Potential of Au Colloids

According to the classical Derjaguin-Landau-Verwey-Overbeek (D.L.V.O) theory, Zeta potential can be used as a good indicator of the colloidal solution stability [148]. In order to confirm the improvement in the stability of the laser-irradiated NPs, the Zeta potential of the colloids prepared by these two methods was measured. Figure 6.7 shows the variation of the Zeta potential of the laser-irradiated (red squares) and $NaBH_4$ reduced 5-nm (blue circles) NPs as a function of the pH value of the colloidal solution. The Zeta potential values for $NaBH_4$ reduced AuNPs vary between -37 mV and -50 mV for pH values between 5.0 and 8.0, which indicates the moderate stability of these AuNPs. In case of laser-irradiated NPs, the Zeta potential value varies between -50 mV and -60 mV which corresponds to the good colloidal stability. Also, as expected, an increase of the pH value in an appropriate range leads to an increase of the absolute value of Zeta potential and thus enhances the stability of the the colloidal solutions, for all investigated samples [149, 150]. All these observations perfectly corroborate the experimental results shown in Figure 6.5 and Figure 6.6, confirming higher stability of laser-irradiated AuNPs vs. the $NaBH_4$ reduced AuNPs.

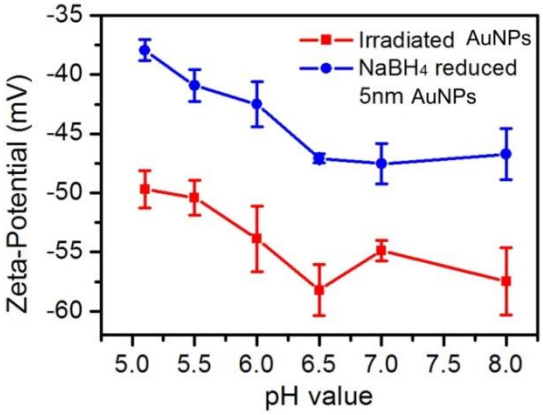

Figure 6.7 Zeta potential of the laser-irradiated and $NaBH_4$ reduced 5-nm AuNPs as a function of pH values of colloidal Au solutions.

6.4 Correlation of Surface Chemistry with Stability

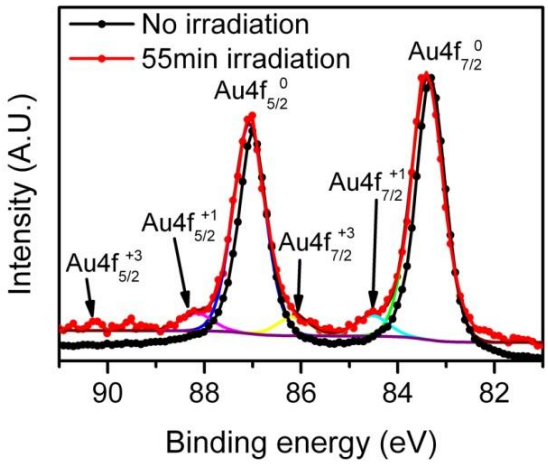

Figure 6.8 High-resolution Au4f XPS spectra of AuNPs before and after 55 minutes of laser irradiation.

To better understand the phenomenon of the increase in colloidal Zeta potential and stability, a property highly dependent on NP surface chemistry [108], upon laser irradiation, the AuNPs have been further characterized by XPS and FTIR. The XPS spectra of AuNPs before (black) and after (red) 55 minutes of laser irradiation are shown in Figure 6.8. Both spectra exhibit two representative sharp peaks at 83.3 and 87.1 eV corresponding to Au $4f_{7/2}$ and $4f_{5/2}$, respectively. For laser irradiated AuNPs, shoulders which can be deconvoluted into four additional peaks were clearly observed. They can be assigned to Au^{+} (84.5 and 88.1 eV) and Au^{3+} (86.1and 90.2 eV), respectively [105]. On

the basis of the relative area of the gold peaks, the respective atomic percentages were estimated to be 89% for Au^0, 11% for Au^+ and Au^{3+}. The XPS spectrum of the laser irradiated sample demonstrates that the laser irradiated AuNPs consist mainly of neutral Au atoms but also contain detectable amounts of oxidized gold species on the surface induced by laser treatment [68, 82]. The surface oxidation of AuNPs is believed to be at the origin of the improved stability of laser irradiated vs. chemically produced AuNPs as it yields $Au\text{-}O^-$ groups which increase the surface negative charges, thus reinforcing the electrostatic repulsion between AuNPs [68, 82].

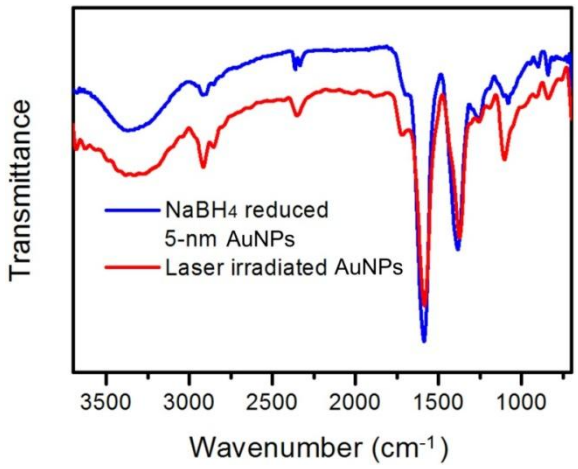

Figure 6.9 FTIR spectra of the same amount of 5-nm AuNP samples prepared by $NaBH_4$ reduction (blue) and laser irradiation (red).

Although the variation of ligands on the surface could be another factor affecting the colloidal stability, we do not think it plays a major role here as the FTIR spectra (Figure 6.9) of the same amount of 5-nm AuNPs prepared by these two methods (and subsequently subjected to the same purification/re-dispersion conditions as those used for the stability comparison) do not exhibit any pronounced difference. Both spectra show the characteristic peaks of asymmetric and symmetric carboxyl (O-C=O) stretching vibration at 1590 and 1394 cm^{-1} for citrate groups [151, 152]. On the other hand, it is worth mentioning that laser treatment does cause some change to sodium citrate, based on our FTIR studies. The appearance of a small peak at 1329 cm^{-1} in the FTIR spectrum of as-

prepared laser irradiated AuNPs (to be shown in Chapter 7) indicates the oxidation of some of citrate into acetonedicarboxylic groups [151]. However, these groups seem to be easily displaced from the AuNP surface by citrate as the peak disappears after the AuNPs are dispersed into 1.25 mM sodium citrate solution for stability testing.

6. 5 Summary

In conclusion, optimized laser irradiation has been applied to reduce the size of chemically prepared AuNPs (20 nm in diameter) in order to produce highly monodispersed Au colloids of ~5 nm in diameter at high concentrations in a hazardous-chemical-free environment. The citrate concentration shows an important effect on NP fragmentation during laser ablation. The stability of such colloids, investigated by using ethanol and salt-induced aggregation, is significantly higher than that of similarly sized AuNPs prepared by a purely chemical approach which involves the use of hazardous $NaBH_4$. This finding is consistent with the considerably increased Zeta potential values of laser irradiated AuNPs, which is believed to be mainly associated with the oxidation of surface Au due to laser processing. An additional benefit of this preparation technique in producing sub-10 nm AuNPs is the quite high particle concentrations that can be achieved. The concentration is estimated to be about 10^3 times higher than that obtainable using laser ablation where the characterization of the AuNPs and their practical applications in biomedicine have been challenging due to low NP concentrations. To summarize, the significant increase in the stability of AuNPs renders this simple technique very promising for the efficient production of highly stable, quite concentrated, ultrasmall nanosized gold colloids for biological applications. This study reveals the significant effect of laser-NP interactions on AuNP surface composition and surface-related properties.

Chapter 7

Modification of Chemically Synthesized AuNPs using Laser Irradiation: (II) Influence on Surface Chemistry and NH_2-AuNP Interaction

Based on the colloidal stability study of laser irradiated AuNPs in Chapter 6, the NP size, surface chemistry and stability have been modified using laser irradiation. The preliminary study on the characterization of surface chemistry verifies that laser treatment oxidizes surface Au. In this Chapter, I go forward to investigate the details of the surface chemistry variation induced by laser treatment, and study its effects on AuNP-NH_2 interactions on the NP surface.

As described in Chapter 1, because of the abundance of amine groups in biological and environmental systems and because the AuNP-amine interaction is the basis of many biomedical applications, the investigation of the interaction between amine molecules and AuNPs and the understanding of their interaction modes become highly important. The formation of oxidized Au species using laser irradition may have an interesting impact on molecular adsorption on AuNPs, the laser technique thus appears to be an excellent tool that offers unexplored possibilities for the investigation of the interaction between amine groups and the oxidized AuNP surface, which has not been reported in literature.

More importantly, it is expected that the surface oxidization of noble metal NPs not only affects their molecule adsorption behavior, but also other surface-sensitive properties. For instance, a recent study reports that a molecule's Raman activity detected from silver (Ag) NP-activated

surface enhanced Raman scattering spectroscopy decreases with the existence of Ag oxide which may change the orientation of molecules as well as induce metal-to-molecule charge transfer [159]. Hence, understanding the influence of surface chemistry on NP properties is not only of great benefit to fundamental research, but is also of significant importance for the development of practical applications.

In this chapter, I address some of the above-mentioned issues and focus on the understanding the effects or the surface chemistry of laser irradiated AuNPs on AuNP-amine interactions.

7.1 Surface Chemistry of AuNP Samples

It is known that the laser irradiation of AuNPs in aqueous solution results in size reduction and surface oxidation [68, 80, 82]. In order to study the effect of surface chemistry modification on particle adsorption properties, optimized irradiation conditions [94] have been applied on the citrate-capped 20-nm AuNPs in order to fabricate 5-nm AuNPs with a narrow size distribution (as mentioned in Chapter 6).

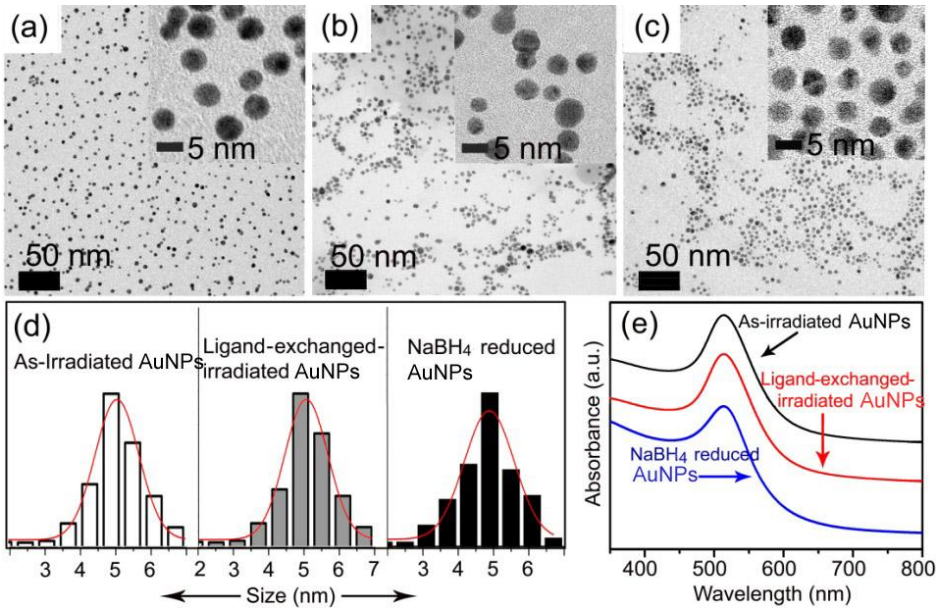

Figure 7.1 TEM images of the AuNPs prepared by laser irradiation before (a) and after (b) citrate ligand-exchange, and by chemical reduction with $NaBH_4$ (c). Insets show corresponding high magnification TEM

images; (d) Histograms of NP size distribution of all three samples. (e) UV-Vis absorption spectra of all three Au colloidal samples.

Figures 7.1-a, b and c show the TEM images of the AuNPs prepared by laser irradiation before and after citrate ligand-exchange, and by the $NaBH_4$ reduction reaction, respectively. TEM analysis reveals that all samples have a similar average particle size (5.0 ± 1.5) nm (see size histograms in Figure 7.1-d).

Figure 7.1-e shows the UV-Vis spectra of these three colloidal samples. The spectra exhibit SPR peaks located at 513 nm for both irradiated AuNPs and 512 nm for the $NaBH_4$ reduced AuNPs, and all show a similar FWHM of about 100 nm. According to TEM observations and UV-Vis spectra analysis, it has been confirmed that the average size and size distribution of NPs are very similar for all the samples investigated herein, which excludes the influence of NP size on the following adsorption capacity assessment.

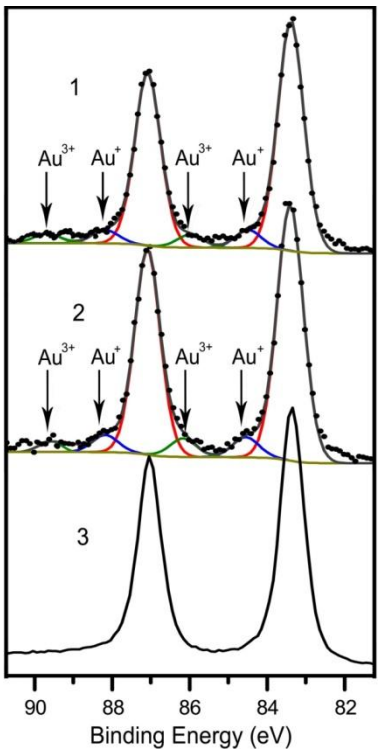

Figure 7.2 High resolution Au4f XPS spectra of the AuNPs modified by laser irradiation before (1) and after (2) citrate ligand-exchange, and the AuNPs produced using the $NaBH_4$ reduction method (3).

In this work, UV-laser irradiation was used to modify the surface chemistry of colloidal AuNPs. In order to examine the modification of surface chemical composition, all samples have been characterized by XPS, FTIR and NMR spectroscopy. Figure 7.2 shows the XPS spectra for the AuNPs prepared by laser irradiation before (curve 1) and after ligand-exchange (curve 2), and by $NaBH_4$ reduction (curve 3), respectively. All spectra exhibit two representative sharp peaks at about 83.3 and 87.1 eV corresponding to Au^0 $4f_{7/2}$ and $4f_{5/2}$, respectively. For the laser irradiated AuNPs both before and after ligand exchange, the deconvolution of their spectra leads to four additional, distinct peaks, which can be assigned to Au^+ (~84.4 and ~88.1 eV) and Au^{3+} (~85.9 and ~89.7 eV) [105]. On the basis of the relative area of the Au peaks, the atomic concentrations were estimated to be ~90% for Au^0, ~10% for Au^+ and Au^{3+}. These data indicate that the laser irradiated AuNPs mainly consist of neutral Au atoms but also contain detectable amounts of oxidized Au components, induced by the laser treatment, on the surface [68, 82]. The chemically produced colloidal Au sample does not show any presence of oxidized Au species (curve 3).

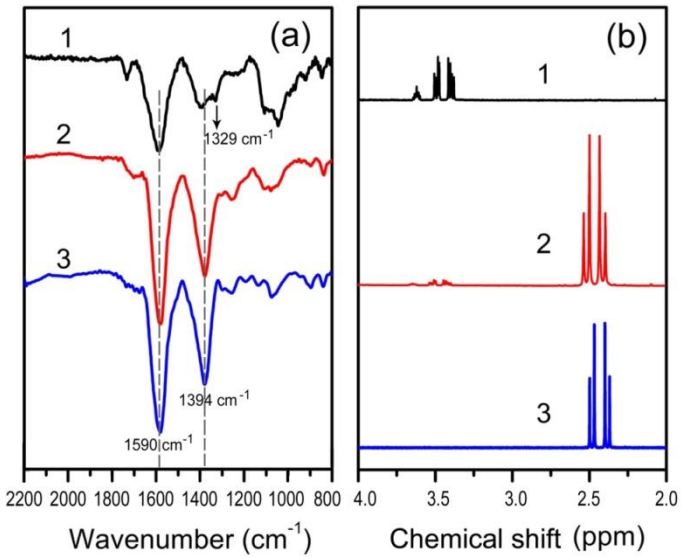

Figure 7.3 FTIR (a) and ^{1}H-NMR (b) spectra of the AuNPs prepared by laser irradiation before (spectrum 1) and after (spectrum 2) ligand-exchange by citrate, and by $NaBH_4$ reduction (spectrum 3).

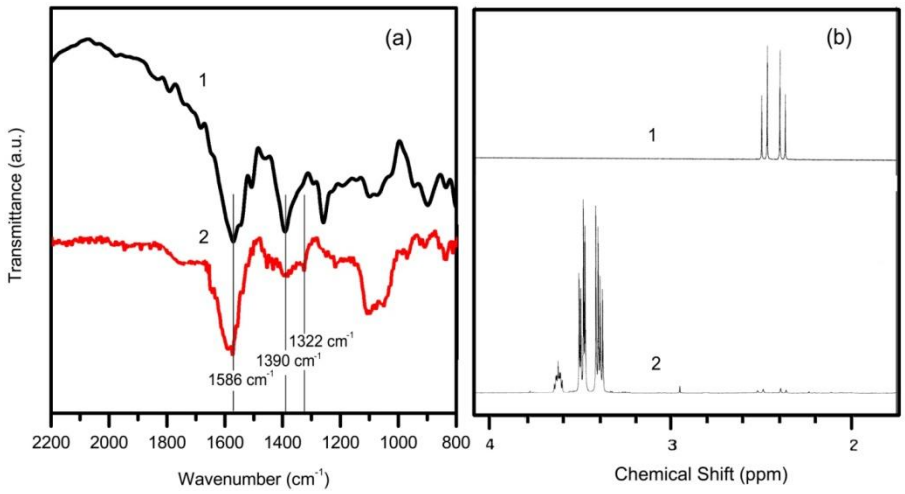

Figure 7.4 FTIR (a) and ^{1}H-NMR (b) spectra of sodium citrate (spectrum 1) and 1, 3-acetonedicarboxylic acid (spectrum 2).

As reported before, highly intense UV light irradiation on sodium citrate and citrate-capped silver colloids photo-oxidizes citrate groups into 1, 3-acetonedicarboxylic groups [151, 152]. In order to verify the surface ligand modification under our specific laser irradiation parameters, all samples have been characterized by FTIR and NMR techniques. Curves 1, 2 and 3 in Figure 7.3-a correspond to the FTIR spectra recorded for the same amount of the as-irradiated, ligand-exchanged-irradiated and $NaBH_4$ reduced AuNPs, respectively. All FTIR spectra show a characteristic peak of the asymmetric carboxyl (O-C=O) stretching vibration at around 1590 cm^{-1}. However, the assignment of the symmetric carboxyl stretching vibration is ambiguous for curve 1 compared with that for curves 2 and 3 at about 1394 cm^{-1} [151, 152]. Moreover, curve 1 displays a new peak at about 1329 cm^{-1}. All these observations are in good agreement with previous reports, implying the oxidization of citrate into 1, 3-acetonedicarboxylate [151, 152]. The FTIR spectra for the ligand-exchanged-irradiated and $NaBH_4$ reduced samples (curves 2 and 3) do not exhibit any pronounced difference and show typical characteristics of citrate ligands. In order to further confirm the deduction from FTIR results, ^{1}H-NMR has been exploited to detect surface ligand variation. Figure 7.3-b shows the ^{1}H-NMR spectra of surface ligands for these three samples. For the as-

irradiated sample, resonances appearing at 3.3-3.5 ppm were observed in spectrum 1, which are assigned to 1, 3-acetonedicarboxylate [160]. After ligand exchange, the NMR spectrum shows intense peaks at 2.3-2.6 ppm (curve 2) assigned to citrate groups are as those shown in curve 3 for the $NaBH_4$ reduced sample [100]. Accordingly both characterization techniques clearly confirm the photo-oxidation of citrate into 1, 3-acetonedicarboxylic groups in the laser irradiated sample. The overlapping of the spectrum 2 and 3 in both characterizations indicates that the ligand exchange process of replacing 1, 3-acetondicarboxylate with citrate is highly successful. To provide more straightforward comparison, FTIR and ^{1}H-NMR spectra of pure sodium citrate and 1, 3-acetonedicarboxylic acid are shown in Figure 7.4. Through the comparison, it is clearly seen that the spectrum shape of the two ligands, citrate and 1, 3-acetonedicarboxylate on the AuNP surface follows perfectly that of the pure sodium citrate and 1, 3-acetonedicarboxylic acid, confirming the analysis of ligand molecule structure on the AuNP surface.

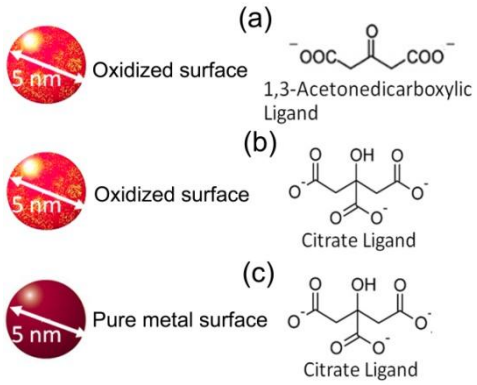

Scheme 7.1 Surface characteristics of the AuNPs prepared by laser-irradiation before (a) and after (b) ligand exchange using citrate, and by $NaBH_4$ reduction (c).

According to these surface chemistry analyses, the characteristics of three different kinds of AuNPs have been recognized and illustrated in Scheme 7.1. The particle size is equal to ~5 nm in diameter for all investigated samples. The surface metal and surface ligand of the as-irradiated AuNPs are, at least partially, oxidized (Scheme 7.1-a). After ligand-exchange, the oxidized ligands

are completely displaced by citrate ligands and therefore, in the ligand-exchanged-irradiated sample the partially oxidized Au metal surface is covered by citrate ligands (Scheme 7.1-b). Only the chemically prepared AuNPs have a pure Au^0 surface, which is capped by citrate ligands (Scheme 7.1-c).

7.2 AuNP-MAP Conjugation

7.2.1 Optimizing MAP Concentration for Conjugation with AuNPs

Before the conjugation of MAP with AuNPs, the particle concentration of all Au colloidal samples has to be adjusted and equalized, which was achieved by using the measurement with UV-Vis spectrometer to get the same absorbance at the SPR peak (specifically, absorbance = 0.5 at 513nm). The Au concentration was further quantified by NAA elemental analysis, which shows the similar Au concentration of 91.8 and 94.1 ppm for the laser treated and chemically prepared samples, respectively. Considering the similar size distribution, the NAA results suggest that all the samples for conjugation have a quite similar particle concentration and therefore are appropriate for a fair comparison. Besides, the pH value of all samples has been adjusted to 5.5 or 7.0, which are higher than the second (4.8) and/or third (6.4) pKa values of citric acid, respectively.

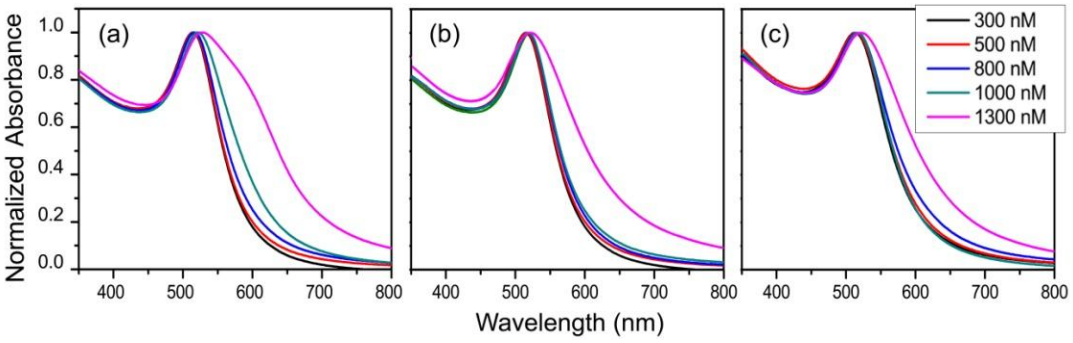

Figure 7.5 UV-Vis spectra for AuNP-MAP conjugation solutions with different MAP concentrations. The AuNP samples were prepared by laser-irradiation before (a) and after (b) ligand exchange using citrate, and by $NaBH_4$ reduction (c). The spectra were taken 6 hours after MAP was introduced into the AuNP solutions.

In order to avoid the aggregation of AuNPs in the conjugation process, the concentration of MAP in colloidal solutions has to be optimized first. To do so, UV-Vis absorption spectroscopy was used to monitor the particle dispersion status in the solutions. Generally, the agglomeration of AuNPs leads to a significant red shift and considerable broadening of the SPR peak in their absorption spectra due to the perturbation in SPR related to the inter-particle electron coupling [16]. Figure 7.5 shows the UV-Vis spectra of the conjugation solutions at pH 5.5 at different MAP concentrations, containing the laser-irradiated AuNPs before (a) and after (b) ligand exchange with citrate, and chemically prepared NPs (c). For relatively low MAP concentrations (less than 1000 nM), the changes in the absorption spectra due to the adsorption of MAP to the AuNP surface are insignificant for all samples. A considerable variation of the dispersion status of all samples was observed when the MAP concentration reaches 1300 nM (pink curves), as evidenced by the obvious peak broadening and red shift shown in the UV-Vis spectra. Although a MAP concentration of 300 nM does not cause any aggregation of AuNPs, it is difficult to calculate the adsorption of MAP on AuNPs accurately using PL spectroscopy (details shown in the following part) due to the rather low PL signal intensity at this conjugation concentration. Accordingly, the MAP concentration in the conjugation solutions was set at 500, 800 or 1000 nM. Similar variations in the spectra have also been observed for the conjugation solutions at pH 7.0.

7.2.2 Quantifying Adsorption of MAP

UV-Vis absorption spectroscopy has often been used to evaluate the concentration of chromophores, such as MAP, by correlating their absorbance with concentration. For assessing the adsorption of MAP on the AuNPs, absorption measurements should be performed on un-conjugated "free" MAP molecules remaining in the filtrate solution, based on which the number of adsorbed MAP molecules can be straightforwardly derived. However, in the current study the concentration

of the "free" MAP molecules in the filtrate solution was too low to be detected accurately. On the other hand, the fluorescence technique is recognized to be more sensitive for measuring MAP at very low concentration [161, 162], where the PL intensity is linearly related to concentration (not shown here). Therefore PL measurements enable us to quantify the "free" un-adsorbed and thereby adsorbed MAP molecules accurately. The proportion of adsorbed MAP molecules (P_{ads}) can be calculated by the following equation:

$$P_{ads} = \left(1 - \frac{I_1}{I_0}\right) \times 100\%$$

Where, I_1 is the PL intensity (at 380 nm) of the "free" MAP in the filtrate solution; and I_0 is the PL intensity (at 380 nm) of the MAP solution at initial concentrations of 500, 800 or 1000 nM.

Figure 7.6-a shows one typical set of PL spectra of the filtrate solutions after conjugation of three colloidal Au samples with 800 nM of MAP at pH=5.5. The PL intensity at 380 nm of the filtrate solution of the irradiated samples before and after ligand exchange is obviously higher than that of the $NaBH_4$ reduced sample. The filtrate of the as-irradiated sample displays the highest PL intensity among all samples. Based on the PL measurements, the adsorption of MAP (%) has been calculated and shown in Figure 7.6-b. It can be seen that the difference in adsorption among samples increases with increasing MAP concentration. Specifically, all samples exhibit similarly high MAP adsorption capacity (~99%) at a lower MAP concentration of 500 nM. In the case of the MAP concentration of 1000 nM, the most noticeable adsorption variation of these three samples was observed. There are only 86% and 94 % of MAP molecules adsorbed on the surface of the laser irradiated samples before and after ligand exchange, respectively, while the $NaBH_4$ reduced sample still shows a good MAP adsorption of ~99 %. A similar trend was observed at pH 7.0. The PL measurements on the filtrates demonstrate that the MAP adsorption capacity decreases in the following order: $NaBH_4$ reduced > ligand-exchanged-irradiated > as-irradiated samples. It is clear

that the MAP adsorption capacity of the AuNPs prepared by the laser irradiation method is inferior to that of similarly sized citrate-capped AuNPs prepared by the purely chemical approach.

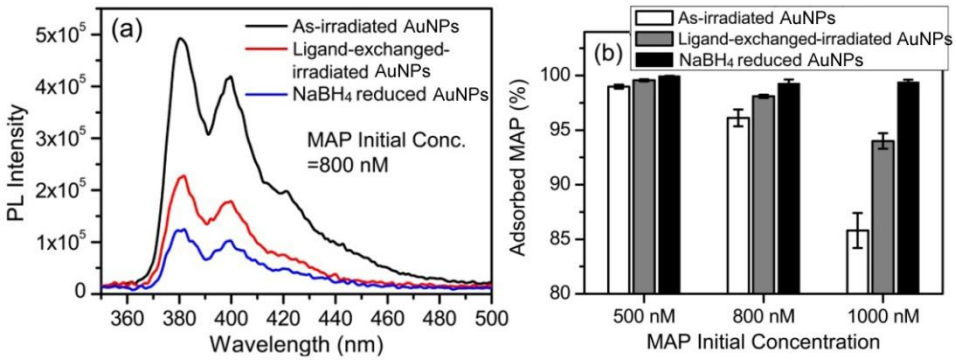

Figure 7.6 (a) PL spectra of the filtrate solutions after conjugating 800 nM MAP with the laser-irradiated samples before and after ligand exchange with citrate, and with the chemically prepared NPs at pH=5.5. (b) Adsorption of 500, 800 and 1000 nM of MAP to the three types of AuNPs at pH=5.5.

In terms of the adsorption of amine groups on the ligand capped AuNP surface, two principal interaction mechanisms have been proposed [150]. The first one is based on electrostatic binding and the second one is the so-called displacement hypothesis. In the first case, the amine groups anchor onto the AuNP surface through the electrostatic attraction between the positively charged amine groups and the negatively charged ligands on the AuNP surface. The displacement hypothesis assumes that the amine groups directly interact with the surface Au to form Au-N bonds by replacing the original ligands. As no such studies have been conducted on the oxidized AuNP surface, detailed investigations need to be performed to identify the dominating interaction mechanism and to understand the interesting decrease in the MAP adsorption observed in the laser irradiated samples.

In order to identify the dominant interaction, the Zeta-potential of all three colloidal Au samples has been measured. Zeta-potential has been widely used as a good indicator of the surface charge of colloidal NPs [148], which can contribute to the electrostatic adsorption [150]. Figure 7.7 shows the Zeta-potential of three types of freshly prepared colloidal samples as a function of their

pH values. The measured Zeta-potential values of the as-irradiated sample vary between -49 and -60 mV in the pH range of 5.5 - 7.0. After ligand exchange, the Zeta-potential values considerably decrease, ranging from -57 to -74 mV, for all pH values. In case of the $NaBH_4$ reduced sample, the Zeta-potential values are in between -30 and -47 mV.

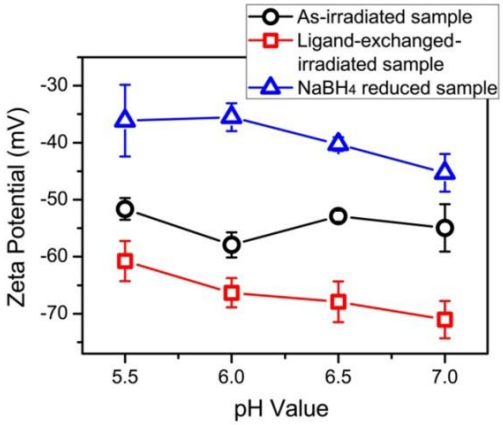

Figure 7.7 Zeta potential of the laser-irradiated AuNPs before and after ligand exchange, and the $NaBH_4$ reduced AuNPs as a function of pH values of Au colloidal solutions.

The increase in the absolute Zeta-potential of the samples prepared by laser irradiation is mainly attributed to the presence of oxidized Au species [68, 80, 82]. The more negative Zeta-potential values of the laser irradiated samples indicate more negative charges on the particle surfaces, which are thus expected to adsorb more positively charged MAP molecules electrostatically [163]. However, this expectation is inconsistent with the observation in the PL measurements, i.e., the chemically prepared AuNPs show a higher MAP adsorption. It may suggest that the electrostatic interaction does not dominate the AuNP-MAP interaction in the laser irradiated samples. Moreover, although the oxidized surface possesses more negative charges, unlike negatively charged ligands, they may not be accessible to the positively charged amine groups.

In order to gain further understanding, it is important to quantify the surface ligands, which are negatively charged as well as easily accessible to MAP, for all samples and make a comparison. To do so, TGA measurements were carried out and the results are shown in Figure 7.8.

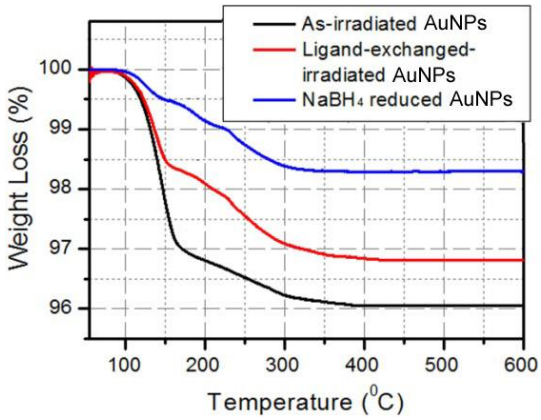

Figure 7.8 TGA data recorded from the as-irradiated AuNPs before and after ligand exchange with citrate, and the $NaBH_4$ reduced citrate-capped AuNPs.

TGA traces for all samples show an initial sharp decrease in mass between 100 and 170 ℃, followed by a gradual mass loss up to 400 ℃. The initial mass loss is likely due to water desorption. As the temperature increases beyond 170 ℃, surface-bound ligands desorb and are volatilized [164, 165], which is responsible for the mass loss of 0.9 wt %, 1.4 wt % and 1.2 wt % in the second stage (170-400 ℃) for the laser irradiated, ligand-exchanged-irradiated and chemically prepared AuNPs, respectively. These values correspond to 0.016 mol %, 0.022 mol % and 0.019 mol % of carboxyl groups, respectively, in these three samples. The lower percentage of the carboxyl groups in the as-irradiated sample, as compared with the other two samples, may partially account for the lower MAP adsorption in this sample. In case of the citrate ligand-exchanged-irradiated sample, the higher percentage of carboxyl groups on the surface should lead to the highest MAP adsorption capacity, if adsorption is solely based on electrostatic attraction. However, the observation that its MAP adsorption capacity is still less than that of the chemical NPs, clarifies that the electrostatic interaction is not the dominating mechanism for the AuNP-MAP interaction. Zeta-potential and TGA measurements together reveal that although in general the as-irradiated AuNPs have a higher total surface charge density as compared with the chemically prepared AuNPs, they have fewer

negatively charged carboxyl groups, which may be more readily involved in the electrostatic interaction than the negatively charged oxidized Au species.

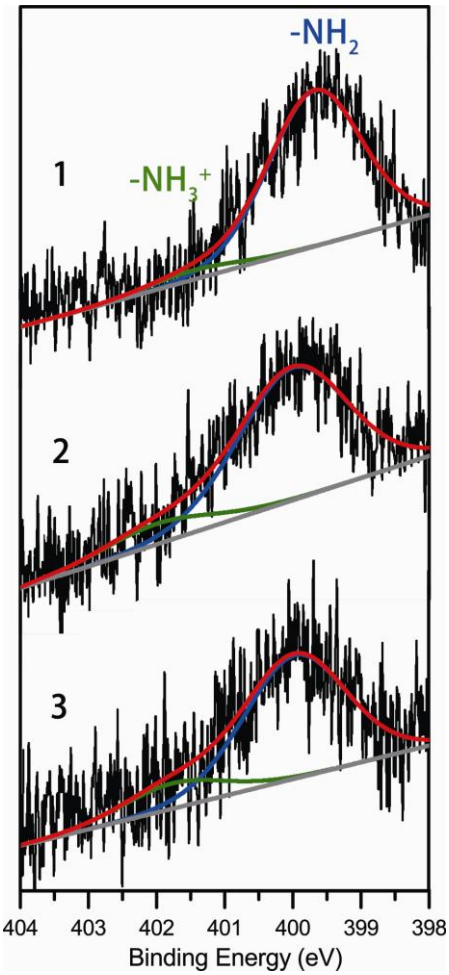

Figure 7.9 N1s XPS spectra of MAP conjugated AuNPs prepared by laser irradiation before (1) and after (2) ligand-exchange with citrate, and by $NaBH_4$ reduction (3).

In order to determine the dominant interaction mode and better understand the nature of bonding between the AuNPs and MAP, XPS analysis was applied on MAP adsorbed AuNP samples. The high resolution N1s XPS spectra of the surface-bound MAP are presented in Figure 7.9. Curves 1 and 2 correspond to the irradiated samples before and after citrate-exchange, respectively, while curve 3 represents the $NaBH_4$ reduced sample. The nitrogen spectrum for each sample could be resolved into two chemically distinct species centered at ~399.9 and ~402.1 eV, respectively. The

higher binding energy component ($N_{indirect}$) is assigned to the electron emission from nitrogen in the protonated amine groups ($-NH_3^+$) electrostatically complexed with the COO^- group of the surface ligands, and/or the oxidized Au species [163]. The lower binding energy part (N_{direct}) is believed to be due to the NH_2R groups which directly interact with Au atoms to form Au-NH_2R bonds [166].

Table 7.1 N1s XPS analysis results of three types of samples.

AuNP sample with MAP adsorbing on surface	Raw area of N1s peaks at different binding energy		Component ratio of $N_{direct}/N_{indirect}$
	399.9 eV	401.1 eV	
As-irradiated	94.3	5.7	16.5/1
Ligand-exchanged-irradiated	86.5	13.5	6.4/1
Chemically reduced	82.9	17.1	4.8/1

On the basis of the relative area of the deconvoluted N1s peaks, the respective proportion of the two components was estimated. Table 7.1 lists the raw areas for the resolved two peaks and the component ratio of directly (Au-NH_2R) to indirectly (electrostatically) bonded MAP reflected by the area ratio for each sample. The ratios of N_{direct} to $N_{indirect}$ for the as-irradiated, ligand-exchanged and chemically prepared samples are 16.5/1, 6.4/1 and 4.8/1, respectively. Clearly, the direct bonding overwhelmingly takes place in all three samples. In other words, the formation of the Au-NH_2R bond dominates the AuNP-MAP interaction. Because of that, the fluctuation of surface charges or accessible surface charges, as measured by a Zeta-potential analyzer or TGA, related to the Au surface oxidation or ligand oxidation, is not necessarily mirrored in the trend of the MAP adsorption. The results from XPS analysis further testify that, as compared with the pure metal surface in the chemically prepared NPs, the oxidized surface from the laser treatment favors more the direct bonding than the indirect, electrostatic interaction. But overall, the chemically prepared AuNPs, with a non-oxidized surface, show the highest MAP adsorption capacity.

The oxidized AuNP surface has clearly shown some interesting impact on the AuNP-MAP interaction. On the other hand, it is universally known that Au oxide is unstable in nature, and will

decompose into gold and oxygen with time [167-169]. If this takes place, then logically, increased MAP adsorption will be observed with time in the laser irradiated samples due to the reduction of Au oxide, which should eventually show a MAP adsorption capacity similar to that of the chemically prepared NPs, if they are capped by the same type of ligands. In order to verify this hypothesis, the AuNPs and MAP with an initial MAP concentration of 800 nM were incubated at pH=5.5 for different times at room temperature and PL measurements were then performed on the filtrate solutions obtained at different conjugation times to examine the variation of AuNP adsorption behavior with time. Figure 7.10 presents the filtrate PL intensity as a function of incubating time for all three samples. As expected, the PL intensity of the filtrates of the laser treated samples before (squares) and after ligand-exchange (circles) shows a similar decay trend, decreasing rapidly in the first three days and then remaining almost constant, while for the chemically prepared sample (triangles), it hardly varies over the same time period. Also as expected, the ligand-exchanged-irradiated sample exhibits PL intensity values very close to the chemically prepared sample after being aged for three days. These observations undoubtedly confirm the important effect of the NP surface oxidation on MAP adsorption, perfectly corroborated with the analysis discussed above. The difference between the two types of irradiated AuNPs mainly arises from the difference in the adsorbed ligands.

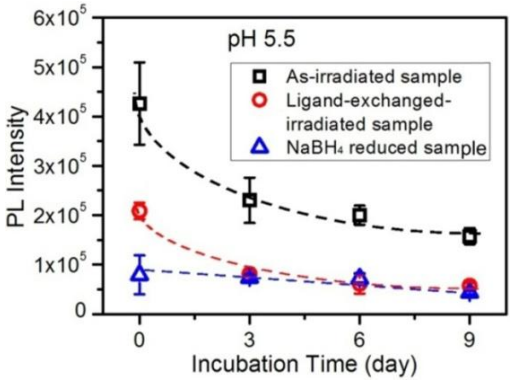

Figure 7.10 PL intensity in filtrates as a function of incubation time for conjugation at pH=5.5 with initial MAP concentration of 800 nM. Broken lines are the guides for the eye.

7.3 Summary

In this chapter, a detailed study of the surface chemistry dependent interaction between MAP and the AuNPs is reported. A UV-laser irradiation technique, that was used to oxidize the AuNP metal surface, was found to simultaneously oxidize the citrate ligands as well. Detailed investigations show that the surface oxidation has two major impacts: it leads to the increase of the surface charge density and significantly alters the ratio of MAP molecules which form direct Au-N bonding to those adsorbed indirectly through the electrostatic interaction between the negatively charged ligands and the positively charged amine groups of MAP. As the direct bonding is dominant in all three samples, the change of the surface charge density does not seem to affect the MAP adsorption significantly, although it may be important for other properties such as colloidal stability. An aging experiment straightforwardly supports the notion that it is the surface oxidation that is responsible for the decrease in the MAP adsorption capacity of the laser irradiated AuNPs. This study demonstrates the high dependency of the AuNP-amine interaction on the AuNP surface chemistry modified by laser irradiation.

Chapter 8

Conclusions and Perspectives

8.1 Conclusions

AuNPs have attracted considerable attention because they show unique properties different from bulk Au. The unique physical and chemical features of AuNPs lead to their wide application in many fields, such as optics, catalysis and biomedicine. The results of this thesis are divided into two sections based on the potential applications of AuNPs. The study of both sections is constructive for understanding the effect of NP-laser interaction on properties and applications.

The first section specifically focuses on the catalytic properties of AuNPs. AuNPs have demonstrated excellent catalytic activity in many reactions, such as selective hydrogenation and oxidation. Compared with the AuNPs synthesized by conventional chemical approaches, PLAL-AuNPs are more promising for catalysis, since their surface is relatively "bare and clean", which favours the interaction between reactants and the catalytically active sites on the NP surface. Notwithstanding, to date few reports show the application of the PLAL-AuNPs in catalysis. The objective of this section was therefore to study the synthesis and catalytic properties of AuNPs prepared by the PLAL technique, and further develop PLAL-AuNP based catalysts to achieve better serviceability and higher activity in catalysis.

In the second section, the colloidal stability of AuNPs and their ability to adsorb amine molecules were investigated, since these two properties are of primary importance to directly the

serviceability of NPs during functionalization for potential bio-applications. To do so, AuNPs were synthesized by a laser irradiation method. The irradiated AuNPs of very small size were obtained in a toxic-chemical-free environment and the use of a laser introduced unique surface chemistry features to NPs, both of which are not easily achievable for conventional chemical methods. However, prior to this thesis, there has been no any investigation of the properties of laser irradiated AuNPs. Therefore, in this section the objective was focused on the surface modification of AuNPs by laser irradiation and its influence on stability and amine-AuNP interactions.

From Chapter 3 to 5 of Section I, the synthesis and catalytic properties of PLAL-AuNP catalyst are studied. In Chapter 3, I describe the synthesis and characterization of a new nanostructured catalyst composed of PLAL-AuNPs and CeO_2 NTs, present its catalytic activity in two important reactions (4-NP reduction in the liquid phase and CO oxidation in the gas phase), and further discuss the mechanisms responsible for its high catalytic activity by comparing it with three different yet similar types of catalysts (fabricated using Chem-AuNPs and/or commercially available CeO_2 powder as a support).

I found that the coupling of the PLAL-AuNPs and CeO_2 NTs is rapid and efficient, not requiring any additional surface modification to either the AuNPs or the CeO_2 NTs. The PLAL-AuNPs/CeO_2-NTs demonstrated a significantly superior catalytic activity in the 4-NP reduction reaction as compared with not only three similar catalysts specifically prepared herein, but also other supported Au catalysts reported recently by other groups. Their superior catalytic activity is found to be due to the unique, relatively "bare" surface of the PLAL-AuNPs as well as oxidized Au species induced by the strong interaction between the "barrier-free" surface of the PLAL-AuNPs and surface defects (oxygen vacancies) of the CeO_2 NTs. The important role of the unique surface chemistry of the PLAL-AuNPs in catalysis was further demonstrated in the CO oxidation reaction in the gas phase. Our results suggest that the use of PLAL-AuNPs enables the easy and efficient

attachment of AuNPs onto the surface of the CeO_2 NTs and that their unique combination leads to the development of highly efficient catalysts.

In Chapter 4, I used a "smart", CO_2-switchable polymer, PDEAEMA, as a stabilizer to functionalize PLAL-AuNPs, to form CO_2-switchable AuNPs (PDEAEMA-AuNPs). The PLAL-AuNPs possess a relatively "bare and clean" surface and therefore favour easy surface functionalization. Gas-responsive testing demonstrates that the dispersion status of the PDEAEMA-AuNPs in the aqueous phase can be readily tuned by bubbling CO_2 into solution or expelling CO_2 from solution using N_2 bubbling, resulting in novel *in situ* recyclable NPs. The PDEAEMA-AuNPs were applied as a catalyst in the 4-NP reduction reaction. The presence of a limited amount of PDEAEMA doesn't seem to noticeably block the catalytically active sites. More interestingly, this novel catalyst can be easily separated and re-dispersed in the reaction solution by CO_2 gas-switching and exhibits a superior colloidal and catalytic stability during reaction cycles, in comparison to the PLAL-AuNPs without polymer functionalization and the Chem-AuNPs of similar size capped with citrate ligands.

In Chapter 5, I present a new approach based on the PLAL technique to prepare clean-surface, stable PtAu alloy colloids with a wide range of compositions, which have a higher catalytic activity than either monometallic Au or Pt NPs in many applications, such as fuel cells and selective hydrogenation. Specifically, a set of novel targets were made by compression molding a mixture of Pt and Au powders at different ratios. The structural characterization of the as-prepared NPs shows that PtAu alloy NPs with an fcc structure are formed. The composition of alloy NPs is close to that of their targets. An experimental parameter study shows that over wide ranges, the solution pH and ablation fluence hardly affect the formation of alloy NPs, whose composition is mainly determined by the target. The surface composition, estimated from electrochemical measurements, is identical

to the overall composition of the NPs calculated from Vegard's law and XRD data, which is a strong indication of the uniform composition on the surface and in the interior of these alloy NPs.

Then, I coupled the PLAL-PtAu alloy NPs with CeO_2 NTs to form hybrid catalysts for 4-NP reduction by simply mixing the two compounds according to the method described in Chapter 3. The "volcano-like" catalytic activity dependence of the alloy NPs on their chemical composition suggests a strong synergistic effect between Au and Pt in the alloy structure, far beyond the simple sum of their individual contributions. This beneficial synergistic interaction leads to the significantly enhanced catalytic activity of $Pt_{30}Au_{70}$ and $Pt_{50}Au_{50}$ alloy NPs, outperforming not only each single constituent, but also their physical mixtures and most recently reported AuNP based nanocatalysts. The unique surface chemistry and structure of the alloy NPs contribute to the excellent catalytic activity observed.

Chapters 6 and 7 of Section II focus on the study of the surface chemistry, colloidal stability and amine-AuNP interactions of laser irradiated AuNPs. In Chapter 6, I used a laser to irradiate "parent" 20-nm AuNPs synthesized by reducing auric acid with sodium citrate. By optimizing the irradiation conditions, 5-nm AuNPs with a narrow size distribution were obtained in a toxic-chemical-free environment. The stability of the AuNPs after laser irradiation has been systematically investigated by varying the dielectric constant and ionic concentration of colloidal solutions. The laser irradiated AuNPs demonstrated a significantly better stability compared to the citrate capped AuNPs of the same size prepared by $NaBH_4$ reduction. The characterization of the surface chemistry characterization, I revealed the presence of gold oxide on the surface of the laser irradiated AuNPs and I correlated it with the stability enhancement.

In Chapter 7, I detail the surface chemistry variation of "parent" AuNPs after laser irradiation and further discuss its effect on the amine-AuNP interaction. Three AuNP samples - laser-irradiated AuNPs, ligand-exchanged-irradiated AuNPs and chemically reduced AuNPs - were prepared; they

differ either in the chemical structure of their ligands or in the Au surface itself (oxidized or metallic Au surface). MAP was used as an amine probe to investigate the effect of the AuNP surface chemistry on the AuNP-amine interaction. Various techniques, such as XPS, NMR, FT-IR, and TGA, have been applied to characterize the surface chemistry of these three types of AuNPs, to study and compare their MAP adsorption capacity and to identify the dominant interaction mechanism. Detailed investigations show that the surface oxidation has two major consequences: it leads to the increase of the surface charge density and significantly alters the ratio of the MAP molecules which form the direct Au-N bonding to those adsorbed indirectly through the electrostatic interaction between the oppositely charged surface ligands and the amine groups of MAP. As the direct bonding is dominant in all three samples, the change of the surface charge density does not seem to affect the MAP adsorption significantly, although it may be important for other properties such as colloidal stability. An aging experiment straightforwardly supports the hypothesis that it is the surface oxidation that is responsible for the decrease in the MAP adsorption capacity of the laser irradiated AuNPs. This study demonstrates the high dependency of the AuNP-amine interaction on AuNP surface chemistry modified by laser irradiation. This study contributes to the understanding of the impact of surface chemistry variation on AuNP surface-related properties.

8.2 Perspectives

My work on the PLAL-AuNPs represents the first demonstration of the use of PLAL-AuNPs in catalysis throught the development of a simple yet efficient approach for preparing a high-activity AuNP/Support nanohybrid catalyst. The simple preparation method can be potentially extended to other hetero-nanostructured materials, made of PLAL-metal NPs (e.g., Pd or Ni) and metal oxides (such as TiO_2 and Al_2O_3). Considering the wide application of AuNPs in catalysis, by choosing a suitable metal oxide support, the PLAL-AuNP nanohybrid catalysts are expected to exhibit good

catalytic activities in many other reactions, such as the selective hydrogenation of unsaturated alcohol, the oxidation of low volatilecomponents, and the photocatalytic generation of O_2 or H_2 from water.

Our PDEAEMA-AuNPs reveal a novel *in situ* recyclability and good catalytic performance during 4-NP reduction. However, the catalytic activity and stability still need to be improved. The structure of current CO_2-switchable polymers for the surface functionalization of AuNPs can be further optimized to minimize the "barrier" effect on catalysis to enhance NP catalytic activity and maintain their catalytic stability during reaction cycles. Furthermore, it is also of high interest to functionalize the PLAL-AuNPs with other "smart" polymers, such as light sensitive polymer, to fabricate environmentally responsive nanocatalysts, sensors or optical devices.

Because of the synergistic effect existing in the PtAu alloy structure, the catalytic activity is significantly increased and many reports have shown that alloying Au with other noble metals, such as Palladium (Pd) and Rhodium (Rh) can enhance the catalytic activity of AuNPs as well. However, the price increases significantly due to the introduction of more expensive noble metals. For this reason, Pt, Pd and other precious metals could only be justified when the performance-to-price ratio of the corresponding alloy catalysts is acceptable for some highly-demanding applications. In most cases, the increased cost prohibits their practicability in industrial application. On the other hand, it has been reported that alloying inexpensive transition metals, such as Ni and Cu, with Au can also increase the catalytic activity of AuNPs, therefore it is possible to develop a method to replace expensive noble metals (such as Pt) with less expensive alternatives to achieve high catalytic activity yet minimize the cost associated with the materials used. Some of these "cheaper" alloy NPs have been synthesized successfully by chemical reduction methods and demonstrated improved activity composed with pure AuNPs. However, as discussed in Chapter 1, strongly adsorbed surface stabilizing molecules or time-consuming post-treatment processes exert negative effects on these

chemically synthesized NPs. I have successfully fabricated stable PtAu alloy NPs using PLAL, which possess a relatively "bare" surface favoring catalysis. The unique surface features of PLAL-PtAu alloy NPs improve catalysis and lead to increased catalytic activity in 4-NP reduction. Based on this, it is highly interesting to use the PLAL technique to produce Au-M alloy NPs, where M could be cheaper transition metals, and study their catalytic properties.

Bibliography

1. Roduner, E. Size matters: why nanomaterials are different, *Chemical Society Reviews*, 35: 583-592, 2006.
2. Chandross, E.A. and Miller, R.D. Nanostructures: Introduction, *Chemical Reviews*, 99: 1641-1642, 1999.
3. Love, J.C., Estroff, L.A., Kriebel, J.K., Nuzzo, R.G. and Whitesides, G.M. Self-Assembled Monolayers of Thiolates on Metals as a Form of Nanotechnology, *Chemical Reviews*, 105: 1103-1170, 2005.
4. Ghosh, S.K. and Pal, T. Interparticle Coupling Effect on the Surface Plasmon Resonance of Gold Nanoparticles: From Theory to Applications, *Chemical Reviews*, 107: 4797-4862, 2007.
5. Mallat, T. and Baiker, A. Oxidation of Alcohols with Molecular Oxygen on Solid Catalysts, *Chemical Reviews*, 104: 3037-3058, 2004.
6. Saha, K., Agasti, S.S., Kim, C., Li, X. and Rotello, V.M. Gold Nanoparticles in Chemical and Biological Sensing, *Chemical Reviews*, 112: 2739-2779, 2012.
7. Corma, A. and Garcia, H. Supported gold nanoparticles as catalysts for organic reactions, *Chemical Society Reviews*, 37: 2096-2126, 2008.
8. Abad, J. A., Mertens, S. F. L., Pita, M., Fernandez, V. M. and Schiffrin, D. J. Functionalization of Thioctic Acid-Capped Gold Nanoparticles for Specific Immobilization of Histidine-Tagged Proteins. *Journal of the American Chemical Society*, 127: 5689-5694, 2005.
9. Haruta, M. When Gold Is Not Noble: Catalysis by Nanoparticles, *The Chemical Record*, 3: 75-87, 2003.

10. Alivisatos, P. The use of nanocrystals in biological detection, *Nature Biotechnology*, 22: 47-52, 2004.

11. Whitesides, G.M. The 'right' size in nanobiotechnology, *Nature Biotechnology*, 21: 1161-1165, 2003.

12. Corma, A. and Serna, P. Chemoselective Hydrogenation of Nitro Compounds with Supported Gold Catalysts, *Science*, 313: 332-334, 2006.

13. Fu, Q., Saltsburg, H. and Flytzani-Stephanopoulos, M. Active Nonmetallic Au and Pt Species on Ceria-Based Water-Gas Shift Catalysts, *Science*, 301: 935-938, 2003.

14. Taton, T.A., Mirkin, C.A. and Letsinger, R.L. Scanometric DNA Array Detection with Nanoparticle Probes, *Science*, 289: 1757-1760, 2000.

15. Parker, S. and Campbell, C. Reactivity and sintering kinetics of Au/TiO_2 (110) model catalysts: particle size effects, *Topics in Catalysis*, 44: 3-13, 2007.

16. Link, S. and El-Sayed, M.A. Spectral Properties and Relaxation Dynamics of Surface Plasmon Electronic Oscillations in Gold and Silver Nanodots and Nanorods, *The Journal of Physical Chemistry B*, 103: 8410-8426, 1999.

17. Kumar, N., Komarala, V.K. and Dutta, V. Deposition of gold nanoparticle films using spray pyrolysis technique: Tunability of SPR band by electric field, *physica status solidi (RRL) – Rapid Research Letters*, 6: 406-408, 2012.

18. Haiss, W., Thanh, N.T.K., Aveyard, J. and Fernig, D.G. Determination of Size and Concentration of Gold Nanoparticles from UV−Vis Spectra, *Analytical Chemistry*, 79: 4215-4221, 2007.

19. Ide, M.S., Hao, B., Neurock, M. and Davis, R.J. Mechanistic Insights on the Hydrogenation of α,β-Unsaturated Ketones and Aldehydes to Unsaturated Alcohols over Metal Catalysts, *ACS Catalysis*, 2: 671-683, 2012.

20. Rashid, M.H. and Mandal, T.K. Templateless Synthesis of Polygonal Gold Nanoparticles: An Unsupported and Reusable Catalyst with Superior Activity, *Advanced Functional Materials*, 18: 2261-2271, 2008.

21. Turner, M., Golovko, V.B., Vaughan, O.P.H., Abdulkin, P., Berenguer-Murcia, A., Tikhov, M.S., Johnson, B.F.G. and Lambert, R.M. Selective oxidation with dioxygen by gold nanoparticle catalysts derived from 55-atom clusters, *Nature*, 454: 981-983, 2008.

22. Enache, D.I., Edwards, J.K., Landon, P., Solsona-Espriu, B., Carley, A.F., Herzing, A.A., Watanabe, M., Kiely, C.J., Knight, D.W. and Hutchings, G.J. Solvent-Free Oxidation of Primary Alcohols to Aldehydes Using Au-Pd/TiO_2 Catalysts, *Science*, 311: 362-365, 2006.

23. Larsson, E.M., Langhammer, C., Zorić, I. and Kasemo, B. Nanoplasmonic Probes of Catalytic Reactions, *Science*, 326: 1091-1094, 2009.

24. Tian, N., Zhou, Z.-Y., Sun, S.-G., Ding, Y. and Wang, Z.L. Synthesis of Tetrahexahedral Platinum Nanocrystals with High-Index Facets and High Electro-Oxidation Activity, *Science*, 316: 732-735, 2007.

25. Zhang, J., Sasaki, K., Sutter, E. and Adzic, R.R. Stabilization of Platinum Oxygen-Reduction Electrocatalysts Using Gold Clusters, *Science*, 315: 220-222, 2007.

26. Haruta, M., Yamada, N., Kobayashi, T. and Iijima, S. Gold catalysts prepared by coprecipitation for low-temperature oxidation of hydrogen and of carbon monoxide, *Journal of Catalysis*, 115: 301-309, 1989.

27. Carrettin, S., McMorn, P., Johnston, P., Griffin, K., Kiely, C.J. and Hutchings, G.J. Oxidation of glycerol using supported Pt, Pd and Au catalysts, *Physical Chemistry Chemical Physics*, 5: 1329-1336, 2003.

28. Prati, L. and Rossi, M. Gold on Carbon as a New Catalyst for Selective Liquid Phase Oxidation of Diols, *Journal of Catalysis*, 176: 552-560, 1998.

29. Hayashi, T., Inagaki, T., Itayama, N. and Baba, H. Selective oxidation of alcohol over supported gold catalysts: methyl glycolate formation from ethylene glycol and methanol, *Catalysis Today*, 117: 210-213, 2006.

30. Marsden, C., Taarning, E., Hansen, D., Johansen, L., Klitgaard, S.K., Egeblad, K. and Christensen, C.H. Aerobic oxidation of aldehydes under ambient conditions using supported gold nanoparticle catalysts, *Green Chemistry*, 10: 168-170, 2008.

31. Corma, A. and Domine, M.E. Gold supported on a mesoporous CeO_2 matrix as an efficient catalyst in the selective aerobic oxidation of aldehydes in the liquid phase, *Chemical Communications*: 4042-4044, 2005.

32. Hayashi, T., Tanaka, K. and Haruta, M. Selective Vapor-Phase Epoxidation of Propylene over Au/TiO_2 Catalysts in the Presence of Oxygen and Hydrogen, *Journal of Catalysis*, 178: 566-575, 1998.

33. Klitgaard, S.K., Egeblad, K., Mentzel, U.V., Popov, A.G., Jensen, T., Taarning, E., Nielsen, I.S. and Christensen, C.H. Oxidations of amines with molecular oxygen using bifunctional gold-titania catalysts, *Green Chemistry*, 10: 419-423, 2008.

34. Zhang, X., Shi, H. and Xu, B.-Q. Catalysis by Gold: Isolated Surface Au^{3+} Ions are Active Sites for Selective Hydrogenation of 1, 3-Butadiene over Au/ZrO_2 Catalysts, *Angewandte Chemie International Edition*, 44: 7132-7135, 2005.

35. Liu, Z.-P., Wang, C.-M. and Fan, K.-N. Single Gold Atoms in Heterogeneous Catalysis: Selective 1, 3-Butadiene Hydrogenation over Au/ZrO_2, *Angewandte Chemie International Edition*, 45: 6865-6868, 2006.

36. Sahiner, N., Ozay, H., Ozay, O. and Aktas, N. A soft hydrogel reactor for cobalt nanoparticle preparation and use in the reduction of nitrophenols, *Applied Catalysis B: Environmental*, 101: 137-143, 2010.

37. Zhang, M., Liu, L., Wu, C., Fu. G., Zhao, H. and He, B. Synthesis, characterization and application of well-defined environmentally responsive polymer brushes on the surface of colloid, *Polymer*, 48: 1989-1997, 2007.

38. Kuroda, K., Ishida, T. and Haruta, M. Reduction of 4-nitrophenol to 4-aminophenol over Au nanoparticles deposited on PMMA, *Journal of Molecular Catalysis A: Chemical*, 298: 7-11, 2009.

39. Zhang, Z., Shao, C., Zou, P., Zhang, P., Zhang, M., Mu, J., Guo, Z., Li, X., Wang, C. and Liu, Y. In situ assembly of well-dispersed gold nanoparticles on electrospun silica nanotubes for catalytic reduction of 4-nitrophenol, *Chemical Communications*, 47: 3906-3908, 2011.

40. Xia, Y., Shi, Z. and Lu, Y. Gold microspheres with hierarchical structure/conducting polymer composite film: Preparation, characterization and application as catalyst, *Polymer*, 51: 1328-1335, 2010.

41. Chang, Y.-C. and Chen, D.-H. Catalytic reduction of 4-nitrophenol by magnetically recoverable Au nanocatalyst, *Journal of Hazardous Materials*, 165: 664-669, 2009.

42. Panigrahi, S., Basu, S., Praharaj, S., Pande, S., Jana, S., Pal, A., Ghosh, S.K. and Pal, T. Synthesis and Size-Selective Catalysis by Supported Gold Nanoparticles: Study on Heterogeneous and Homogeneous Catalytic Process, *The Journal of Physical Chemistry C*, 111: 4596-4605, 2007.

43. Rashid, M.H. and Mandal, T.K. Templateless Synthesis of Polygonal Gold Nanoparticles: An Unsupported and Reusable Catalyst with Superior, *Advanced Functional Materials*, 18: 2261-2271, 2008.

44. Boronat, M. and Corma, A. Origin of the Different Activity and Selectivity toward Hydrogenation of Single Metal Au and Pt on TiO_2 and Bimetallic Au−Pt/TiO_2 Catalysts, *Langmuir*, 26: 16607-16614, 2010.

45. Zhu, Y., Qian, H., Drake, B.A. and Jin, R. Atomically Precise Au25(SR)18 Nanoparticles as Catalysts for the Selective Hydrogenation of α,β-Unsaturated Ketones and Aldehydes, *Angewandte Chemie International Edition*, 49: 1295-1298, 2010.

46. Haruta, M. Size- and support-dependency in the catalysis of gold, *Catalysis Today*, 36: 153-166, 1997.

47. Chen, G., Desinan, S., Rosei, R., Rosei, F. and Ma, D. Synthesis of Ni–Ru Alloy Nanoparticles and Their High Catalytic Activity in Dehydrogenation of Ammonia Borane, *Chemistry, A European Journal*, 18: 7925-7930, 2012.

48. Milone, C., Ingoglia, R., Tropeano, M.L., Neri, G. and Galvagno, S. First example of selective hydrogenation of unconstrained α,β-unsaturated ketone to α,β-unsaturated alcohol by molecular hydrogen, *Chemical Communications*, 868-869, 2003.

49. Website information, http://en.wikipedia.org/wiki/4-Nitrophenol.

50. He, L., Yu, F.-J., Lou, X.-B., Cao, Y., He, H.-Y. and Fan, K.-N. A novel gold-catalyzed chemoselective reduction of α,β-unsaturated aldehydes using CO and H_2O as the hydrogen source, *Chemical Communications*, 46: 1553-1555, 2010.

51. Hugon, A., Delannoy, L., Krafft, J.-M. and Louis, C. Selective Hydrogenation of 1,3-Butadiene in the Presence of an Excess of Alkenes over Supported Bimetallic Gold−Palladium Catalysts, *The Journal of Physical Chemistry C*, 114: 10823-10835, 2010.

52. Yu, T., Zeng, J., Lim, B. and Xia, Y. Aqueous-Phase Synthesis of Pt/CeO_2 Hybrid Nanostructures and Their Catalytic Properties, *Advanced Materials*, 22: 5188-5192, 2010.

53. Zhang, M., Liu, L., Wu, C., Fu, G., Zhao, H. and He, B. Synthesis, characterization and application of well-defined environmentally responsive polymer brushes on the surface of colloid particles, *Polymer*, 48: 1989-1997, 2007.

54. Toshima, N. and Yonezawa, T. Bimetallic nanoparticles-novel materials for chemical and physical applications, *New Journal of Chemistry*, 22: 1179-1201, 1998.

55. Hostetler, M. J., Green, S. J., Stokes, J. J. and Murray, R. W. Monolayers in Three Dimensions: Synthesis and Electrochemistry of ω-Functionalized Alkanethiolate-stabilized Gold Cluster Compounds, *Journal of the American Chemical Society*, 118: 4212-4213, 1996.

56. Frens, G. Controlled nucleation for the regulation of the particle size in monodisperse gold suspensions, *Nature (London)*, 241: 3, 1973.

57. Terrill, R. H., Postlethwaite, T. A., Chen, C., Poon, C., Terzis, A., Chen, A., Hutchison, J. E., Clark, M. R., Wignall, G., Londono, J. D., Superfine, R., Falvo, M., Johnson Jr., C. S., Samulski, E. T. and Murray, R. W. Monolayers in Three Dimensions: Nmr, Saxs, Thermal and Electron Hopping Studies of Alkanethiol Stabilized Gold Clusters, *Journal of the American Chemical Society*, 117: 12537-12548, 1995.

58. Lopez-Sanchez, J.A., Dimitratos, N., Hammond, C., Brett, G.L., Kesavan, L., White, S., Miedziak, P., Tiruvalam, R., Jenkins, R.L., Carley, A.F., Knight, D., Kiely, C.J., and Hutchings, G.J. Facile removal of stabilizer-ligands from supported gold nanoparticles, *Nature Chemistry*, 3: 551-556, 2011.

59. Long, C.G., Gilbertson, J.D., Vijayaraghavan, G., Stevenson, K.J., Pursell, C.J. and Chandler, B.D. Kinetic Evaluation of Highly Active Supported Gold Catalysts Prepared from Monolayer-

Protected Clusters: An Experimental Michaelis−Menten Approach for Determining the Oxygen Binding Constant during CO Oxidation Catalysis, *Journal of the American Chemical Society*, 130: 10103-10115, 2008.

60. Xiao, F., Wang, F., Fu, X. and Zheng, Y. A green and facile self-assembly preparation of gold nanoparticles/ZnO nanocomposite for photocatalytic and photoelectrochemical applications, *Journal of Materials Chemistry*, 22: 2868-2877, 2012.

61. Comotti, M., Li, W.-C., Spliethoff, B. and Schüth, F. Support Effect in High Activity Gold Catalysts for CO Oxidation, *Journal of the American Chemical Society*, 128: 917-924, 2005.

62. Camellone, M.F. and Fabris, S. Reaction Mechanisms for the CO Oxidation on Au/CeO_2 Catalysts: Activity of Substitutional Au^{3+}/Au^{+} Cations and Deactivation of Supported Au^{+} Adatoms, *Journal of the American Chemical Society*, 131: 10473-10483, 2009.

63. Zheng, N. and Stucky, G.D. A General Synthetic Strategy for Oxide-Supported Metal Nanoparticle Catalysts, *Journal of the American Chemical Society*, 128: 14278-14280, 2006.

64. Ivanova, S., Pitchon, V., Petit, C., Herschbach, H., Dorsselaer, A.V. and Leize, E. Preparation of alumina supported gold catalysts: Gold complexes genesis, identification and speciation by mass spectrometry, *Applied Catalysis A: General*, 298: 203-210, 2006.

65. Xu, Q., Kharas, K.C.C. and Datye, A.K. The Preparation of Highly Dispersed Au/Al_2O_3 by Aqueous Impregnation, *Catalysis Letters*, 85: 229-235, 2003.

66. Han, M., Wang, X., Shen, Y., Tang, C., Li, G. and Smith, R.L. Preparation of Highly Active, Low Au-Loaded, Au/CeO_2 Nanoparticle Catalysts that Promote CO Oxidation at Ambient Temperatures, *The Journal of Physical Chemistry C*, 114: 793-798, 2009.

67. Glaspell, G., Fuoco, L. and El-Shall, M.S. Microwave Synthesis of Supported Au and Pd Nanoparticle Catalysts for CO Oxidation, *The Journal of Physical Chemistry B*, 109: 17350-17355, 2005.

68. Sylvestre, J.-P., Poulin, S., Kabashin, A.V., Sacher, E., Meunier, M. and Luong, J.H.T. Surface Chemistry of Gold Nanoparticles Produced by Laser Ablation in Aqueous Media, *The Journal of Physical Chemistry B*, 108: 16864-16869, 2004.

69. Mafuné, F., Kohno, J.-Y., Takeda, Y. and Kondow, T. Formation of Stable Platinum Nanoparticles by Laser Ablation in Water, *The Journal of Physical Chemistry B*, 107: 4218-4223, 2003.

70. Cristoforetti, G., Pitzalis, E., Spiniello, R., Ishak, R. and Muniz-Miranda, M. Production of Palladium Nanoparticles by Pulsed Laser Ablation in Water and Their Characterization, *The Journal of Physical Chemistry C*, 115: 5073-5083, 2010.

71. Zhang, J., Oko, D.N., Garbarino, S., Imbeault, R., Chaker, M., Tavares, A.C., Guay, D. and Ma, D. Preparation of PtAu Alloy Colloids by Laser Ablation in Solution and Their Characterization, *The Journal of Physical Chemistry C*, 116: 13413-13420, 2012.

72. Zhang, J., Riabinina, D., Chaker, M. and Ma, D. Effect of Surface Oxidation on the Interaction of 1-Methylaminopyrene with Gold Nanoparticles, *Langmuir*, 28: 2858-2865, 2012.

73. Burakov, V., Butsen, A. and Tarasenko, N. Laser-induced plasmas in liquids for nanoparticle synthesis, *Journal of Applied Spectroscopy*, 77: 386-393, 2010.

74. Sinha, A.K., Suzuki, K., Takahara, M., Azuma, H., Nonaka, T., Suzuki, N. and Takahashi, N. Preparation and Characterization of Mesostructured γ-Manganese Oxide and Its Application to VOCs Elimination, *The Journal of Physical Chemistry C*, 112: 16028-16035, 2008.

75. Guczi, L., Beck, A. and Frey, K. Role of promoting oxide morphology dictating the activity of Au/SiO_2 catalyst in CO oxidation, *Gold Bulletin*, 42: 5-12, 2009.

76. Guczi, L., Horváth, D., Pászti, Z., Tóth, L., Horváth, Z.E., Karacs, A. and Petõ, G. Modeling Gold Nanoparticles: Morphology, Electron Structure, and Catalytic Activity in CO Oxidation, *The Journal of Physical Chemistry B*, 104: 3183-3193, 2000.

77. Irissou, E., Laplante, F., Garbarino, S., Chaker, M. and Guay, D. Structural and Electrochemical Characterization of Metastable PtAu Bulk and Surface Alloys Prepared by Crossed-Beam Pulsed Laser Deposition, *The Journal of Physical Chemistry C*, 114: 2192-2199, 2010.

78. Mafuné, F., Kohno, J.-y., Takeda, Y. and Kondow, T. Nanoscale Soldering of Metal Nanoparticles for Construction of Higher-Order Structures, *Journal of the American Chemical Society*, 125: 1686-1687, 2003.

79. Mafuné, F., Kohno, J.-Y., Takeda, Y., Kondow, T. and Sawabe, H. Formation and Size Control of Silver Nanoparticles by Laser Ablation in Aqueous Solution, *The Journal of Physical Chemistry B*, 104: 9111-9117, 2000.

80. Muto, H., Yamada, K., Miyajima, K. and Mafuné, F. Estimation of Surface Oxide on Surfactant-Free Gold Nanoparticles Laser-Ablated in Water, *The Journal of Physical Chemistry C*, 111: 17221-17226, 2007.

81. Kabashin, A.V. and Meunier, M. Synthesis of colloidal nanoparticles during femtosecond laser ablation of gold in water, *Journal of Applied Physics*, 94: 7941-7943, 2003.

82. Sylvestre, J.-P., Kabashin, A.V., Sacher, E., Meunier, M. and Luong, J.H.T. Stabilization and Size Control of Gold Nanoparticles during Laser Ablation in Aqueous Cyclodextrins, *Journal of the American Chemical Society*, 126: 7176-7177, 2004.

83. Kamat, P.V., Flumiani, M. and Hartland, G.V. Picosecond Dynamics of Silver Nanoclusters. Photoejection of Electrons and Fragmentation, *The Journal of Physical Chemistry B*, 102: 3123-3128, 1998.

84. Niu, K.Y., Yang, J., Kulinich, S.A., Sun, J., Li, H. and Du, X.W. Morphology Control of Nanostructures via Surface Reaction of Metal Nanodroplets, *Journal of the American Chemical Society*, 132: 9814-9819, 2010.

85. Amendola, V. and Meneghetti, M. What controls the composition and the structure of nanomaterials generated by laser ablation in liquid solution? *Physical Chemistry Chemical Physics*, 15: 3027-3046, 2013.

86. Nichols, W.T., Sasaki, T. and Koshizaki, N. Laser ablation of a platinum target in water. II. Ablation rate and nanoparticle size distributions, *Journal of Applied Physics*, 100: 114912-114916, 2006.

87. Jakobi, J., Petersen, S., Menéndez-Manjón, A., Wagener, P. and Barcikowski, S. Magnetic Alloy Nanoparticles from Laser Ablation in Cyclopentanone and Their Embedding into a Photoresist, *Langmuir*, 26: 6892-6897, 2010.

88. Sobhan, M.A., Withford, M.J. and Goldys, E.M. Enhanced Stability of Gold Colloids Produced by Femtosecond Laser Synthesis in Aqueous Solution of CTAB, *Langmuir*, 26: 3156-3159, 2009.

89. Tarasenko, N.V. and Butsen, A.V. Laser synthesis and modification of composite nanoparticles in liquids, *Quantum Electronics*, 40: 986, 2010.

90. Kneipp, J., Li, X., Sherwood, M., Panne, U., Kneipp, H., Stockman, M.I. and Kneipp, K. Gold Nanolenses Generated by Laser Ablation-Efficient Enhancing Structure for Surface Enhanced Raman Scattering Analytics and Sensing, *Analytical Chemistry*, 80: 4247-4251, 2008.

91. Kawasaki, M. and Masuda, K. Laser Fragmentation of Water-Suspended Gold Flakes via Spherical Submicroparticles to Fine Nanoparticles, *The Journal of Physical Chemistry B*, 109: 9379-9388, 2005.

92. Zhang, J., Chen, G., Chaker, M., Rosei, F. and Ma, D.L. Gold nanoparticle decorated ceria nanotubes with significantly high catalytic activity for the reduction of nitrophenol and mechanism study, *Applied Catalysis B: Environmental*, 12: 6, 2012.

93. Zhang, J., Han, D., Zhang, H., Chaker, M., Zhao, Y. and Ma, D. In situ recyclable gold nanoparticles using CO_2-switchable polymers for catalytic reduction of 4-nitrophenol, *Chemical Communications*, 48: 11510, 2012.

94. Zhang, J., Riabinina, D., Chaker, M. and Ma, D. Significant Stability Enhancement of Gold Colloids via Nanosecond Laser Irradiation, *Advanced Science Letters*, 4: 59-64, 2011.

95. Chen, G., Rosei, F. and Ma, D. Interfacial Reaction-Directed Synthesis of Ce–Mn Binary Oxide Nanotubes and Their Applications in CO Oxidation and Water Treatment, *Advanced Functional Materials*, 22: 3914-3920, 2012.

96. Chen, G., Xu, C., Song, X., Zhao, W., Ding, Y. and Sun, S. Interface Reaction Route to Two Different Kinds of CeO_2 Nanotubes, *Inorganic Chemistry*, 47: 723-728, 2007.

97. Dubin, P.L. and Tong, P. *Colloid-Polymer Interactions: Particulate, Amphiphilic, and Biological Surfaces; American Chemical Society*, Oxford University Press. New York, USA, 1993.

98. Huang, J., Vongehr, S., Tang, S., Lu, H. and Meng, X. Highly Catalytic Pd−Ag Bimetallic Dendrites, *The Journal of Physical Chemistry C*, 114: 15005-15010, 2010.

99. JCPDS Card File No. 00-004-0784 (Au), 00-004-0802 (Pt) and 34-0394 (CeO_2).

100. Ojea-Jiménez, I. and Puntes, V. Instability of Cationic Gold Nanoparticle Bioconjugates: The Role of Citrate Ions, *Journal of the American Chemical Society*, 131: 13320-13327, 2009.

101. Horváth, A., Beck, A., Sárkány, A., Stefler, G., Varga, Z., Geszti, O., Tóth, L. and Guczi, L. Silica-Supported Au Nanoparticles Decorated by TiO_2: Formation, Morphology, and CO Oxidation Activity, *The Journal of Physical Chemistry B*, 110: 15417-15425, 2006.

102. Si, R. and Flytzani-Stephanopoulos, M. Shape and Crystal-Plane Effects of Nanoscale Ceria on the Activity of Au-CeO_2 Catalysts for the Water–Gas Shift Reaction, *Angewandte Chemie International Edition*, 47: 2884-2887, 2008.

103. Abad, A., Concepción, P., Corma, A. and García, H. A Collaborative Effect between Gold and a Support Induces the Selective Oxidation of Alcohols, *Angewandte Chemie International Edition*, 44: 4066-4069, 2005.

104. Horváth, A., Beck, A., Stefler, G., Benkó, T., Sáfrán, G., Varga, Z., Gubicza, J. and Guczi, L. Silica-Supported Au Nanoparticles Decorated by CeO_2: Formation, Morphology, and CO Oxidation Activity, *The Journal of Physical Chemistry C*, 115: 20388-20398, 2011.

105. Crist, V.B. *PDF Handbooks of Monochromatic XPS Spectra, Volume 1: The Elements and Native Oxides*, XPS International, LLC. California, USA, 1999.

106. Celardo, I., De Nicola, M., Mandoli, C., Pedersen, J.Z., Traversa, E. and Ghibelli, L. Ce^{3+} Ions Determine Redox-Dependent Anti-apoptotic Effect of Cerium Oxide Nanoparticles, *ACS Nano*, 5: 4537-4549, 2011.

107. Shan, J. and Tenhu, H. Recent advances in polymer protected gold nanoparticles: synthesis, properties and applications, *Chemical Communications*, 4580-4598, 2007.

108. Daniel, M.-C. and Astruc, D. Gold Nanoparticles: Assembly, Supramolecular Chemistry, Quantum-Size-Related Properties, and Applications toward Biology, Catalysis, and Nanotechnology, *Chemical Reviews*, 104: 293-346, 2003.

109. Zhu, M.-Q., Wang, L.-Q., Exarhos, G.J. and Li, A.D.Q. Thermosensitive Gold Nanoparticles, *Journal of the American Chemical Society*, 126: 2656-2657, 2004.

110. Liu, X.-Y., Cheng, F., Liu, Y., Liu, H.-J. and Chen, Y. Preparation and characterization of novel thermoresponsive gold nanoparticles and their responsive catalysis properties, *Journal of Materials Chemistry*, 20: 360-368, 2010.

111. Housni, A. and Zhao, Y. Gold Nanoparticles Functionalized with Block Copolymers Displaying Either LCST or UCST Thermosensitivity in Aqueous Solution, *Langmuir*, 26: 12933-12939, 2010.

112. Han, D., Tong, X., Boissière, O. and Zhao, Y. General Strategy for Making CO_2-Switchable Polymers, *ACS Macro Letters*, 1: 57-61, 2011.

113. Hammer, B., Norskov, J. K. Theoretical surface science and catalysis—calculations and concepts, *Advanced Catalyst*, 45: 71-129, 2000.

114. Budroni, G. and Corma, A. Gold and gold–platinum as active and selective catalyst for biomass conversion: Synthesis of γ-butyrolactone and one-pot synthesis of pyrrolidone, *Journal of Catalysis*, 257: 403-408, 2008.

115. Luo, J., Maye, M.M., Petkov, V., Kariuki, N.N., Wang, L., Njoki, P., Mott, D., Lin, Y. and Zhong, C.-J. Phase Properties of Carbon-Supported Gold−Platinum Nanoparticles with Different Bimetallic Compositions, *Chemistry of Materials*, 17: 3086-3091, 2005.

116. Schrinner, M., Proch, S., Mei, Y., Kempe, R., Miyajima, N. and Ballauff, M. Stable Bimetallic Gold–Platinum Nanoparticles Immobilized on Spherical Polyelectrolyte Brushes: Synthesis, Characterization, and Application for the Oxidation of Alcohols, *Advanced Materials*, 20: 1928-1933, 2008.

117. Liu, Y., Yuan, J., Polzer, F., Drechsler, M. and Preussner, In Situ growth of catalytic active Au-Pt bimetallic nanorods in thermoresponsive core-shell microgels, *ACSNano*, 4: 7078-7086, 2010.

118. Hu, Y., Zhang, H., Wu, P., Zhang, H., Zhou, B. and Cai, C. Bimetallic Pt-Au nanocatalysts electrochemically deposited on graphene and their electrocatalytic characteristics towards oxygen reduction and methanol oxidation, *Physical Chemistry Chemical Physics*, 13: 4083-4094, 2011.

119. Zhang, Z., Wang, Y. and Wang, X. Nanoporous bimetallic Pt-Au alloy nanocomposites with superior catalytic activity towards electro-oxidation of methanol and formic acid, *Nanoscale*, 3: 1663-1674, 2011.

120. Luo, J., Njoki, P.N., Lin, Y., Mott, D., Wang and Zhong, C.-J. Characterization of Carbon-Supported AuPt Nanoparticles for Electrocatalytic Methanol Oxidation Reaction, *Langmuir*, 22: 2892-2898, 2006.

121. Wang, J., Yin, G., Liu, H., Li, R., Flemming, R.L. and Sun, X. Carbon nanotubes supported Pt–Au catalysts for methanol-tolerant oxygen reduction reaction: A comparison between Pt/Au and PtAu nanoparticles, *Journal of Power Sources*, 194: 668-673, 2009.

122. Obradović, M.D., Rogan, J.R., Babić, B.M., Tripković, A.V., Gautam, A.R.S., Radmilović, V.R. and Gojković, S.L. Formic acid oxidation on Pt–Au nanoparticles: Relation between the catalyst activity and the poisoning rate, *Journal of Power Sources*, 197: 72-79, 2012.

123. Ruban, A., Hammer, B., Stoltze, P., Skriver, H. L. and Norskov, J. K. Surface electronic structure and reactivity of transition and noble metals, *Journal of Molecule Catalyasis A: Chemistry*, 115: 421-429, 1997.

124. Hernández-Fernández, P., Rojas, S., Ocón, P., Gómez de la Fuente, J.L., San Fabián, J., Sanza, J., Peña, M.A., García-García, F.J., Terreros, P. and Fierro, J.L.G. Influence of the Preparation Route of Bimetallic Pt−Au Nanoparticle Electrocatalysts for the Oxygen Reduction Reaction, *The Journal of Physical Chemistry C*, 111: 2913-2923, 2007.

125. Bai, Y.-C., Zhang, W.-D., Chen, C.-H. and Zhang, J.-Q. Carbon nanotubes-supported PtAu-alloy nanoparticles for electro-oxidation of formic acid with remarkable activity, *Journal of Alloys and Compounds*, 509: 1029-1034, 2011.

126. Zhang, S., Shao, Y., Liao, H.-g., Liu, J., Aksay, I.A., Yin, G. and Lin, Y. Graphene Decorated with PtAu Alloy Nanoparticles: Facile Synthesis and Promising Application for Formic Acid Oxidation, *Chemistry of Materials*, 23: 1079-1081, 2011.

127. Yu, R., Machavariani, V.S., Voronel, A., Garber, S., Rubshtein, A., Frenkel, A.I. and Stern, E.A. Strain energy density in the x-ray powder diffraction from mixed crystals and alloys, *Journal of Physics: Condensed Matter*, 12: 8081, 2000.

128. Tian, Z.Q., Jiang, S.P., Liang, Y.M. and Shen, P.K. Synthesis and Characterization of Platinum Catalysts on Multiwalled Carbon Nanotubes by Intermittent Microwave Irradiation for Fuel Cell Applications, *The Journal of Physical Chemistry B*, 110: 5343-5350, 2006.

129. Xu, J.B., Zhao, T.S. and Liang, Z.X. Synthesis of Active Platinum−Silver Alloy Electrocatalyst toward the Formic Acid Oxidation Reaction, *The Journal of Physical Chemistry C*, 112: 17362-17367, 2008.

130. Wanjala, B.N., Luo, J., Loukrakpam, R., Fang, B., Mott, D., Njoki, P.N., Engelhard, M., Naslund, H.R., Wu, J.K., Wang, L., Malis, O., and Zhong, C.-J. Nanoscale Alloying, Phase-Segregation, and Core−Shell Evolution of Gold−Platinum Nanoparticles and Their Electrocatalytic Effect on Oxygen Reduction Reaction, *Chemistry of Materials*, 22: 4282-4294, 2010.

131. Mei, Y., Lu, Y., Polzer, F. and Ballauff, M. Catalytic activity of Palladium nanoparticles encapsulated in spherical polyelectrolyte brushes and core-shell microgels, *Chemistry of Materials*, 19: 1062-1069, 2007.

132. Woods, R. The surface composition of platinum-gold alloys, *Electrochimica Acta*, 16: 655-658, 1971.

133. Breiter, M.W. Electrochemical Characterization of the Surface Composition of Heterogeneous Platinum-Gold Alloys, *The Journal of Physical Chemistry*, 69: 901-904, 1965.

134. Hyman, M.P. and Medlin, J.W. Effects of Electronic Structure Modifications on the Adsorption of Oxygen Reduction Reaction Intermediates on Model Pt(111)-Alloy Surfaces, *The Journal of Physical Chemistry C*, 111: 17052-17060, 2007.

135. Bommersbach, P., Chaker, M., Mohamedi, M. and Guay, D. Physico-Chemical and Electrochemical Properties of Platinum-Tin Nanoparticles Synthesized by Pulsed Laser Ablation for Ethanol Oxidation, *The Journal of Physical Chemistry C*, 112: 14672-14681, 2008.

136. Angerstein-Kozlowska, H., Conway, B.E., Hamelin, A. and Stoicoviciu, L. Elementary steps of electrochemical oxidation of single-crystal planes of Au Part II. A chemical and structural basis of oxidation of the (111) plane, *Journal of Electroanalytical Chemistry and Interfacial Electrochemistry*, 228: 429-453, 1987.

137. Heyd, D.V. and Harrington, D.A. Platinum oxide growth kinetics for cyclic voltammetry, *Journal of Electroanalytical Chemistry*, 335: 19-31, 1992.

138. Mayrhofer, K.J.J., Blizanac, B.B., Arenz, M., Stamenkovic, V.R., Ross, P.N. and Markovic, N.M. The Impact of Geometric and Surface Electronic Properties of Pt-Catalysts on the Particle Size Effect in Electrocatalysis, *The Journal of Physical Chemistry B*, 109: 14433-14440, 2005.

139. Friedrich, K.A., Henglein, F., Stimming, U. and Unkauf, W. Size dependence of the CO monolayer oxidation on nanosized Pt particles supported on gold, *Electrochimica Acta*, 45: 3283-3293, 2000.

140. Corma, A., Serna, P., Concepción, P. and Calvino, J.J. Transforming Nonselective into Chemoselective Metal Catalysts for the Hydrogenation of Substituted Nitroaromatics, *Journal of the American Chemical Society*, 130: 8748-8753, 2008.

141. Bus, E. and van Bokhoven, J.A. Hydrogen chemisorption on supported platinum, gold, and platinum−gold-alloy catalysts, *Physical Chemistry Chemical Physics*, 9: 2894-2902, 2007.

142. Fernández, J.; Walsh, D. A. and Bard, A. J. Thermodynamic guidelines for the design of bimetallic catalysts for oxygen electroreduction and rapid screening by scanning electrochemical microscopy, *Journal of the American Chemical Society*, 127: 357-365, 2005.

143. Kim, C. K., Ghosh, P., Pagliuca, C., Zhu, Z., Menichetti, S. and Rotello, V. M. Entrapment of Hydrophobic Drugs in Nanoparticle Monolayers with Efficient Release into Cancer Cells, Journal of the American Chemical Society, 131: 1360-1361, 2009.

144. Sokolov, K., Follen, M., Aaron, J., Pavlova, I., Malpica, A., Lotan, R. and Richards-Kortum, R. Real-Time Vital Optical Imaging of Precancer Using Anti-Epidermal Growth Factor Receptor Antibodies Conjugated to Gold Nanoparticles, *Cancer Research*, 63: 1999-2004, 2003.

145. Kim, C., Ghosh, P., and Rotello, V. M. Multimodal drug delivery using gold nanoparticles, *Nanoscale*, 1: 61-67, 2009.

146. Inasawa, S., Sugiyama, M. and Yamaguchi, Y. Bimodal Size Distribution of Gold Nanoparticles under Picosecond Laser Pulses, *The Journal of Physical Chemistry B*, 109: 9404-9410, 2005.

147. Takami, A., Kurita, H. and Koda, S. Laser-Induced Size Reduction of Noble Metal Particles, *The Journal of Physical Chemistry B*, 103: 1226-1232, 1999.

148. Zhitomirsky, I. Cathodic electrodeposition of ceramic and organoceramic materials. Fundamental aspects, *Advances in Colloid and Interface Science*, 97: 279-317, 2002.

149. Mei, B.C., Susumu, K., Medintz, I.L., Delehanty, J.B., Mountziaris, T.J. and Mattoussi, H. Modular poly(ethylene glycol) ligands for biocompatible semiconductor and gold nanocrystals with extended pH and ionic stability, *Journal of Materials Chemistry*, 18: 4949-4958, 2008.

150. Brewer, S.H., Glomm, W.R., Johnson, M.C., Knag, M.K. and Franzen, S. Probing BSA Binding to Citrate-Coated Gold Nanoparticles and Surfaces, *Langmuir*, 21: 9303-9307, 2005.

151. Borer, P., Hug, S.J., Sulzberger, B., Kraemer, S.M. and Kretzschmar, R. Photolysis of Citrate on the Surface of Lepidocrocite: An in situ Attenuated Total Reflection Infrared Spectroscopy Study, *The Journal of Physical Chemistry C*, 111: 10560-10569, 2007.

152. Redmond, P.L., Wu, X. and Brus, L. Photovoltage and Photocatalyzed Growth in Citrate-Stabilized Colloidal Silver Nanocrystals, *The Journal of Physical Chemistry C*, 111: 8942-8947, 2007.

153. Freeman, R.G., Grabar, K.C., Allison, K.J., Bright, R.M., Davis, J.A., Guthrie, A.P., Hommer, M.B., Jackson, M.A., Smith, P.C., Walter, D.G., and Natan, M.J. Self-Assembled Metal Colloid Monolayers: An Approach to SERS Substrates, *Science*, 267: 1629-1632, 1995.

154. Colvin, V.L., Schlamp, M.C. and Alivisatos, A.P. Light-emitting diodes made from cadmium selenide nanocrystals and a semiconducting polymer, *Nature*, 370: 354-357, 1994.

155. Grabar, K.C., Smith, P.C., Musick, M.D., Davis, J.A., Walter, D.G., Jackson, M.A., Guthrie, A.P. and Natan, M.J. Kinetic Control of Interparticle Spacing in Au Colloid-Based Surfaces: Rational Nanometer-Scale Architecture, *Journal of the American Chemical Society*, 118: 1148-1153, 1996.

156. Leff, D.V., Brandt, L. and Heath, J.R. Synthesis and Characterization of Hydrophobic, Organically-Soluble Gold Nanocrystals Functionalized with Primary Amines, *Langmuir*, 12: 4723-4730, 1996.

157. Thomas, K.G., Zajicek, J. and Kamat, P.V. Surface Binding Properties of Tetraoctylammonium Bromide-Capped Gold Nanoparticles, *Langmuir*, 18: 3722-3727, 2002.

158. Porta, F., Krpetić, Z.e., Prati, L., Gaiassi, A. and Scarì, G. Gold-Ligand Interaction Studies of Water-Soluble Aminoalcohol Capped Gold Nanoparticles by NMR, *Langmuir*, 24: 7061-7064, 2008.

159. Erol, M., Han, Y., Stanley, S.K., Stafford, C.M., Du, H. and Sukhishvili, S. SERS Not To Be Taken for Granted in the Presence of Oxygen, *Journal of the American Chemical Society*, 131: 7480-7481, 2009.

160. Xue, C., Métraux, G.S., Millstone, J.E. and Mirkin, C.A. Mechanistic Study of Photomediated Triangular Silver Nanoprism Growth, *Journal of the American Chemical Society*, 130: 8337-8344, 2008.

161. Ipe, B.I. and Thomas, K.G. Investigations on Nanoparticle−Chromophore and Interchromophore Interactions in Pyrene-Capped Gold Nanoparticles, *The Journal of Physical Chemistry B*, 108: 13265-13272, 2004.

162. Dulkeith, E., Morteani, A.C., Niedereichholz, T., Klar, T.A., Feldmann, J., Levi, S.A., van Veggel, F.C.J.M., Reinhoudt, D.N., Möller, M. and Gittins, D.I. Fluorescence Quenching of Dye Molecules near Gold Nanoparticles: Radiative and Nonradiative Effects, *Physical Review Letters*, 89: 203002, 2002.

163. Takeda, Y., Mafuné, F. and Kondow, T. Selective Degradation of Proteins by Laser Irradiation onto Gold Nanoparticles in Solution, *The Journal of Physical Chemistry C*, 113: 5027-5030, 2009.

164. Sweeney, S.F., Woehrle, G.H. and Hutchison, J.E. Rapid Purification and Size Separation of Gold Nanoparticles via Diafiltration, *Journal of the American Chemical Society*, 128: 3190-3197, 2006.

165. Kim, S.-G., Wang, W.-N., Iwaki, T., Yabuki, A. and Okuyama, K. Low-Temperature Crystallization of Barium Ferrite Nanoparticles by a Sodium Citrate-Aided Synthetic Process, *The Journal of Physical Chemistry C*, 111: 10175-10180, 2007.

166. Kumar, A., Mandal, S., Pasricha, R., Mandale, A.B. and Sastry, M. Investigation into the Interaction between Surface-Bound Alkylamines and Gold Nanoparticles, *Langmuir*, 19: 6277-6282, 2003.

167. Tsai, H., Hu, E., Perng, K., Chen, M., Wu, J.-C. and Chang, Y.-S. Instability of gold oxide Au_2O_3, *Surface Science*, 537: L447-L450, 2003.

168. Ono, L.K. and Roldan Cuenya, B. Formation and Thermal Stability of Au_2O_3 on Gold Nanoparticles: Size and Support Effects, *The Journal of Physical Chemistry C*, 112: 4676-4686, 2008.

169. Cuenya, B.R., Baeck, S.-H., Jaramillo, T.F. and McFarland, E.W. Size- and Support-Dependent Electronic and Catalytic Properties of Au^0/Au^{3+} Nanoparticles Synthesized from Block Copolymer Micelles, *Journal of the American Chemical Society*, 125: 12928-12934, 2003.

170. Zhou, Z., Kooi, S., Flytzani-Stephanopoulos, M. and Saltsburg, H. The Role of the Interface in CO Oxidation on Au/CeO_2 Multilayer Nanotowers, *Advanced Functional Materials*, 18: 2801-2807, 2008.

171. Zhou, Z., Flytzani-Stephanopoulos, M. and Saltsburg, H. Decoration with ceria nanoparticles activates inert gold island/film surfaces for the CO oxidation reaction, *Journal of Catalysis*, 280: 255-263, 2011.

172. Venezia, A. M., Pantaleo, G., Longo, A., Cario, G. D., Casaletto, M. P., Liotta, F. L. and Deganello, G. Relationship between Structure and CO Oxidation Activity of Ceria-Supported Gold Catalysts, *The Journal of Physical Chemistry B*, 109: 2821-2827, 2005.

173. Huang, P. X., Wu, F., Zhu, B. L., Gao, X. P., Zhu, H. Y., Yan, T. Y., Huang, W. P., Wu, S. H. and Song, D. Y. CeO_2 Nanorods and Gold Nanocrystals Supported on CeO_2 Nanorods as Catalyst, *The Journal of Physical Chemistry B*, 109: 19169-19174, 2005.

Appendix A

List of Acronyms

4-AP	4-Aminophenol
4-NP	4-Nitrophenol
AuNP(s)	Gold Nanoparticle(s)
Chem-AuNPs	Chemically prepared AuNPs
FTIR	Fourier Transform Infrared spectroscopy
MAP	1-methylaminopyrene
NMR	Nuclear Magnetic Resonance Spectroscopy
NP(s)	Nanoparticle(s)
NT(s)	Nanotube(s)
PDEAEMA	Poly(N,N-diethylaminoethylmethacrylate)
PL	Photoluminescence
PLAL	Pulsed Laser Ablation in Liquid
PLD	Pulsed Laser Deposition
TEM	Transmission Electron Microscopy
UV-Vis	UV-Visible
XPS	X-ray Photoelectron Spectroscopy
XRD	X-Ray Diffraction

Appendix B

List of Chemical Formulas

4-AP

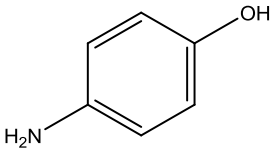

4-NP

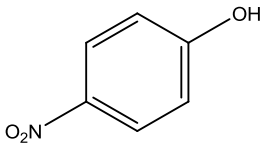

MAP

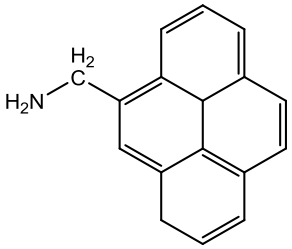

PDEAEMA

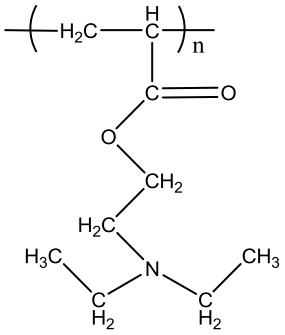

Appendix C

Résumé de la Thèse

Introduction

Depuis plusieurs années, les nanomatériaux ont attiré beaucoup d'attention de la part de la communauté scientifique et ce, grâce à leurs propriétés uniques très différentes des matériaux sous forme volumique. Ils représentent un grand potentiel scientifique dans le domaine des sciences physiques, chimiques, biologiques et sciences de la santé, ainsi que dans les domaines interdisciplinaires de la science et de l'ingénierie [1, 2]. En nanotechnologies, les nanoparticules d'or (AuNPs) occupent une place tout à fait particulière grâce à l'énorme potentiel de leurs applications dans les domaines aussi variés que la biomédecine, le développement de dispositifs optiques et la catalyse qui se base sur leurs propriétés uniques de résonance de plasmon de surface (SPR) et la fonctionnalisation pour les molécules qui contiennent les groupes sulfuré et amine.

A ce jour, deux techniques ont été mises en place pour la synthèse des AuNPs [54]. La première est la méthode chimique, qui est la voie la plus largement utilisée et la mieux étudiée pour synthétiser les nanostructures d'Au de taille et de forme variées. Cette méthode utilise les sels d'or, par exemple, l'acide aurique ($HAuCl_4$), pour la formation de NPs [7]. La formation et la croissance de AuNPs se produit par réduction des ions d'or en atomes neutres après l'introduction d'un agent réducteur [55, 56]. Généralement, les petites NPs s'agglomèrent facilement à cause de leur énergie de surface élevée, ce qui mène à la diminution de leurs propriétés et du champ d'application. Elles sont également sensibles à l'environnement, i.e. à la haute concentration ionique et à la température

qui peut occasionner l'agrégation de NPs [57, 58]. Afin d'atteindre la taille idéale des particules et d'éviter cette problématique, des agents stabilisants (par exemple des ligands ou des molécules tensioactives) sont nécessaires pour stabiliser les NPs [34, 35, 57, 59].

Il existe une autre méthode pour la synthèse des AuNPs communément appelée « méthode physique ». Différente de la méthode chimique, cette méthode préconise la formation de NPs à partir d'un matériau volumique sans l'utilisation de précurseurs chimiques. Ablation laser pulsé sur une cible solide est la méthode physique la plus largement utilisée. Dans cette approche, l'utilisation d'agents stabilisants peut être évitée. Il a été démontré que des petites AuNPs peuvent être déposées sur un substrat par ablation laser pulsée (PLD) [74-76] et testées dans les réactions en phase gazeuse [74-76].

Récemment, une technique d'ablation laser alternative, l'ablation laser pulsée en milieu liquide (PLAL) a attiré beaucoup d'intérêt [68, 69, 71, 73, 78, 79, 81, 82, 85, 87, 88]. En outre, dans un procédé optimisé, elle permet de produire de petites NPs mono-dispersées stables sans l'introduction d'agents stabilisants, même si le liquide utilisé est un solvant pur sans additifs, par exemple l'eau pure ou l'éthanol, et donc la contamination d'AuNPs peut être évitée. En particulier, puisque la plume du plasma en PLAL est confinée dans un liquide environnant, le plasma présente les caractéristiques différentes de celles de la PLD conventionnelle [71, 73, 85, 89]. Il crée les conditions de haute température, haute pression et haute densité, qui sont très favorables à la réaction chimique [73]. Par conséquent, cette technique permet de fonctionnaliser la surface des PLAL-AuNPs de manière très différente des autres approches synthétiques [73]. Par exemple, Luong et al. et Mafune et al. ont rapporté ce que les atomes d'or sur la surface des AuNPs fraîchement préparées par la technique d'ablation laser dans l'eau sont partiellement oxydées [68, 80, 82], Kondow [69], Muniz-Miranda et al. [70] ont également montré que les petits groupes OH^-

dans l'environnement aqueux sont adsorbés à la surface de nanoparticules métalliques produites par PLAL pour former une surface chargée négativement qui stabilise les NPs en suspension.

Malgré la nature inerte de l'or sous forme volumique, les AuNPs démontrent une forte activité catalytique dans de nombreuses réactions, par exemple, l'hydrogénation de composés aromatiques nitrés, l'oxydation de CO et la décomposition de l'eau [2-23], ce qui est extrêmement prometteur de point de vue de la protection de l'environnement et le développement de nouvelles énergies. Depuis cette découverte, de grands efforts ont été concentrés sur l'optimisation de l'activité catalytique des AuNPs. Plusieurs types de catalyseurs à base d'AuNPs ont été synthétisés par la methode chimique mentionnée ci-haut. Toutefois, les produits résiduels de la réaction (par exemple, Cl^-) et les agents stabilisants sont adsorbés la surface des NPs et peuvent éventuellement « empoisonner » le catalyseur et bloquer l'accès des agents réactifs aux sites actifs des NPs (effet «barrière»), en diminuant ainsi leur activité catalytique [58]. Bien que certains protocoles de post-traitement ont été développés pour éliminer ces agents stabilisants à l'aide du lavage, de méthodes thermiques et d'oxydation, ces techniques mènent à une augmentation importante de la taille des NPs et altèrent ainsi leurs propriétés catalytiques [59, 61]. Les petites AuNPs peuvent être synthétisées en utilisant la méthode chimique modifiée, par exemple la méthode par dépôt-précipitation (DP), croissance dans une couche de mouillage et les méthodes de croissance *in-situ*, sur des substrats sans l'introduction d'agents stabilisateurs [15, 59, 61-65], ce qui permet d'éviter l'effet «barrière» tel que décrit plus haut. Cependant, les impuretés telles que Cl^- en provenance du précurseur $HAuCl_4$ ou du carbonate de sodium utilisé dans la méthode DP, qui restent dans le catalyseur, doivent être complètement éliminées à l'aide d'un traitement de lavage ou d'un traitement thermique puisque celles-ci ont un impact négatif sur les catalyseurs à base d'or [7]. En particulier, les résidus de Cl^- non seulement nuisent aux propriétés catalytiques des nanomatériaux mais également favorisent l'agrégation de NPs à haute température en activant les atomes d'or [64, 65].

En résumé de cette introduction, il est clair que le principal inconvénient de la synthèse chimique des catalyseurs à base de NPs d'or est la contamination de la surface des nanoparticules due au procédé de synthèse, ce qui est difficile à éviter car la présence des précurseurs chimiques et / ou des additifs sont nécessaires.

La contamination chimique et l'effet « barrière » peuvent être évités dans le cas des AuNPs produits par ablation laser puisque aucun produit chimique tel que agents stabilisateurs n'est utilisé dans cette méthode de synthèse. Comparé à la synthèse chimique, les AuNPs produites par ablation laser sont ainsi plus adéquates pour les applications en catalyse. Des petites AuNPs déposées sur un substrat utilisées pour des réactions en phase gazeuse telles que l'oxydation de CO [74] ont montré une bonne activité catalytique. Cependant, la mise en place et le fonctionnement du système PLD relativement compliqué et le temps de production élevé font partie des inconvénients de cette technique de synthèse. En comparaison avec la méthode PLD, la PLAL est un système relativement simple qui ne nécessite pas d'utilisation de chambre à vide et, par conséquent, offre une commodité importante dans la manipulation expérimentale. Les petits groupes OH^- sont susceptibles d'exercer beaucoup moins d'effets de "barrière" sur la catalyse que la plupart d'agents stabilisants, dont la taille est généralement beaucoup plus élevée, de sorte qu'ils peuvent bloquer accès aux molécules réactives à la surface du catalyseur. Par conséquent, il est très intéressant d'utiliser les PLAL-AuNPs stables et bien dispersées avec des surfaces réactives relativement « propres » dans des réactions catalytiques en milieu aqueux. Un autre avantage de la technique PLAL réside dans le fait que la surface recouverte de OH^- interagit facilement avec d'autres matériaux, par exemple, l'oxyde métallique avec de groupes hydroxyles en solution aqueuse, pour former des structures hybrides de NP / oxyde métallique qui ont un grand potentiel d'applications. L'effet de différentes conditions sur la fabrication de NPs, telles que les paramètres laser, les solvants, les valeurs de pH, la température

et les électrolytes ainsi que la chimie de surface de PLAL-AuNPs [68, 69, 79, 81, 88, 90, 91] ont été étudiés. Cependant, l'activité catalytique des PLAL-AuNPs n'a pas été encore bien étudiée.

Outre l'effet des propriétés de surface des AuNPs sur la catalyse, il est important d'adresser deux défis de taille en catalyse d'AuNPs en phase liquide :

i) La récupération et la réutilisation des NPs. La difficulté de ce défi réside dans la séparation efficace des petites AuNPs des produits de réaction en minimisant les pertes, leur re-dispersion après la centrifugation ou la filtration et leur stabilité colloïdale en nouvelle solution réactive. Bien que la centrifugation soit largement utilisée pour séparer les NPs des produits de réaction, elle mène généralement à l'agrégation irréversible des NPs et ainsi la réduction considérable de leur activité catalytique. Pour obtenir une excellente activité catalytique et stabilité à long terme, et afin d'assurer la réutilisabilité des AuNPs, une technique de séparation simple et efficace doit être développée.

ii) L'augmentation de l'activité catalytique des AuNPs. Bien que la réduction de taille permet d'augmenter l'activité catalytique des AuNPs, la diminution additionnelle de la taille des nanoparticules en synthèse chimique ou par PLAL préconise l'utilisation des additifs tensio-actifs ou des ligands ce qui annule les avantages de la technique de PLAL.

Mis à part leurs propriétés catalytiques, les AuNPs ont été également largement utilisées pour la recherche dans le domaine de biologie, grâce à leur propriétés optiques et électroniques, et leur non-toxicité [4-15]. Pour ces applications, il est important que la taille des NPs soit très petite (moins de 10 nm) et que leur attachement aux espèces biologiques soit suffisamment fort dans le but de faciliter leur passage à travers les barrières biologiques (i.e. membranes cellulaires) [10. 11]. La

plupart des applications biologiques requiert la modification de surface de AuNPs à l'aide des molécules fonctionnelles. Lors de cette étape, il est important que s'assurer d'une bonne stabilité colloïdale des AuNPs et d'éviter leur agglomération, en particulier dans le cas de haute concentration [57]. La stabilité colloïdale est ainsi primordiale pour conserver l'utilisabilité des nanoparticules pendant leur fonctionnalisation.

Il a été démontré que les nanoparticules d'or peuvent facilement s'attacher aux groupes amines [150, 156-158]. L'abondance de groupes amines dans les systèmes biologiques et la force de l'interaction entre NPs Au et les groupes amines sont à la base de plusieurs applications biomédicales des NPs Au. Les études sur l'interaction entre les groupe amines et les AuNPs démontrent clairement une forte influence de la chimie de surface des AuNPs (surface métallique vs ligands variés) sur cette interaction.

Récemment, la technique de l'irradiation par laser a été utilisée pour la synthèse de très petites nanoparticules à partir des AuNPs produites initialement par méthode chimique et ensuite irradiées par faisceau laser [68, 82, 91, 146, 147]. Le traitement par irradiation laser permet de fractionner les NPs en milieu liquide. Comparée à la synthèse de très petites AuNPs (moins de 10 nm) par méthode chimique, l'irradiation laser est une technique de synthèse relativement «verte» qui évite l'utilisation des produits chimiques toxiques ce qui la rend plus appropriée pour les applications biologiques. Aussi, le traitement laser des nanoparticules d'or permet de créer une fine couche d'oxyde d'or à la surface de nanoparticules ce qui serait impossible dans le cas de la synthèse chimique dû à la nature inerte de l'or [68, 82, 91]. Cette modification de surface pouvant affecter la stabilité colloïdale et l'adsorption des molécules à la surface des AuNPs, la technique d'irradiation laser se révèle d'être un excellent outil qui offre une multitude de possibilités pour l'étude de la stabilité et l'interaction groupes amines avec la surface oxydée des NPs d'or.

Les objectifs de la thèse

Cette thèse est divisée en deux sections. La première section est consacrée à l'étude de la synthèse des nanoparticules d'or par PLAL et leurs propriétés catalytiques. Dans cette partie, nous avons également étudié l'influence de la chimie de surface sur la catalyse à travers la comparaison avec les nanoparticules synthétisées chimiquement.

La deuxième section porte sur l'étude de la modification de surface par irradiation laser des NPs Au synthétisées chimiquement et son influence sur les propriétés fonctionnelles de ces nanoparticules.

De façon plus détaillée, les objectifs de la thèse sont divisés en deux volets :

1. a) Préparer un catalyseur à base de PLAL-AuNPs pour évaluer ses propriétés catalytiques dans la réaction de réduction de 4-NP et comprendre l'effet de la chimie de surface dans cette réaction catalytique; b) développer une nouvelle méthode, simple et efficace, pour permettre un meilleur recyclage et la possibilité de réutilisation des PLAL-AuNPs en catalyse; c) trouver une nouvelle méthode basée sur la technique PLAL pour améliorer l'activité catalytique des PLAL-AuNPs. Grâce aux études systématiques, cette thèse offre une meilleure compréhension de l'influence de la chimie de surface sur les propriétés catalytiques des AuNPs et le potentiel d'applications des AuNPs en catalyse.

2. Étudier l'influence de l'irradiation laser sur la chimie de surface des Au NPs synthétisées chimiquement et investiguer l'effet de l'oxydation de surface sur la stabilité colloidale des AuNPs et leur interaction avec les groups amines dans le but de mieux comprendre l'influence de la chimie de surface sur les propriétés fonctionnelles des AuNPs.

Les résultats de cette thèse sont résumés sous forme de cinq chapitres et divisés en deux sections tel que suit :

SECTION (I): Les AuNPs synthétisées par PLAL et leurs propriétés catalytiques

Chapitre 3. Activité catalytique des PLAL-AuNPs.

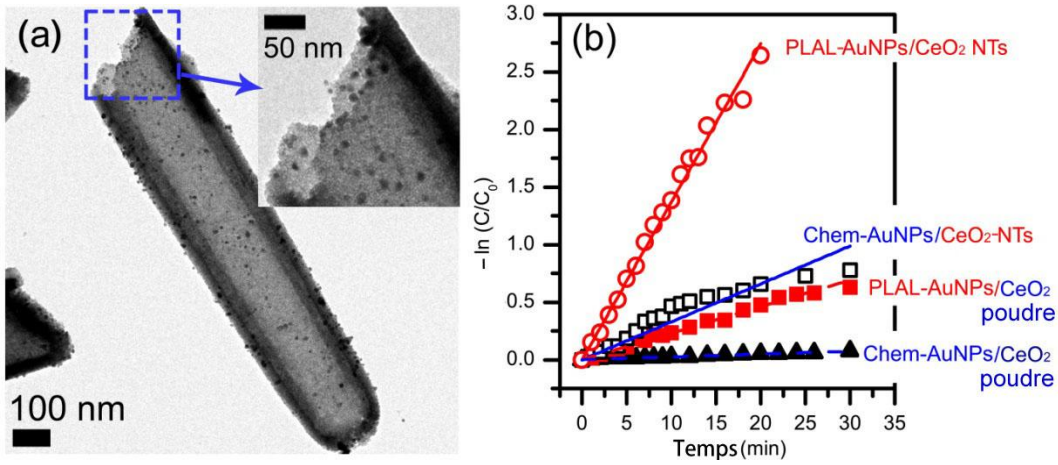

Figure R1. (a) Image MET d'un nanocatalyseur PLAL-AuNP/CeO_2-NT. (b)-ln (C/C_0) en fonction du temps de réaction catalytique calculé à partir des spectres UV-Vis (C_0 et C sont la concentration initiale des ions 4-nitrophénolate et la concentration au moment t, respectivement).

Un nouveau catalyseur nanostructuré a été fabriqué à partir des AuNPs petites et uniformes et les nanotubes de CeO_2 (NTs), tel que présenté sur les images MET (voir la Figure R1-a). Nous avons démontré que les AuNPs synthétisées par PLAL sur une cible d'or solide sont assemblées à la surface des CeO_2-NTs sans aucune fonctionnalisation de surface de chaque composante. Cet assemblage est dû au couplage des liaisons pendantes -OH à la surface des PLAL-AuNPs. La réaction de réduction du 4-NP en 4-AP à l'aide du catalyseur PLAL-AuNP/CeO_2-NT présente une vitesse de réaction remarquablement plus élevée que dans le cas des catalyseurs similaires composés de AuNPs synthétisées chimiquement (Chem-AuNPs) et de la poudre de CeO_2 commerciale, tel que présenté à la Figure R1-b. La forte activité catalytique des catalyseurs basés sur les PLAL-AuNPs est due à leur surface unique, relativement «propre» ainsi qu'à la présence d'oxyde d'or à la surface des NPs. Le rôle important de la chimie de surface unique des PLAL-AuNPs en catalyse a été également démontré dans la réaction d'oxydation du CO en phase gazeuse. Nos résultats

suggèrent que les PLAL-AuNPs peuvent être facilement attachées à la surface des CeO_2-NTs et que cette combinaison unique mène à des propriétés catalytiques très efficaces. Nos nano-catalyseurs mettent à profit les caractéristiques uniques des PLAL-AuNPs et offrent potentiellement une solution efficace pour la synthèse de catalyseurs métal-NP/métal-oxyde-support.

L'article relatif aux résultats décrits dans ce chapitre:

[92] Zhang, J., Chen, G., Chaker, M., Rosei, F. and Ma, D. Gold Nanoparticle Decorated Ceria Nanotubes with Significantly High Catalytic Activity for the Reduction of Nitrophenol and Mechanism Study, *Applied Catalysis B: Environmental*, 132-133: 107-115, 2013.

Chapitre 4. Un nouveau catalyseur recyclable *In Situ* d'AuNPs sensibles au gaz

Dans ce travail, nous avons développé de nouvelles AuNPs sensibles au gaz pour produire des nano-catalyseurs d'AuNPs très stables et réutilisables. Pour assurer une bonne activité catalytique et une bonne fonctionnalité des AuNPs, les PLAL-AuNPs avec surface "propre" sont utilisées dans ce projet. Pour la première fois, le polymère sensible au CO_2, PDEAEMA, est introduit dans la préparation de NPs «intelligentes» pour la catalyse.

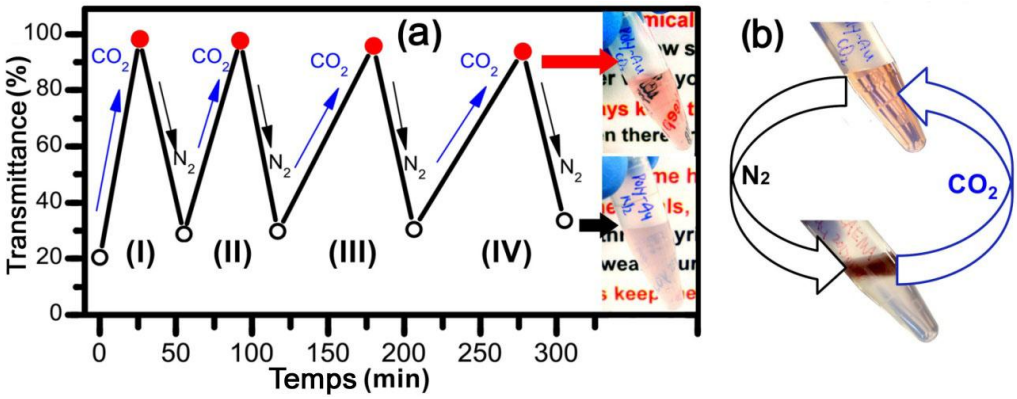

Figure R2 (a) la variation réversible de la transmission à quatre cycles CO_2/N_2, (b) séparation de phase réversible in-situ et re-dispersion de PDEAEMA-AuNPs dans l'eau au cours du bullage alterné de CO_2 / N_2.

La Figure R2 montre que la transmission et l'état de dispersion des PDEAEMA-AuNPs en solution aqueuse peuvent être ajustés par bullage de CO_2/N_2 en alternance, résultant en changement

d'opacité (Figure R2-a encadrée) et en séparation de phase (Figure R2-b) dû à la présence des NPs sensibles à gaz. Cette transition entre la séparation de phase et la re-dispersion des AuNPs dans la solution est réversible et se produit lors du bullage de CO_2/N_2. Les PDEAEMA-AuNPs montrent une haute sensibilité au CO_2, ce qui offre un bon contrôle de leur état de dispersion dans une solution aqueuse.

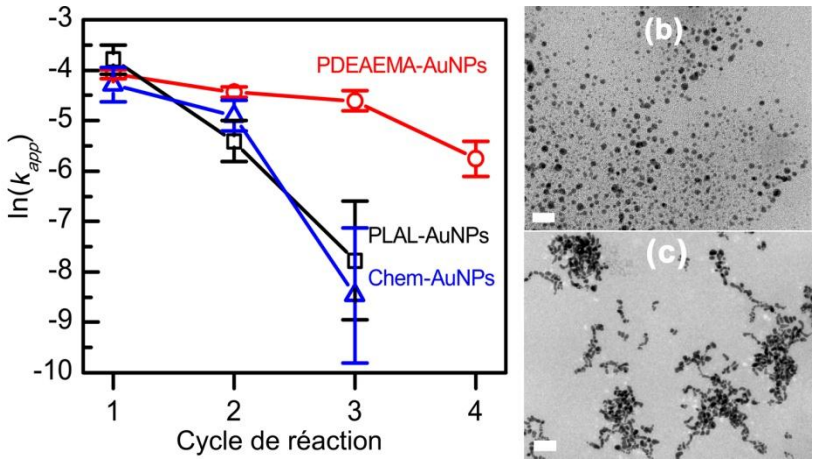

Figure R3 (a) Cuvres de $\ln(k_{app})$ en fonction du cycle de réaction en présence de PDEAEMA-AuNPs, PLAL-AuNPs et Chem-AuNPs, (b) et (c) images MET de PDEAEMA-AuNPs et PLAL- AuNPs, respectivement, après le troisième cycle de réaction (la longueur du trait est de 20 nm).

L'activité et la réutilisabilité du catalyseur PDEAEMA-AuNP recyclable *in situ* ont été évaluées dans la réaction de réduction 4-NP. Tel que montré à la figure R3-a, les PDEAEMA-AuNPs montrent une activité catalytique beaucoup plus élevée dans tous les cycles de réaction que les PLAL-AuNPs et les Chem-AuNPs. L'analyse MET (Figure R3-b, c) confirme que l'agglomération des PDEAEMA-AuNPs est faible après trois cycles de réaction. Ces observations suggèrent fortement que la stabilité et le potentiel de récupération des AuNPs fonctionnalisées avec PDEAEMA sont supérieurs à celles des AuNPs sans modification polymérique, offrant ainsi un catalyseur stable et facilement réutilisable. La présence d'une faible quantité de PDEAEMA ne semble pas influencer les sites catalytiques actifs des PLAL-AuNPs. Ce travail présente un nouveau

concept d'utilisation des polymères sensibles au CO_2 qui permettent une récupération facile de NPs, ce qui mène à des applications potentielles en catalyse en phase liquide homogène.

L'article relatif aux résultats décrits dans ce chapitre:

[93] Zhang, J., Han, D., Zhang, H., Chaker, M., Zhao, Y. and Ma, D. In situ recyclable gold nanoparticles using CO_2-switchable polymers for catalytic reduction of 4-nitrophenol, *Chemical Communications*, 48: 11510, 2012.

Chapitre 5. Augmentation de l'activité catalytique de PLAL-AuNPs par l'utilisation de l'alliage Pt-Au

Les alliages d'or avec d'autres métaux de transition, i.e. Pt, peut fortement augmenter l'activité catalytique des AuNPs du à l'effet synergique dans la structure d'alliage. En utilisant la technique de PLAL modifiée, les stables colloïdes d'alliage PtAu avec une large gamme de compositions ont été synthétisées à partir de cibles fabriquées par moulage de compression d'un mélange de poudres Pt et Au de concentration variée.

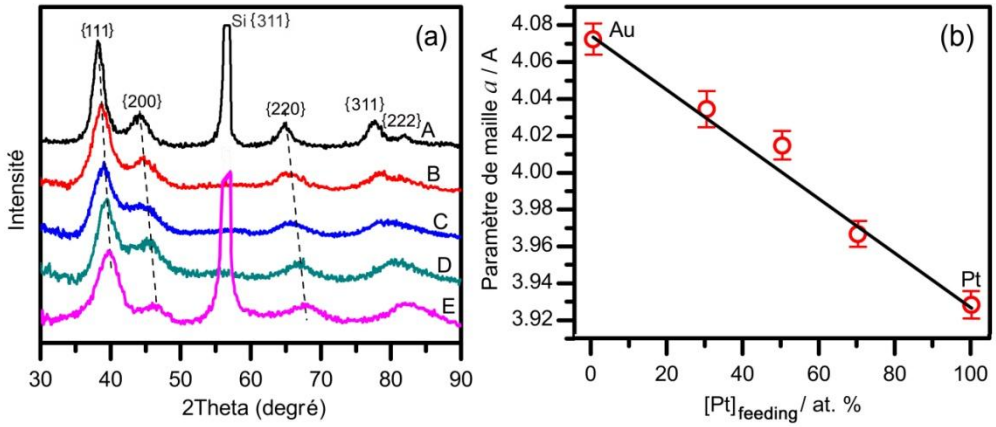

Figure R4 (a) les spectres DRX des colloïdes en alliage PtAu préparés par PLAL avec la fluence de 150,0 J/cm^2 et le pH de 11,0. La teneur en Pt est (A) 0, (B) 30, (C) 50 (D) 70, et (E) 100 %-at. (b) Paramètre de maille estimé à partir des spectres DRX, en fonction de la concentration de platine.

La Figure R4-a montre les spectres DRX des NPs préparées par différentes teneurs en Pt ($[Pt]_{feeding}$), à savoir la concentration de Pt dans les cibles. Chaque spectre montre quatre pics de diffraction qui correspondent à une structure CFC. Aucun autre pic n'est observé et la forme des spectres DRX est similaire pour chaque concentration. La position des pics se déplace progressivement vers des plus grandes valeurs de 2-théta lorsque la concentration de $[Pt]_{feeding}$ augmente de 0 à 100% (A-E). La position des pics et leur déplacement indiquent clairement la présence d'une structure d'alliage. Le paramètre de maille CFC *a* a été extrait à partir d'une analyse des pics de diffraction {111}. Il varie de façon quasi-linéaire en fonction de la concentration de $[Pt]_{feeding}$ (voir la Figure R4-b). Non seulement cette linéarité confirme la formation d'alliages dans une large gamme de concentrations [77, 115, 120] mais il démontre également que la teneur de Pt dans l'alliage des NPs est proche de celle des cibles utilisées.

L'étude de l'influence du pH de la solution et de la fluence du laser sur la synthèse de NPs montre que la formation d'alliage est essentiellement insensible à ces deux facteurs et que cette technique de synthèse de nanoparticules d'alliage est très fiable. En outre, la composition chimique à la surface, estimée à partir des mesures électrochimiques, est identique à la composition globale des NPs calculées à partir de la loi de Vegard et les données de DRX, ce qui est une bonne indication de l'uniformité de la composition chimique à la surface et à l'intérieur des NPs.

Les NPs d'alliages PtAu préparées par PLAL ont été assemblées sur CeO_2-NTs pour former des nano-catalyseurs hybrides, en utilisant la même méthode de préparation que celle décrite au chapitre 3, pour la réduction de 4-NP. La constante de vitesse de réaction catalytique *k* pour la réduction de 4-NP en fonction de la concentration de Pt dans le catalyseur Pt_xAu_{100-x}-NP/CeO_2-NT est présentée à la Figure R5 (ronds rouges). La valeur de *k* pour les nanohybrides contenant les NPs d'alliage AuPt est beaucoup plus élevée que celle obtenue avec les PLAL-AuNPs (à une concentration Pt égale à 0). En particulier, l'échantillon $Pt_{50}Au_{50}$-NP/CeO_2-NT montre la vitesse de

réaction maximale (~ 5,11 $\times 10^{-2}$ s^{-1} m^{-2}), ce qui est largement supérieur aux catalyseurs à base d'or ou de Pt pur et au mélange de NPs des deux types (carrés noirs) ainsi que d'autres nano-catalyseurs à base d'alliage d'or tel que trouvé dans la littérature [20, 39-42, 53]. Par conséquent, nous avons clairement démontré que l'alliage Au-Pt permet d'améliorer de manière significative l'activité catalytique par effet synergique.

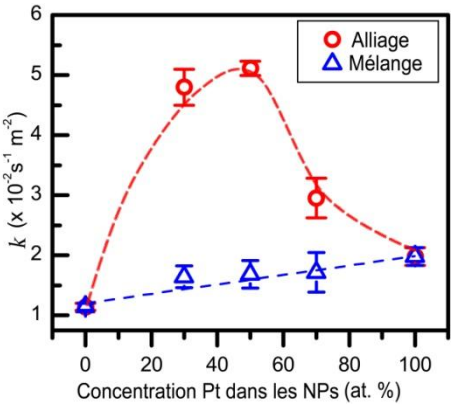

Figure R5 La vitesse de réaction *k* de NPs/CeO_2-NTs en fonction de la concentration de Pt dans les NPs.

Les publications relatives aux résultats présentés dans ce chapitre sont :

[71] Zhang, J., Oko, D., Garbarino, S., Imbeault, R., Chaker, M., Tavares, A. C., Guay, D. and Ma, D. Preparation of PtAu Alloy Colloids by Laser Ablation in Solution and their Characterization, *Journal of Physical Chemistry C*, 116: 13413-13420, 2012.

Zhang, J., Chen, G., Chaker, M. and D. Ma, Synergistic Catalysis of PtAu Alloy Nanoparticle in the Reduction of 4-Nitrophenol, *Journal of Physical Chemistry Letters*, to be submitted.

SECTION (II): La modification de surface par irradiation laser des Au NPs synthétisées chimiquement et son influence sur leur stabilité colloidale et leur interaction avec les groupes amines.

Chapitre 6. Modification des AuNPs synthétisées chimiquement par irradiation laser: (I) Effet sur la stabilité colloïdale des NPs

Des AuNPs synthétisées par la méthode de Frens « verte » ont été modifiées par irradiation laser afin de produire des AuNPs mono-dispersées avec un diamètre inférieur à 10 nm. La stabilité des AuNPs irradiées a été étudiée par ajustement de la constante diélectrique (introduction de l'éthanol) et de la concentration ionique (introduction du sel) des suspensions colloïdales. Après l'introduction de l'éthanol dans la solution aqueuse des AuNPs irradiées, de très petites variations de la position du pic (décalage vers le rouge) et de la largeur de pic d'absorption ont pu être observées. La même opération avec la suspension des AuNPs de 5 nm préparées par réduction de $NaBH_4$ montre un déplacement et un élargissement important du pic d'absorption vers le rouge (Figure R6-a).

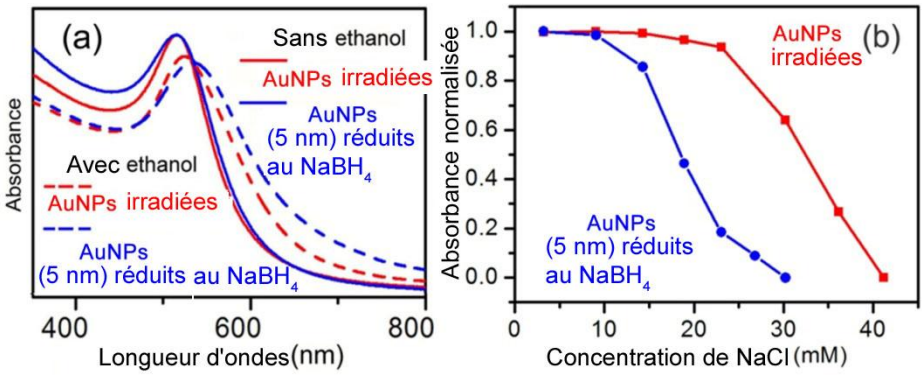

Figure R6. (a) spectres UV-Vis de AuNPs irradiées (rouge) et de AuNPs préparées par réduction de $NaBH_4$ (bleu) avant (ligne continue) et après (ligne pointillée) l'introduction de l'éthanol; (b) l'intensité d'absorption normalisée à 514 nm des AuNPs irradiés (rouge carrés) et $NaBH_4$ réduit (cercle bleu) AuNPs en fonction de la concentration de NaCl.

Figure R6-b montre l'évolution du spectre UV-Vis de la suspension des AuNPs irradiées et de la suspension des Chem-AuNPs en fonction de l'introduction de différentes quantités de solution de 0,1 M de NaCl. Pour les Chem-AuNPs, l'augmentation de la concentration de NaCl (plus de 10 mm) mène à une diminution rapide de l'intensité du pic SPR à 514 nm ce qui indique la formation

d'agglomérats d'AuNPs. La concentration de NaCl au «point critique» associé à l'agglomération de NPs est beaucoup plus élevée pour les AuNPs irradiées (~ 27 mM de NaCl) que pour les NPs réduites au $NaBH_4$ (~ 10 mM de NaCl). Ces résultats démontrent que la stabilité des AuNPs traitées par l'irradiation laser est supérieure à celle des AuNPs préparées par la méthode chimique non-modifiée. Cette stabilité colloïdale renforcée est également confirmée par une augmentation importante du potentiel de Zêta des colloïdes d'or et peut être expliquée par l'oxydation de la surface d'or sous l'effet de l'irradiation laser.

Ces travaux ont fait l'objet d'une publication:

[94] Zhang, J., Riabinina, D., Chaker, M. and Ma, D. Significant Stability Enhancement of Gold Colloids via Nanosecond Laser Irradiation, *Advanced Science Letters*, 4: 59-64, 2011.

Chapitre 7. Modification d'AuNPs synthétisées chimiquement en utilisant l'irradiation laser: (II) Effet sur la chimie de surface et sur l'interaction NH_2-AuNP

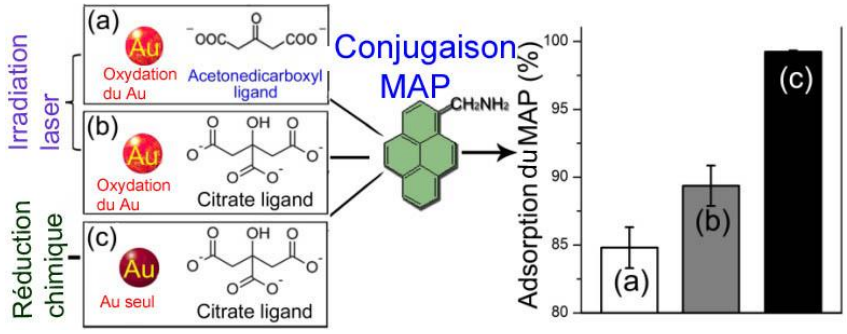

Figure R7. La conjugaison et l'adsorption de la molécule MAP sur la surface des AuNPs avec différentes caractéristiques de chimie de surface.

AuNPs synthétisées par voie chimique ont été modifiées par la technique d'irradiation laser. Trois échantillons d'or colloïdale avec la même taille de particules ont été préparés par i) l'irradiation laser de colloïdes d'or préparés chimiquement (l'échantillon irradié), ii) l'échange de ligands par citrate des NPs irradiées et iii) la méthode de réduction chimique. XPS, FTIR et la caractérisation NMR ont été effectuées sur les trois types d'échantillons pour étudier la chimie de

surface des AuNPs. Les résultats de cette analyse confirment que la surface des NPs irradiées et des NPs irradiées après le traitement d'échange de ligands est recouverte avec des ligands acétonedicarboxylique (en raison de l'oxydation du citrate) et des ligands citrate, respectivement, et les deux contiennent de l'oxyde d'or (Figure R7).

L'influence de la chimie de surface des AuNPs sur l'interaction d'AuNP-amine ($-NH_2$) a été étudiée par la conjugaison d'une sonde amine ─ 1- chromosphères methylaminopyrene (MAP) ─ avec les colloïdes d'or (Figure R7). L'adsorption du MAP a été analysée par spectroscopie de photoluminescence pour les trois échantillons d'or colloïdale. La capacité d'adsorption inférieure pour les deux échantillons irradiés par laser a été observée (Figure R7). La caractérisation de surface montrent que les AuNPs irradiées après l'échange de ligands possèdent une densité plus élevée de charge négative à la surface et plus de COO^-, cependant, ils adsorbent moins de MAP que celles préparées chimiquement. Cette observation démontre que l'interaction électrostatique ne domine pas le mécanisme d'adsorption et la présence d'oxyde d'or peut diminuer l'absorption. La caractérisation XPS sur le pic N1s révèle la nature de l'interaction AuNPs-amine, montrant que les molécules de MAP créent un lien directement avec des atomes d'or via les liaisons $Au-NH_2R$, et le niveau d'oxydation de la surface d'or influence fortement la proportion de cette liaison directe. L'impact de la surface oxydée d'or est confirmé par l'expérience du vieillissement sur les systèmes de conjugaison d'AuNPs-MAP, qui vérifie que l'oxydation de surface conduit à la diminution dans l'absorption de MAP sur la surface des AuNPs. Cette étude montre une forte dépendance de l'interaction d'AuNPs-amine de la chimie de surface d'AuNPs modifiée par irradiation laser.

L'article relatif aux résultats décrits dans ce chapitre:

[72] Zhang, J., Riabinina, D., Chaker, M. and Ma, D. Effect of Surface Oxidation on the Interaction of 1-Methylaminopyrene with Gold Nanoparticles, *Langmuir* 28: 2858-2865, 2012.

En résumé, dans cette thèse nous avons étudié, pour la première fois, la performance catalytique des PLAL-AuNPs et nous avons développé le catalyseur recyclable à base de nanoparticules d'or produites par PLAL. Nous avons également amélioré la performance catalytique du matériau en créant des alliages PtAu sous forme de nanoparticules par PLAL. Aussi, nous avons étudié la stabilité et l'interaction entre les groupements amine et les nanoparticules d'or irradiées par laser en vue de leurs applications potentielles dans le domaine de biologie; ainsi nous avons découvert l'oxydation de surface des nanoparticules d'or induite par irradiation laser.

Les hybrides basés sur les nanoparticules d'or produites par PLAL développés dans le cadre de cette thèse peuvent également être utilisés pour d'autres applications catalytiques, telles que dissociation de l'eau par photocatalyse (photocatalytic water splitting). De plus, il est indispensable de réduire le coût des catalyseurs en diminuant la proportion des matériaux nobles en vue de leur utilisation à l'échelle industrielle. Ainsi, il est intéressant d'exploiter le potentiel d'utilisation de la technique PLAL pour la production des nanoparticules pour la catalyse en vue de remplacement des métaux nobles par des matériaux moins couteux.